UNIVERSITÀ DEGLI STUDI DI PALERMO

NEEMO: NEW ELECTRICAL ENERGY FROM MARINE OSCILLATION

By Alessia Viola
A thesis submitted in fulfillment of the requirements for the PhD degree in Energy.
Supervised by Dr. Vincenzo Franzitta, Dr. Marco Trapanese

UNIVERSITÀ DEGLI STUDI DI PALERMO

Dottorato in Energia indirizzo Energetica
D.E.I.M. Dipartimento di Energia, Ingegneria dell'Informazione e Modelli Matematici
Settore Scientifico Disciplinare : ING/IND11

NEEMO: New Electrical Energy from Marine Oscillation

IL DOTTORE
ALESSIA VIOLA

IL COORDINATORE
PROF. ALDO ORIOLI

IL TUTOR
DOTT. ING. VINCENZO FRANZITTA

CO TUTOR
DOTT. ING. MARCO TRAPANESE

CICLO XXV
ANNO CONSEGUIMENTO 2015

LIST OF CONTENTS

To my parents

Acknowledgments

Completing the PhD and writing this thesis has been an amazing journey that would not have been possible without the support and encouragement of many outstanding people.

My greatest appreciation and gratitude goes to my advisors Vincenzo Franzitta and Marco Trapanese for their trust and support. I would like to thank them for advising me during all phases of my PhD, but also for giving me the freedom to find my own way in the project IMPETUS. During these years I've learned what it means to do research and to open my mind in different areas. I would like to thank them for giving me great possibilities to travel worldwide and do life experience that will stay with me for ever.

Finally, I would like to express my deepest gratitude to my family, Fabrizio and my friends. They have all been standing by me and shared with me both the great and the difficult moments of life. I owe them much more then I would ever be able to express, so I keep it plain and simple: Thank you so much for your love and care!

I dedicate this thesis to my parents Anna and Alfredo that support me in every moment and have always encouraged me in every decision.

Introduction

Among the actions that the Kyoto Protocol indicates in order to reduce CO_2 emissions, innovative technologies are promoted, in particular the particular renewable energy.

The penetration of renewable energy into the energy system of human settlements on Earth is from one point of view nearly 100%. The energy system seen by the inhabitants of the Earth is dominated by the environmental heat associated with the greenhouse effect, which captures solar energy and stores it within a surface-near sheet of topsoil and atmosphere around the Earth. Only 0.02% of this energy system is currently managed by human society. Within this economically managed part of the energy sector, renewable energy sources currently provide about 25% of the energy supplied[1].

Energy use and resource depletion does not, of course, constitute the primary goals of any society or individual within a society. For example, average Europeans or Japanese use about half as much energy as the average North American, but have a living standard, which certainly is not lower than that of the North American citizens. This underlines the fact that the living standard and welfare depends on having primary (food, shelter, relations) as well as secondary standards of individual preference fulfilled and that this can be done in different ways with different implications for energy use[1].

In the last years the interest of research and policy is focused attention on new system able to exploit energy from nature or economical source of energy.

Electricity generation from clean, safe and sustainable energy sources is nowadays a priority for many industrialized countries to meet increased energy demand and to reduce CO_2 emissions. An extremely promising renewable resource, which could provide substantial clean energy supply, is represented by surface ocean waves.

Very important is the contribution of coastal areas in which the water can be used as driving force or exploited to its thermal and saline gradient .Even though the coastal areas have a great importance for energy production by waves, so far the main projects of generation systems have involved the installation in open oceans, because of the greater energy of these waves rather the coastal ones. Near the coast, in fact, the waves are shorter and with a more little period so that there's a lower energy potential. However, in closed basins such as the Mediterranean, coastal installations for wave energy recovery allow the

integration of generators in coastal builds, producing a reduction of return on investment and the decentralized production of electricity in fixed small systems.

Wave energy is a type of well-concentrated and predictable renewable energy, and its resources are huge (IEA's estimation of the total wave energy is up to 80,000 TWh a year[1], compared to the worldwide electricity production 17,400 TWh in the year of 2004). Extracting wave energy from seas may significantly contribute to the green target of sustainable development around the world.

In the past three decades, it has been shown that the wave energy conversions are practically difficult, although the principles of wave energy conversion have been proven, and different technologies can be used for extracting wave energy from seas. One question is how expensive we can convert wave energy into useful energy, and this question must be answered by researchers and developers before any commercial wave energy farm is built.

Although difficulties, wave energy conversions have been seen some successful stories. It is reported a few hundred navigational buoys (oscillating water columns) have been deployed in the remote and harsh areas where the access for frequently changing batteries is not viable .Also, the breakthroughs in wave energy conversion in 1970e1980s on some prototype devices once convinced people that massive wave energy production would soon become a reality. Considerable works have been undertaken on wave energy assessment in several areas of the European coastline. The total wave power was found to range from 1GW in Sweden, to 120 GW in UK, passing through 3.4 GW of Denmark, 10 GW in Portugal, 21 GW in Ireland and over 28 GW in the area of Gulf of Gascoigne, France. Recent works focused on the Spanish coastline reveal an enormous potential in several coastal areas facing the Atlantic, with a wave power which frequently reaches 200 MWh/m and exceeds 400 MWh/m along the Death Coast.

Optimal and control technologies for improving wave energy conversion have been proposed and developed since 1970s and the developed optimal theories have shown if an ideal power take-off (PTO)[2] can provide the required performance, the wave energy capture by the device can be made to or close to the theoretical maximum. However, such as ideal PTO cannot be achievable in practice due to the very high demands for the control optima and the mechanical limitation for the PTO device and some other issues. As a result of the difficulties in realizing the full optimal/control strategy, more practical control technologies have been proposed and developed by partially fulfilling the optimal conditions, thus they are often called the sub-optimal controls[3].

The planning and fulfilment have as principal difficulty the installation of WEC in marine environment. The corrosion and high cost of the type of energy system influence the planning choice. So a correct and specific pre-sizing is a

necessary step to achieve the work. In fact, in this study is been adopted FEM sizing that allows to optimize performances of energy system. All FEM simulations are approached using the steps described in figure below inserted

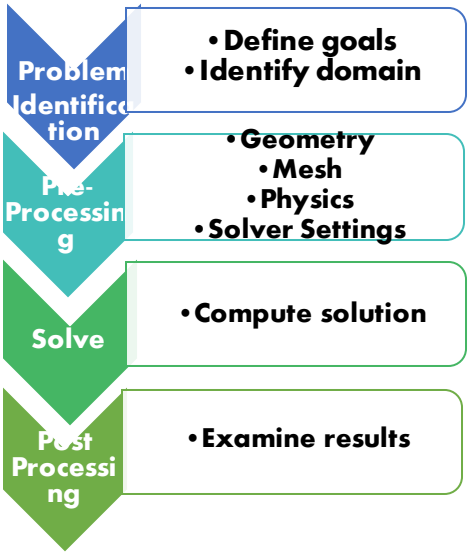

Figure I FEM Scheme

In this thesis I describe the numerous steps that allow the design and fulfilment of wave energy converters. In particular, I analyse a case study of installation of this type of electrical device. The optimum plan of wave energy system should follow a specific pattern:

- To identify the installation site;
- To describe its wave climate;
- To obtain minimal wavy parameters to device a wave energy converter (WEC)
- To select type of electrical available generator;
- To choose sustainable and low cost materials,

The methodology above described is been used to realize the electrical system that is the content of this work. In particular, I divided my work into five chapter where in everyone I've described a part of scheme above mentioned.

In the Chapter I, there is a detailed description of wave climate studies: laws, equations and physical principles of wave generated by wind. So I identify the main parameters that are necessary to design an electrical wave converter. The Chapter II shows a characterization of measuring and prediction instruments of marine oscillation: a buoy realized in the Department of Energy, Information engineering and Mathematical models at University of Palermo.

A state of the art of wave energy converters is inserted in Chapter III. In particular , it's been reported the term "Technology Readiness Level".A number of steps have been set in place to pave the way for a staged growth of a new wave energy concept or design.

As for the Chapter IV, in it I examined the procedures adopted for the choice of type of electric generator to be used for the realization of the converter. In particular, the analysis is made using a specific FEM (finite element method) software that is necessary to could be a comparison among different electrical structure. The research is based on the design, modelling and optimization of: A Ferrite Tubular Linear Permanent Magnet Generator (FTLPMG), A Transverse Flux Machine and a Linear Permanent Magnet Generator (LPM).

In the end, the final Chapter V represents a case and experimental study of the system "WECs + electrolyzer" that is designed in Sicily. In the previous chapter they were separately analysed the operation of wave buoy of DEIM and the numerical simulation of numerous electrical device. The Permanent Magnet Generator (PMG) was chosen as electrical system to be implemented. In particular, we introduce all electrical structure of PMG (stator and shifter), a FEM transient simulation of it that shams a sea wave condition and test bench of generator. So we obtain a real energy production. Its production in connected to the working of an electrolyzer.Sea water electrolysis is a mechanism of production of Hydrogen; in fact we analysed the process, studying operative variable as Temperature and Pressure. As for the conclusion of this work is based on the environmental valuation of the system realized: produce clean hydrogen from sea.

If the main aim of this thesis is a description of new electrical energy from marine oscillation, in this work I inserted two annex that represent new kind of energy harvesting.

So the Annex I presents a Thermomagnetic Motor. The design of the motor is based on a thermal-magnetic coupled dynamic model, which is obtained by assuming the use of a ferromagnetic material working at temperatures near the curie point. The motor is modeled in terms of both its magnetic as well thermal properties (magnetic permeability and thermal conductivity) and the thermal processes are supposed to be influenced by the thermal conductivity, the convection and the advection. An analytical expression of the generated torque, which links this quantity to the magnetic, thermal and geometrical parameters of the generated torque is given. A design of a machine, based on this theory is proposed and the related performances are numerically simulated. The motor has been built and its rotor has been manufactured by using Gadolinium.

As for Annex II, I propose an approach to the design of a magnetostrictive electric power generator and we validate it experimentally. We use Dynamic Preisach hysteresis Model (DPM) for magnetostrictive materials operating in hysteretic and time varying nonlinear regimes to design and simulate a magnetostrictive electrical power generator. DPM is a development of classical Preisach Model which is able to include dynamical features in the mathematical model of hysteresis. We measure the output power capability of the generator and we show how it is comparable to other energy harvesting technologies.

CHAPTER I

Wave Climate Studies

Introduction

Wave energy is defined as the energy produced by motion of wave that is a directly consequence of wind and different superficial temperature of the soil. It is usually expressed in power per meter of wave front and is generally measured in kW / m.

Waves are disturbances of a fluid medium through which energy is moved. Sea waves travel on the interface between oceans and the atmosphere. Waves are caused by friction between wind and the water surface, gravitational attraction, earthquakes or volcanic eruptions. As will be elaborated on later, we focus on waves caused by wind[4].

The waves can be generated by various forces such as wind, gravitational action of the sun and the moon, changes in atmospheric pressure, earthquakes. Anyway, the wave created by the wind represents a concentrated source of the energy and daily variations smaller than those of other renewable resources such as wind, the sun or the ocean currents[5].

The main methods to outline the waves are those random zero upcrossing and zero downcrossing, thus waves zero upcrossing are identified by two crossings of the level of quiet with positive derivative while waves zero downcrossing are identified by two successive crossings of the level of quiet top to bottom.[6]

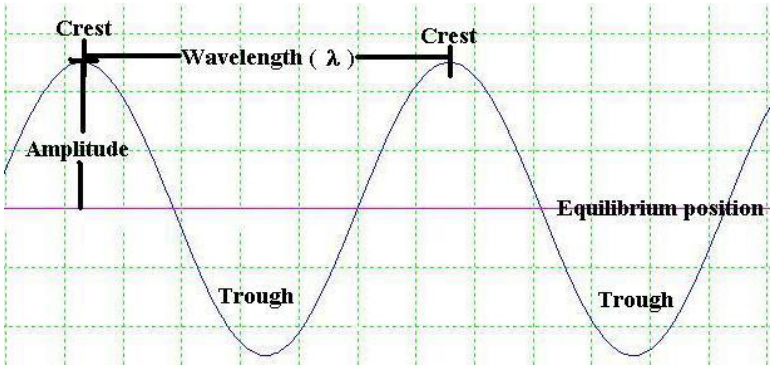

Figure 1.1-Characteristic of Wave

It's important describe main principal characteristic of a wave:

- Crest: the highest maximum of this wave;
- Trough: the relative minimum of less ordinate;
- Height of wave: the sum of the height of the crest and the depth of the trough ($H = \eta_{crest} - \eta_{trough}$)

As illustrated in this figure, wave length (λ) is the distance between two crests. The time it takes the wave to travel this distance is called wave period.

Wave class	Period	Wavelength	Cause	Wave type
Capillary	<0.1 s	<2cm	Local winds	Deep to shallow
Chop	1-10 s	1-10 cm	Local winds	Deep to shallow
Swell	10-30 s	Up to hundreds of m	Distant storms	Deep to shallow
Seiche	10 min-10 hrs	Up to hundreds of km	Wind, tsunami, tidal resonance	Shallow or intermediate
Tsunami	10-60 min	Up to hundreds of m	Earthquakes or under or near the ocean	Shallow or intermediate
Tide	12.4-24.8 hr	Thousands of km	Gravitational attraction of sun and moon	Shallow

Table 1.1Different waves

Sea states can be described through the concept of "characteristic wave" namely regular waves specified according to a fraction of the highest waves.

1.1 Sea Wave parameters

Characteristic wave is defined as wave that has a height $\mathbf{H_{1/c}}$ equal to the average of the heights of random waves that make up the fraction of the highest waves and a period equal to the average in the periods of the waves that build the wave $H_{1/c}$. [7]

The parameters used are:

- Mean wave $H_{1/1}$;
- Significant wave $H_{1/3}$: it is obtained by averaging the wave height of the one third highest waves.
- Wave one-tenth $H_{1/10}$: it' calculated as the average of tenth of the highest waves.
- Maximum wave H_{max}: it represents maximum height that is independent by the period T. It's usually used to design structure that are sensitive to attacking of the wave motion.

The main parameters used for the definition of climate state are the period (T_e) and the height of wave (H_s). In fact, the buoys as almost all other stations

located off the Italian coast, don't supply directly the energy period, so there are different mathematical relations that connect T_e with mean period T_m.

In particular, it's possible define two forms of energy:[8]

- Kinetic energy: where the water molecules of a single wave move continuously according to circular orbits;
- Potential energy:the water molecules of the single wave are lifted above the free surface, and then equipped with energy potential.

For regular waves, the sum of kinetic and potential energy density per unit area, can be expressed according to the known relationship:

$$\boldsymbol{E_t = \frac{\rho g H^2}{8}} \tag{1.1}$$

where with ρ is sea water density, g is the gravity acceleration ad H is mean height.

.

In this study the expression used is:

$$\boldsymbol{T_e = \alpha T_p} \tag{1.2}$$

where α depends on the shape of the spectrum waveform associated with samplings and its value is 0.9 while T_p is the peak period.[9]

As regards the value of H_s is obtained by:

$$\boldsymbol{H_{\frac{1}{3}} = \frac{1}{\frac{n}{3}} \sum_{j=1}^{\frac{n}{3}} H_j} \tag{1.3}$$

The estimation of wave power transmitted per unit width is represented below:

$$\boldsymbol{P_{wave} = E \cdot c_g} \tag{1.4}$$

where c_g is the group velocity.

In deep water, when the depth is greater than half the wavelength, the equation above mentioned can be rewritten as:

$$\mathbf{P} = \boldsymbol{\frac{\rho g^2}{64\pi} H_s^2 T_e} \tag{1.5}$$

A wave energy converter needs to be dimensioned to its intended wave climate just as the generator of a hydro power plant is dimensioned with regard to the head of its dam. Knowledge of the average sea states and extreme waves are vital, and a natural and important step in designing a wave energy converter for a particular location is therefore to determine the wave climate of the site.

1.2 Wave Climate

A particular sea state, i.e. the waves appearing at a location over a relatively short period of time, is generally described by its significant wave height and energy period (or sometimes average period). So wave characteristic of the same place is called *Wave Climate*, and is generally given only in terms of the average energy flux. To define sea state, generally, we study two different statistical and probabilistic distribution: frequency distribution of combined occurrence of wave height (source direction) and frequency of exceeding of thresholds of significant wave height.[10]

The design wave must represent the environmental conditions that are considered dangerous fort the stability of maritime structure (as wave energy converters) and in in general to indicate a sea state, it is defined by means of its height , period and original directions. We can study different methodology to determine significant wave height, but it's possible to find three different stage:

1. Selection of homogeneous independent data;
2. Identification of the probability model;
3. Determination of wave heights within a given return period;

As for the first phase, is very difficult to identify what data is included in the probabilistic model. We can use:

- complete data set: direct surveys containing all the wave heights measured in the long term;
- annual data set: collection of the series of annual maximum wave heights;
- partial data set: series of the maximum wave heights in every single storm that have exceeded a threshold value

There are two different approach: the first procedure is based on regular sampling of observed data generating a time-aggregated population, while the second provides for event sampling and generates a time disaggregated population (called *PTO Peak Over Threshold*). With particular reference to wave measurements, the second procedure is generally adopted, in fact it's simple to

assure that data are independent while it is difficult to define homogeneous because different sea states have different origin and characteristics.

Therefore, the statistical inference applied to the wave measurement series is complicated by the directional dependence of data and their relation with the meteorological condition of the same site.in particular, a definition of a "sea storm" appears to be fundamental for the characterization climate of the site in question. Sea storms are typically represented by values of wave height, period and direction that correspond to the peak of the sea state.

As regards directional homogeneity can be guaranteed by classifying mean sea storm directions into directional sectors.

The choice of probabilistic model is a critic phase of characterization of wave climate.[6]

The most common distributions in the analysis of extreme wave heights are type I (Gumbel), type II (Fretchet) and type III with lower limit (Weibull) and in each model the cumulated probability of not exceedance above threshold, indicated as P(x), is been studied as principal parameter. It's a function of different variables: scale factor A; position factor B and shape factor k. The most common are Weibull or Gumbel distribution.

As regards Weibull distribution, the cumulated probability of not exceedance:

$$\boldsymbol{P\ (X < x) = 1 - e^{-\left(\frac{x-B}{A}\right)^{k}}} \tag{1.6}$$

with X indicates wave height characteristic and x is the realization of X.

As for Gumbel distribution:

$$\boldsymbol{P\ (X < x) = 1 - e^{-e^{\left(\frac{x-B}{A}\right)}}} \tag{1.7}$$

So it is possible to identify a simplified procedure which provides:

1) To sort in descending order samples of wave height;
2) To calculate the non- exceedance frequency for each sample element. The value of m-th element is calculated by the equation:

$$\boldsymbol{P_m = 1 - \frac{m-\alpha}{N+\beta}} \tag{1.8}$$

where N is the number of samples and if you have deleted the data, as less than a fixed threshold, the sample size to be included in the formula is the original.

As for α and , values are constants that we report in table.

	α	β
Gumbel	0.44	0.121
Weibull	$0.20 + 0.27/\sqrt{k}$	$0.20 + 0.23/\sqrt{k}$
Fretchet	0.0	1.0

3) After you find all parameters of the probability distributions, it is necessary to select among all probability methods considered the "true" distribution probability or, the most similar one.

It can be assumed that the probability law is the one that better fits to observation and therefore, from the Least Squares point of view, it is the one that has the smallest residual between observed and statically forecasted values. We can use the absolute correlation coefficient *(r)* or its complement to 1 called residual *(Δr)*. Some authors propose new criteria based on the normalization of the correlation coefficient residual with to respect to its mean value.

Another important parameter that is calculated is the determination of wave heights within a given return period. To identify the length of time over which you want to extend the statistical prediction, ca be used *return period* (T_R) which by definition is shown as the mean number of years within which the general H value is not exceeded, or simply as interval of time between two events at not lower height .

$$\boldsymbol{T_R = \frac{1}{\lambda(1-P(x)}} \qquad (1.9)$$

where λ is a parameter of intensity of data and the expression (1- P(x)) is probability of exceedance. In particular, probability of exceedance is connected with lifetime of the structure L_s :

$$\boldsymbol{P_S = 1 - \left(1 - \frac{1}{T_R}\right)^{L_s}} \qquad 1.10)$$

In conclusion, the probability of risk, at least one episode of the return period to be taken as given project will occur during the design life of the

structure will be assigned according to the importance of the work. So to calculate return period connected to lifetime of the structure can be defined:

$$\boldsymbol{T_R = \frac{V_P}{-\ln[1-P(T_R;V_P)]}} \qquad (1.11)$$

As can be seen from the equation above mentioned, it is a function of the risk P (T_R;V_P) event and the life of the project V_P.

CHAPTER II

Wave measurement and prediction

Introduction

Weather buoys are devices designed to collect weather and ocean data within the world's oceans. Drifting buoys have been used since 1979 while moored buoys have been in used since 1951, Moored buoys are connected with the ocean bottom using either chains, nylon, or buoyant polypropylene.

With the decline of the weather ship, they have taken a more primary role in measuring conditions over the open seas since the 1970s. During the 1980s and 1990s, a network of buoys in the central and eastern tropical Pacific Ocean helped study the El Niño-Southern Oscillation. Drifting buoys are the dominant form of weather buoy in sheer number, with 1250 located worldwide. Wind data from buoys have smaller error than that from ships. There are differences in the values of sea surface temperature measurements between the two platforms as well, relating to the depth of the measurement and whether or not the water is heated by the ship which measures the quantity.

Weather buoys, like other types of weather stations, measure parameters such as air temperature above the ocean surface, wind-speed (steady and gusting),barometric pressure, and wind direction. Since they lie in oceans and lakes, they also measure water temperature, wave height, and dominant wave period. Raw data is processed and can be logged on board the buoy and then transmitted via radio, cellular, or satellite communications to meteorological centers for use in weather forecasting and climate study[11].

Both moored buoys and drifting buoys (drifting in the open ocean currents) are used. Fixed buoys measure the water temperature at a depth of 3 metres (9.8 ft). Many different drifting buoys exist around the world that vary in design and the location of reliable temperature sensors varies. These measurements are beamed to satellites for automated and immediate data distribution. Other than their use as a source of meteorological data, their data is used within research programs, emergency response to chemical spills, legal proceedings, and engineering design. Moored weather buoys can also act as a navigational aid, like other types of buoys.

There are numerous applications for buoy data, which complement data collected through other means such as satellites:

- Weather forecasts: Meteorological models routinely assimilate observational data, under the World Weather Watch, from various sources including satellites, weather balloons, land stations, floats, ships, and data buoys. Most of the models are global and assimilate observational data from all sources to generate national forecasts. Buoy data are crucial because deployed in data sparse ocean area where no other source of valuable data are available.
- Marine forecasting: Buoy data are critical for producing improved marine forecasts.
- Hurricane or Cyclone forecasts can be improved by placing drifting buoys (with sub surface temperature measurements) into hotspots.
- Seasonal Forecasting: Using data buoys and other instruments such as sub-surface floats, many advanced oceanographic models now can be used to predict global or regional events and other ocean disturbances.
- Safety at sea: Several nations have successfully used surface wind and ocean current information from the buoys to help locate missing or overdue boats.
- Assistance to fisheries: Sea surface temperature is an important tool to find many different species of fish. The buoys provide this information to weather centres daily. These centres, in turn, produce charts of sea surface temperature and distribute them to assist and also control fishing activity.
- Environmental observations required in support of meteorological and oceanographic services and research.

The first step to an appropriate research towards the exploitation of the energy source in question is to identify the most effective method to calculate the potential energy extractable from the sea.

The main limitation of such a system of acquisition of the data is found in the excessive costs of the devices used. Another fundamental problem is the difficulty of installing buoys due to the different characteristics of marine areas.

For these different motivations is useful to design and implement a buoy measure waves

2.1 The Design of Buoy

The DEIM buoy system suitable either for shallow water or lagoons areas or no sheltered deeper sea sites. This buoy have important advantages and features, as[12]:

- On line aerial data transmission (telephone line);
- Easy assembling and installation;
- Low cost;
- Solar panels maintenance free for the power supply.

In the following Fig. 1-2 we can see the dimension of the DEIM weather buoy".

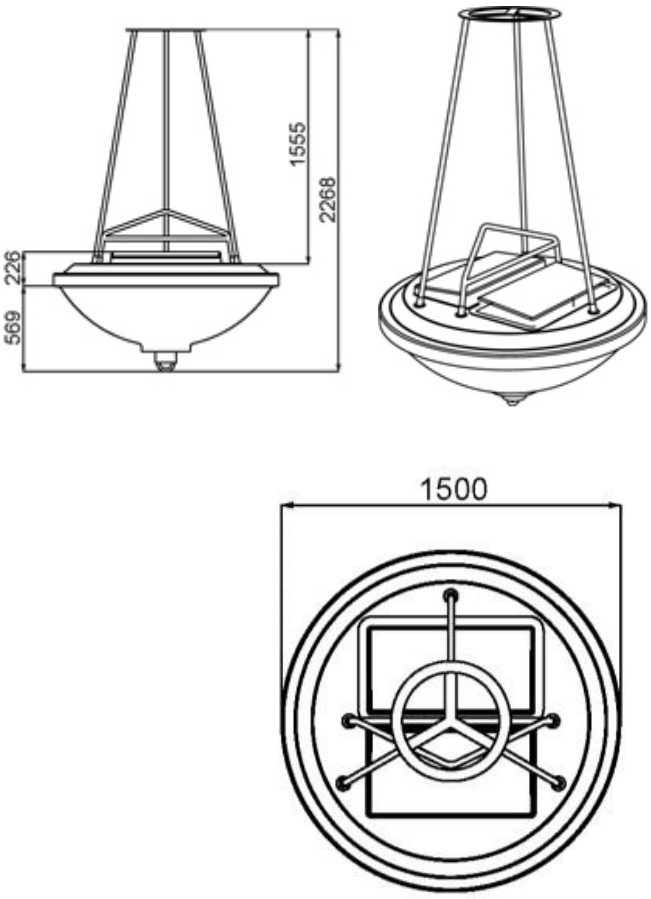

Figure 2.1 Design of Buoy: Real Dimension

The images below represent some of the phases of construction and processing of the buoy.

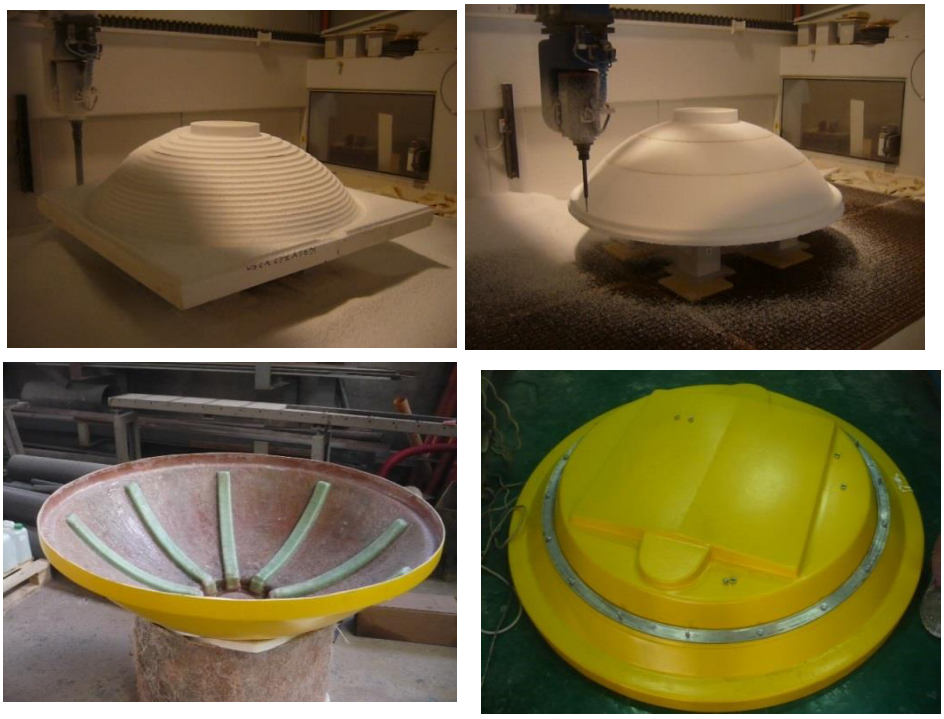

Figure 2.2 Images of Construction of Buoy

The heart of the system consists of a RISC microcontroller Microchip PIC 18F2620 with an internal crystal oscillator with a clock frequency of 40MHz that allows programs to run at a speed of no less than 10 MIPS. The microcontroller supervises all the operations required for operating the device data acquisition, in the monitoring and remote management.

The digital multiplexer allows you to share serial port of the PIC module with the Telit GSM / GPRS / GPS and with the removable mass storage, managed by the micro SD card reader, which is carried on the back-up your data.A suitable network allows to adapt the logic levels of the PIC to those of the Telit module and the reader µDrive.

The figure below shows the block diagram of the geo-referenced acquisition and transmission dates mounted inside the buoy.

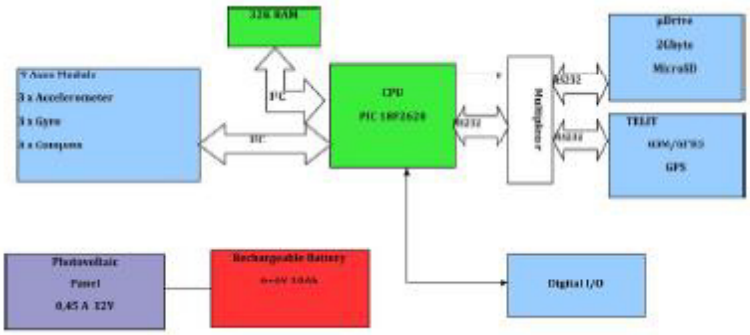

Figure 2.3 Geo-referenced acquisition and transmission dates

The main sensor is represented by a tab SMD assembling on board a triaxial accelerometer, a triaxial gyroscope and a compass triaxial; connection to the microcomputer is bidirectional I2C. The resolution of the sensors of the modul to 9 axes is as follows:

- Compass 12-bit
- Accelerometer 13-bit
- Gyroscope 16-bit

For a total of 41 bits each of the axes (X, Y, Z) will therefore have 123 bits for each sample (16 8-bit byte). Using the maximum possible speed sampling is possible to have an acquisition every 0.1 sec.

To manage this flow of information is required to adopt a compression technique. The digital inputs mounted are contacts On / Off to inform the system of any openings or openings of the buoy; Taking advantage of the multi-channel ADC converter of the microcontroller can monitor the charge level of the battery, the voltage supplied by the solar panel and the charging current of the battery. Data is stored on a microSD card with a maximum capacity of 2Gigabyte allowed by the card reader (µDrive).

Considering that the data can be stored using a compression algorithm such as that described later, it is possible to estimate a back-up of over 5 months of data.The Telit module with phone SIM card, manages the connection to the telephone network GSM / GPRS network and then to the Internet Web. On board the same module is also mounted a GPS receiver to 12 satellites.

The GPS module also allows you to capture the exact values of date and time, eliminating the need to mount on a board RTC (Real Time Clock) for the timing of activities related to the operation of the module.

The 32K RAM with I2C output is expected to function as a buffer to store the sampled data prior to compression, storing them on the microSD card and the final submission to the Internet Server. Only after the ackowledgement

receiving valid data sent in response from the remote server RAM will be erased and rewritten.

A backup battery and a solar panel to complete the system for what concerns the power of the module. Alternatively, they can be studied Power Systems-pack high capacity batteries to be mounted outside of the buoy for easy replacement. The module is powered by a switching regulator that provides 4.2V voltage necessary for the proper functioning of the Telit module and the remaining devices.

A careful analysis of the running times of various devices and run-time management program ensures that you can easily sampled 10 times per second for the 9 parameters from the acceleration sensor (3 for accelerations, 3 for position and 3 for gyroscopic the magnetic field), compress them within the static RAM 32K and generate data packets that will be sent to the remote server using the Telit module .

The machine time remaining is more than sufficient to ensure also the other auxiliary services such as the position control, alarm management and control of the voltages.

As mentioned above, the acquired data are sent via the GSM / GPRS module directly to an Internet server through a PHP script residing on the server. With the POST method sends the entire compressed package. The PHP code will unpack the received data and insert them into a MySQL database. An HTML page, to which access will be password protected, it will allow for consultation or downloading on the part of authorized users.

Given the inertia of the system, the acquired data should vary relatively slowly, so it is conceivable that the difference between a sample value and the next is quite small. Determined the maximum variation for each type of data, it is possible to adopt a compression system simple, effective and which requires few resources of calculation by the CPU.

A data packet can be formed by the 9 initial values of the relative sensors (123 bit) followed by 4/5/6 ... bits per channel that indicate the change compared to the previous value. For example, suppose for a minute of uncompressed samples are needed 73800 bits or 9225 bytes. The following table shows the possible compression with different resolutions.

The number of bits required can be determined experimentally by analyzing a data stream is not compressed. A reduction of the amount of data means more space available in the memory for the data, smaller packets and less transmission time thus saving energy stored in batteries.

In addition to the simple task of acquisition, storage and transmission of data, the system must also be able to ensure the following functions:

- Automatic reset due to errors or unexpected random block system (watchdog function);
- Restore the system configuration (time, location, historical data acquired) after reset (using scratchpad RAM);
- Check the connection of GSM and GPS data before sending;
- Check validity of data from the mean value of previous data;
- Control successful reception of the data (acknowledgment) from the remote system;
- Immediate notice of tampering or opening of the buoy;
- Immediate notice of the emergency situation in case the buoy moves significantly from the point of installation;
- Low battery alert;
- Contract failure of the solar panel;
- Setting up a remote time of sending data;
- - Setting the remote execution of some basic parameters.

These functions are carried out directly by the software resident on board. Other alarm functions or management of particular events may be entrusted to the Internet.

Server such as sending specific alerts in case the buoy does not transmit more for a certain period. Messages can be sent via email by the system itself or from the Internet Server and, if necessary, for critical alarms can be sent a text message to a predefined number.

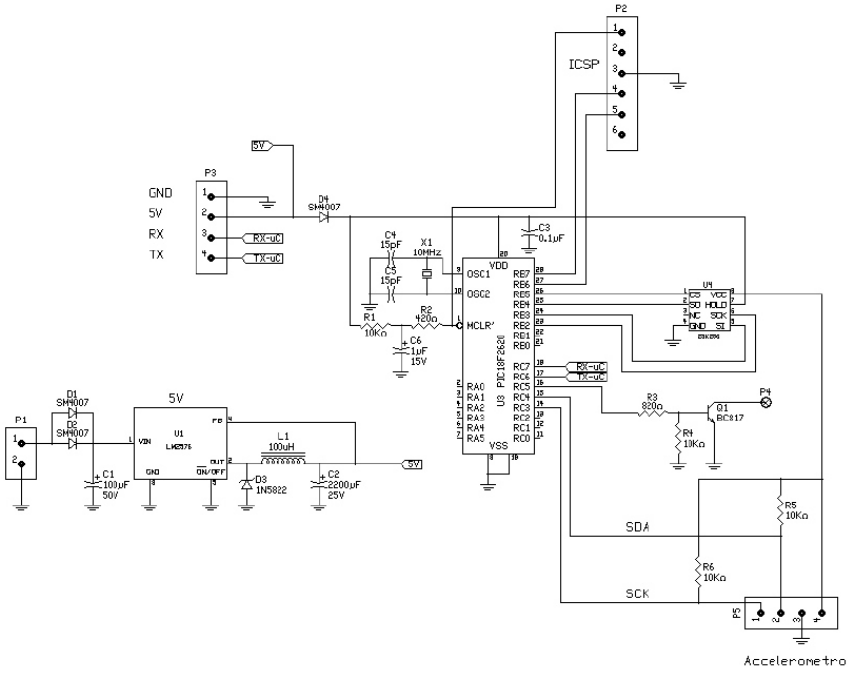

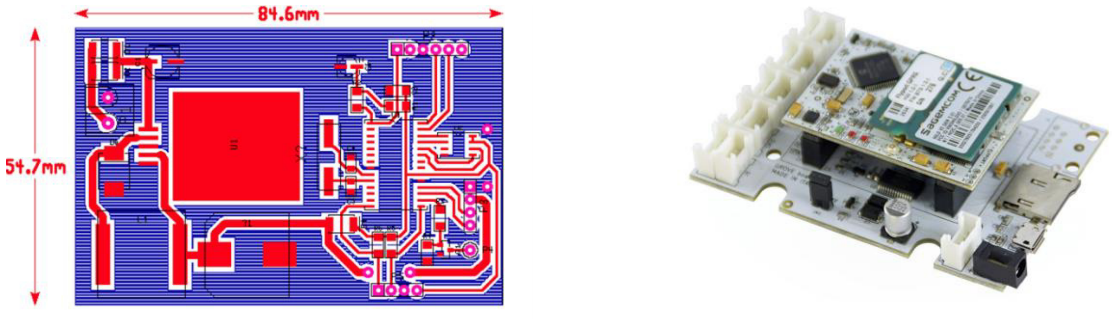

Figure 2.4 PCB (Printed Circuit Board) and Module with sensor board

The motion sensor (9 Axes Module) that includes a triaxial accelerometer, a gyroscope and a compass triaxial was tested together with the data transmission system to check the possibility of carrying out a pre-processing of data aboard the buoy and limit the number of bytes to send.

In particular, it is addressed the problem of filtration of signals acquired through the development of software that implements a Kalman filter, which, as is known, is an efficient recursive algorithm which evaluates the state of a dynamic system from a series of measures subject to noise.

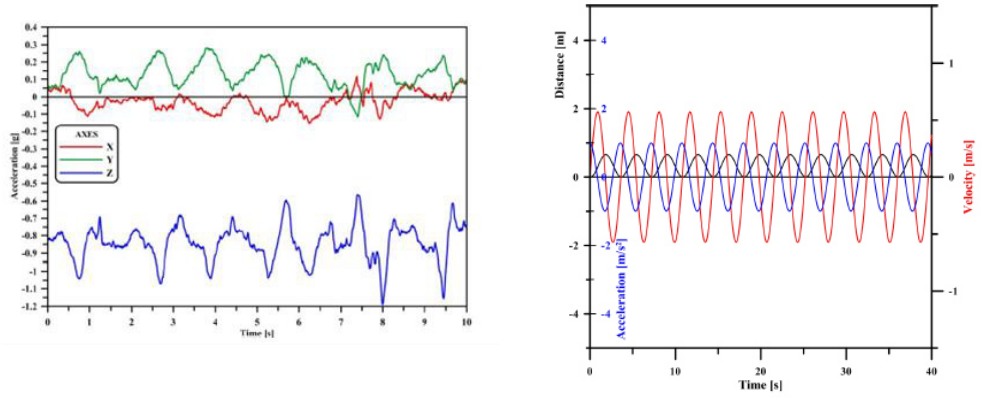

Figure 2.5 Example of transmission of filtered data in horizontal and vertical motion

Figure 2.5 shows an example of transmission of filtered dataduring a test of displacement in the horizontal of the sensor subject to slight shifts in the vertical direction. Note the presence of constant vertical component directed downwards and equal to 1 g.

The acquisition interval is 0.01 seconds, equal to 100 samples / second.

Figure xx shows an example of vertical motion more energetic, associated with a rotation of the sensor in the horizontal plane. It's shows the excellent sensitivity of the module and the effectiveness of the filtering carried out by software. Also in this example, the acquisition interval was of 0.01 seconds. The acceleration data may be further processed and used to calculate the

displacements of the module. In figure2.6 is shown a test carried out by placing the module on an object in vibration, free to move on the horizontal plane.

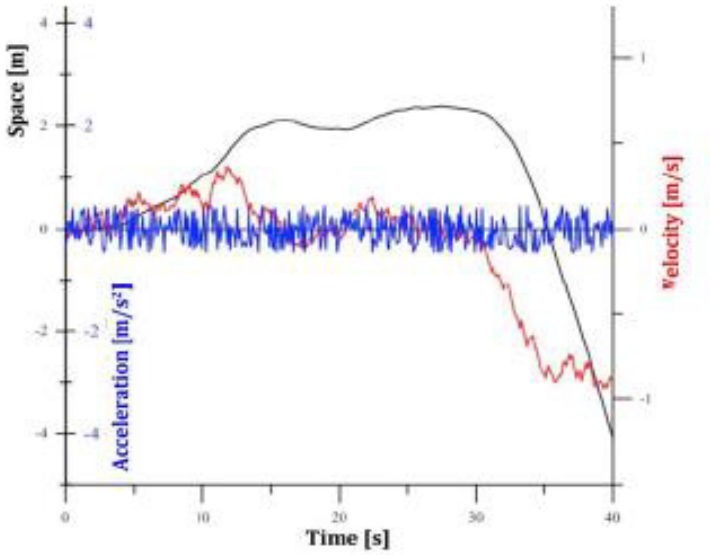

Figure 2.6 Example of test in vibration motion

As for transmission data, the buoy has Sagem module, equipped with a SIM (Subscriber Identity Module) that commonly used in every mobile device has the ability to transmit data either via SMS or via connection package.

The first method is been used when you want to install a system that alerts the user directly in the event of a possible malfunction of the buoy (opening or tampering, detachment from the mooring, low battery, etc ...). The connection to the package instead is working to transmit data from the sensors useful for the study in question. The data, after having been compressed by the method above analyzed, should be sent to an Internet server in which they are collected and stored. Finally, a specific software allows you to read the data in raw form and turn them into graphs and numerical values. The figures below show descriptive images of the software used.

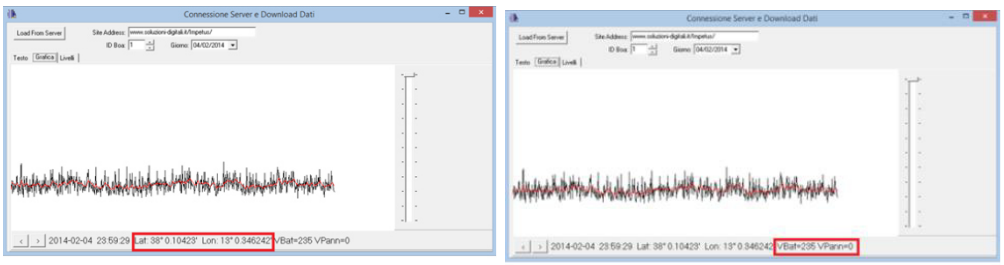

Figure 2.7 Images of Software IMPETUS

2.2 *Wave monitoring: Algorithm Implementation*

In the previous paragraph we emphasize the innovative aspects of buoy realized. In this paragraph we introduce the algorithm used to obtain values of wave height.

This section explains on the algorithm we use to approximate vertical acceleration and detect wave periods, giving us wave height and frequency.

The accelerometer sensor gives us measurement real time of acceleration that must be double integrated to get height. In fact, with the first integration we calculate *velocity* while the second integration allows us to obtain the displacement. Some buoy's sensor using a particular software that does double integration using discrete Fourier Transform[13] (eq. 2.1)

$$\boldsymbol{\varsigma(t) = \frac{a_0}{2} + \sum_{n=1}^{\infty}(a_n \cos 2\pi nft + b_n \sin 2\pi nft)} \qquad (2.1)$$

Another approach to measure wave height is the knowledge of vertical movement of the buoy. One way of determining the vertical movement would be to keep the accelerometer horizontal with gimbals or similar, and use only z-axis readings.

A second way to determine the vertical movement is to measure acceleration along all 3 axes and compensate these readings for rotational movement. That would require a (digital) gyroscope in addition to the accelerometer. A big disadvantage is that adding more measurements means adding more errors.

A third solution is to use only one accelerometer and turn the nuisance of gravity influencing the accelerometer into something useful, as is explained in the below equations.

As we are not aware of the accelerometer's orientation, we calculate the acceleration magnitude ($amag$) from the measurements on all three axes (ax, ay and az), defined as[14]:

$$\boldsymbol{a_{mag} = \sqrt{a_x^2 + a_y^2 + a_z^2}} \qquad (2.2)$$

The vertical distance covered between the trough and crest equals the wave height. This vertical distance is caused by the vertical component of a_O, from now on referred to as a_{Oz} (not to be confused with a_z, the accelerometer z-axis measurement). Now this is where gravity proves to be useful. For relatively

small accelerations, because of gravity, the acceleration magnitude is hardly affected by acceleration perpendicular to gravity, while it is fully affected by acceleration parallel to gravity. Hence the acceleration magnitude can be used to approximate a_{Oz} by subtracting gravity from it. We define the approximated (vertical) acceleration (a_A) as

$$\boldsymbol{a_A = a_{mag} - g} \tag{2.3}$$

The approximation of aOz by aA is visualised in Figure 2.8

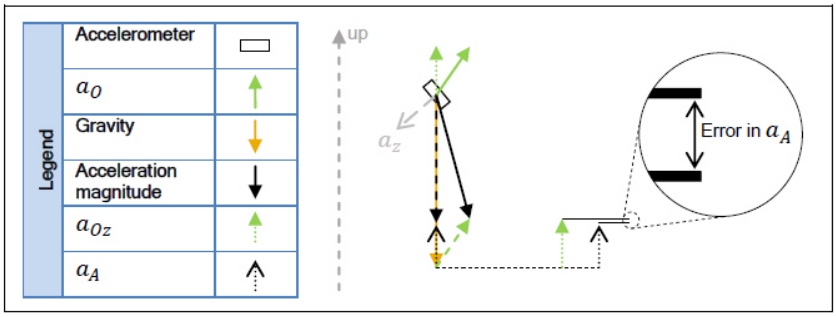

Figure 2.8 Approximated acceleration vs the vertical component of a_0

So we identify a general method to calculate wave height[14]:

1. Calculting a_A (eq. 2.3) ;
2. We detect each local maximum and local minimum for aA to determine when we are passing a crest or trough;
3. In between a crest and trough, we compute the vertical distance covered. After detecting a crest, to keep processing and memory requirements low, each sample is processed immediately into a distance by adding a_A to speed (v_A) and this speed to distance (d_A);
4. Compensating the approximation error with statistical formula

In our case we adopt procedure explained in second point namely the determination of vertical height is obtained by the knowledge of component Z of acceleration.

CHAPTER III

Wave Energy: State of the Art of Technology

Wave energy devices need large investment of money throughout the process of producing a valid device: overcoming successive steps that can lead them to validate their concepts, build and test prototypes and optimise parameters with the final outcome of a successful product that can be deployed in arrays and sold.

The current panorama with many concepts being patented in every country can be confusing; some technologies have the potential of being successful, whereas many others will not pass the concept phase. Therefore, it is important to assess the real degree of advancement of these technologies, to calibrate the state of the industry and that both private investors and public bodies have some criteria when it comes to awarding funds[15].

There are several steps that developers must progress through on the journey between initial concept and commercial product.

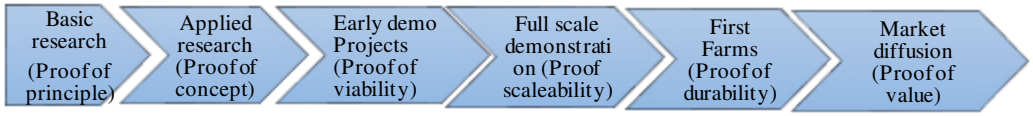

Figure 3.1 The Technology Journey[15]

It would be pertinent to define here the term "Technology Readiness Level". A number of steps have been set in place to pave the way for a staged growth of a new wave energy concept or design.

Technology development, from first concept to commercial operation, is expected to progress through defined stages. In order to track the progress of ocean energy devices from concept through to final product a table of Technology Readiness Levels (TRL) has been produced.

TRL	*Description*	*Indicative Ocean Energy Device*
1	Basic principles observed and reported	**Discovery/Concept Definition;** Scientific research begins to be translated into applied research and development where basic principles are observed and reported. Technology concept and application are formulated and investigated through analytic studies and in-depth investigations of principal design considerations. This stage is characterised by paper studies, concept exploration, and planning. **Scale Guide** 1:25 – 1:100 (Small Scale)
2	Technology concept and/or application formulated	

3	Analytical and experimental critical function and/or characteristic proof of concept	**Early Stage Development**, Design and Engineering;Active research is initiated, including engineering studies and laboratory studies to physically validate analytical predictions of separate elements of the technology. **Scale Guide** 1:25 – 1:100 (Small Scale)
4	Component and/or partial system validation in a laboratory environment	**Proof of Concept**; Early stage proof-of-concept system or component development, testing and concept validation. Critical technology elements are developed and tested in a laboratory environment, and computer simulation of the device will be carried out. **Scale Guide** 1:10 – 1:25 (Medium Scale)
5	Component and/or partial system val idation in a relevant environment	**Technology Laboratory Demonstration**; Basic technological components are fabricated at a scale relevant to full scale and integrated to establish and verify subsystem and system level functionality and preparation for testing in a simulated environment. Subsystem level interfacing testing demonstrated at model scale. **Scale Guide**: 1:2 – 1:5 (Large Scale)
6	System/subsystem model validation in a relevant environment	**System Integration and System Technology Laboratory Demonstration;** System level interfacing/integration testing demonstrated at model or prototype scale. At this level, representative model or prototype system at a scale relevant to full scale, which is beyond that of TRL 5, is tested in a relevant environment, such as a test facility capable of producing simulated waves/currents and other operational conditions, while monitoring device response and performance. Furthermore, the devices foundation concept shall be incorporated and demonstrated. This stage represents a major step up in a technology's demonstrated readiness and risk mitigation and is the stage leading to open water testing. **Scale Guide**: 1:2 – 1:5 (Large Scale)
7	System prototype demonstration in an operational environment	**Open Water System Testing and Demonstration**; Testing may be initially performed in water at a relatively benign location, with the expectation that testing then be performed in a fully exposed, open water environment, where representative operating environments can be experienced. The final foundation/mooring design shall be incorporated into testing at this stage. **Scale Guide**: 1:1 – 1:3 (Large Scale)
8	Actual system completed and service qualified through test and demonstration	**Open Water System Operation;** The prototype in its final form (at or near full scale) is to be tested, and qualified in an open water environment under all expected operating conditions to demonstrate readiness for commercial deployment in a demonstration project. Testing should include extreme conditions. Production of

		GWh scale electricity, operating continuously for at least one year. **Scale Guide**: 1:1 – 1:2 (Pre Commercial Demonstrator)
9	Actual system proven through successful mission operation	**Commercial Scale Production / Operation**; Final commercial unit, economic deploymentwhen the technology is ready for mass production and has proven to operate as designed for several years. Array scale projects. **Scale Guide**: 1:1 (Full Scale1)

Table 3-1 Technology Readiness Levels*[15]*

The wave energy sector is reaching a significant milestone in the development of the industry, with positive steps towards commercial viability being taken.

The more advanced device developers are now progressing beyond single unit demonstration devices and are proceeding to array development and multi-megawatt projects. The backing of major utility companies is now manifesting itself through partnerships within the development process, unlocking further investment and, in some cases, international co-operation.

In general, we can find five principle requirements of WECs (Wave Energy Converters)[16]:

- must be " storm proof": that have to resist harsh weather conditions;
- don't have environmental impact to surrounding ecosystem;
- should not have an excessive weight;
- should require reduced maintenance;
- devices must be tested several times.

The next sections describe the classification of devices:

- by position;
- by principle;
- by size and orientation.

3.1 Classification by position

This first sorting is based on the position of devices in relation to the costline. The first criterion is the distance of the wave energy converter to the shore: this leaves onshore, nearshore and offshore devices.

As for *onshore devices*[17], lie on the bottom or on very shallow waters, commonly integrated into coastal structures, such as breakwaters or rocky cliffs. Their advantages are easy installation, absence of moorings, reduced cost of maintenance and short distance to the shore and the grid. On the other hand, they

present location constraints, less energy, and high visual impact. These devices have a less power to extract energy by wave respect offshore devices.

As regards *nearshore device* or second generation, it is located at depths between 20 and 30 m and relatively close to the shore. This depth range is suitable for big devices mounted on the bottom by gravity or floating.

Those that are bottom mounted can also use the whole movement of the wave, which is impossible for floating devices. Major disadvantages are high unit cost and extreme loads experienced by the devices.

In the end we distinguish *offshore device*, offshore or third generation devices are usually floating structures, but can also be submerged at depths of more than 40 m.

They are the most promising type of device of them all, because at those depths, losses due to friction with the bottom are small, so they are installed where the highest energy flow is. Reliability and survival are the biggest challenges this kind of devices are facing.

3.2 Classification by principle

In this case we can examine three main classes: Overtopping Device, Oscillating Water Column, Wave Activated Bodies and Buoyant.

In the *overtopping device* waves run up on a structure and raise their potential energy, kinetic energy or both of them. Overtopping devices force water to go over their structure, while impact devices make water break against an articulated body that transfers the energy[18]. Onshore overtopping devices exist but they present high building cost and technical difficulties, and hence offshore ones are more common.

These devices can have a water storage reservoir. Water from waves is temporarily stored in a reservoir above sea level. The water again leaves the reservoir through low pressure hydraulic turbines to produce the electrical power.

Oscillating Water Column represent the most prevalent category. it is a chamber open on its bottom side under sea level, in which the alternant movement of the waves makes the water level go up and down and move the air kept in the chamber. When the crest of the wave approaches the chamber, the air is compressed inside the chamber and moves a turbine. In the same way,

when the wave withdraws, the air flows into the chamber and moves the turbine again.

A special design of the turbine is required so that it can cope with airflows in both directions, even though this involves a lower performance than a regular turbine. Even though most of these are located onshore, there are also devices that use this principle in near shore and offshore water depths. This system is characterised by none of its moving elements being in contact with water.

Wave Activated Bodies are devices where the waves active different movements of relative oscillating among modular components of the system or among the parts of system and fixed reference.The mainly movements that are used to extract energy are: heave, roll and pitch movements. In general, however, the possibility of a segment to interact with the nearby element gives rise to an autonomous system, avoiding rigidly each active part of the device to the bottom of sea.

In conclusion we find *buoyant system* [19]that these are devices formed by a floating body that is moved by waves. Energy is extracted in different ways by using the alternant movement of this element. The movement can be vertical, horizontal, around an axis or a combination of the previous. The movement can be absolute between the floating body and a fixed element or relative between two moving parts. Fixed reference devices are more common, even though the moorings of this kind of devices bear important forces and are sensitive to tides, so their installation and O&M is not simple.

3.3 Classification by size and orientation

The third type of classification is based on the capacity of devices to exploit wave energy in function of the ability to intercept the wave. We study: point absorbers, attenuator and terminators.

Point Absorbers: they are small structures in relation to the wavelength of the incoming waves and they are non-directional, as they can receive incoming waves from any incident angle They are usually cylinders, so they have radial symmetry and are indifferent to the direction of the waves.

A remarkable characteristic is that they can concentrate wave energy around them and thus use a larger wave front than their own diameter. Ideally, in a monochromatic wave and resonance situation, their effective wave ront can be up to L/2p, being L the wavelength.

Attenuator is an example of energy converters that use the energy within oncoming waves to induce an oscillatory motion between two (or more) adjacent structural components. The motion can be resisted by hydraulic rams which pump high pressure hydraulic fluid through a motor, or by a direct drive power take off system, to generate electricity.

Attenuator can be surface floating or fully submerged, the former is most common. Attenuators tend to yaw automatically to face the predominant wave direction

Terminator are placed in parallel to the wave front. Considering a wave that strikes perpendicular to the coast, the device is placed parallel to the coastline.

These devices are called terminator because they are able to provide a significant obstacle to the propagation of the waves, going to capture and reflect wave energy. They are typically placed on shore or coast, but have been designed devices which are also floating installations for off - shore.

CHAPTER IV

Generators for Wave Energy Applications

Introduction

As discussed in the previous chapter, the classification of wave energy converter is based on the internal characteristic of its device (position in relation of the cost line or the arrangements of wave power conversion) or the generator used to exploit wave energy in electrical. The choice of the better generator is fundamental phase of the design of WECs.

My research has been focused on a simplification of processes, i.e., replacing systems employing intermediate hydraulics or pneumatics with direct-drive approaches to allow generators to respond directly to the movement of the sea. The term "direct" drive describes the direct coupling of the buoy's velocity and force to the generator without the use of hydraulic fluid or air.[20]

The aim of this chapter is to describe the procedures adopted for the choice of type of electric generator to be used for the realization of the converter. In particular, the analysis is made using a specific FEM (finite element method) software that is necessary to could be a comparison among different electrical structure.

The research was based on the design, modelling and optimization of: A Ferrite Tubular Linear Permanent Magnet Generator (FTLPMG), A Transverse Flux Machine and a Linear Permanent Magnet Generator (LPM).

4.1 A Ferrite Tubular Linear Permanent Magnet Generator (FTLPMG)

A tubular linear induction electric generator can be ideally realized by winding around an axis parallel to the direction of motion of a monolateral linear motor induction.

The shot agent on the mobile part of a TLG is generated to the electromagnetic interaction between the magnetic field oriented radially translating[21] obtained by supplying the inductor with a tern of symmetrical sinusoidal voltages out of phase by 120 °, in time between them, and the currents circulating in are produced by the induced electromotive forces induced by the same magnetic field.

The tubular structure has some advantages compared to the linear device as the absence of effects at the edges and the vanishing of the resultant of the forces normal to the direction of motion.

In general, a tubular generator can present a circular or polygonal section, so it's usually defined as cylindrical generator.

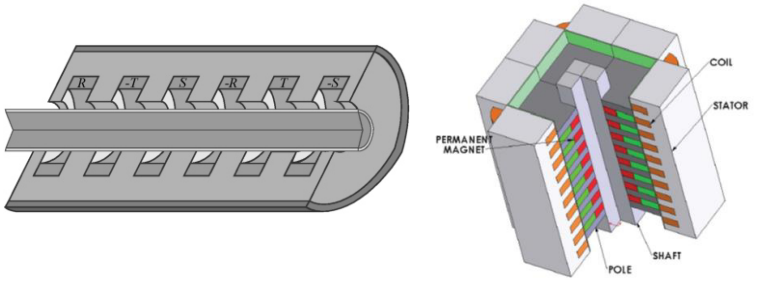

Figure 4.1 Example of square and tubular generator

More general considerations can be made as to length of the inductor and the stator and the fact that they can function as either fixed or mobile machine. The magnetic structure is made by laminations normally bundled in four cores.

The lamination is necessary to reduce the magnitude of the eddy currents that are caused[22] by the radial magnetic field in the translating direction of the axis. It can be longitudinal or transverse to the direction of motion.

In the first case the main disadvantage is:

- The difficulty to align accurately the laminations of each core (given their length).

In the second possibility:

- The reluctance of the magnetic circuit due to the significant total thickness of isolation of the laminations.

Translator can be realized to cylindrical foil or circular rings. The first example is constituted by a sheet-iron or a copper or aluminium foil and it is supported by a sleeve translating massive iron solidly to the foil or fixed with respect to this.

The shifter rings could be constituted by a series of copper rings mounted on an iron support that is laminated transversely to the direction of the axis, or by iron rings alternating with solid copper rings.

4.1.1 Design of a Ferrite PM Tubular Linear Generator

Several solutions have been considered to build both the translator and the stator of a designed ferrite PM Tubular Linear Generator [23]. In particular, the translator can be arranged with magnets in conventional or in Halbach configuration and with a different assembling system.

One solution is presented in fig 4.2 in which both the magnets (in Halbach configuration) and the associated iron spacers are cylindrical shaped and contained in nonmagnetic tube (orange).

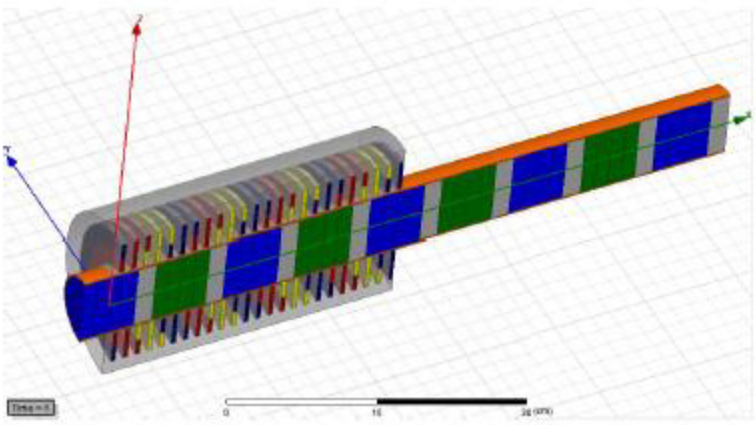

Figure 4.2 Axially magnetized tubular linear PM Generator. Magnets contain in a nonmagnetic tube (orange)

Another solution (fig. 4.3) uses annular shaped magnets in Halbach configuration; in this case the magnets and the iron spacers are supported by a non-ferromagnetic (aluminum) rod (grey).

The last solution offers several advantages over the topology shown in Fig. 1. First, it eliminates the need for a nonmagnetic tube (orange) to contain the magnets and spacers, so that the effective magnetic air gap between the stator and armature is reduced.[24] It also reduces the volume and the moving mass of permanent magnetic material, thereby increasing the attainable speed.

Furthermore, in order to inhibit corrosion and/or to satisfy technical standards, the surface of both the machine stator and translator can be covered with relatively thin protective coating.

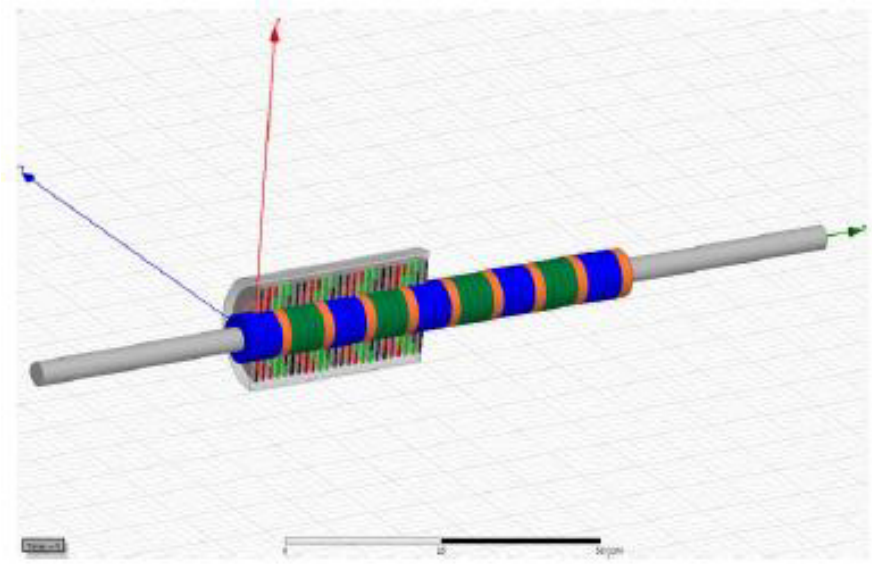

Figure 4.3 Axially magnetized tubular linear PM Generator. Magnets supported by a non-ferromagnetic (aluminium) rod (grey)

Even the stator can be designed, built and assembled in different ways. The stator iron core laminations can be either longitudinal or transversal with respect to the direction of motion.

In the case of transversal lamination, the magnetic core of the inductor is composed of either one block in which each sheet has a crown shape or more block in which each sheet has the shape of a crown sector.

The main disadvantage of longitudinal lamination is the difficulty to align the sheets of each core with precision, because of their length. The main disadvantage of transversal lamination is the thickness between the sheets which increases the reluctance of the magnetic circuit[25].

The Stator core lamination is transversal to the direction of motion and the sheets are 0.5 mm thick, sheared in two different shapes. With the repeated alternation of 10 sheets of the kind shown in fig. 4.4a and 16 sheets of the kind shown in fig. 4.4b, it was possible to obtain the alternation of respectively slots and teeth. The machine has a total of 24 slots.

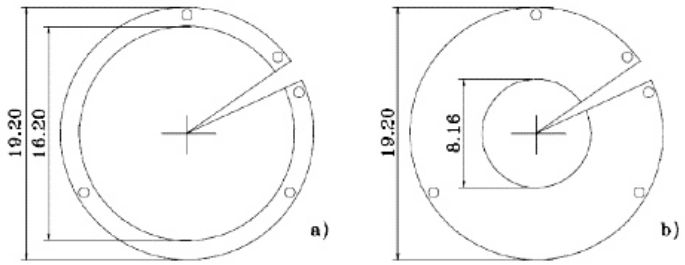

Figure 4.4 Stator magnetic sheets having different inner diameters

The stator winding is made up of 48 concentric cylindrical coils, located inside the 24 slots (2 concentric coils for each slot), as shown in fig 4.5.

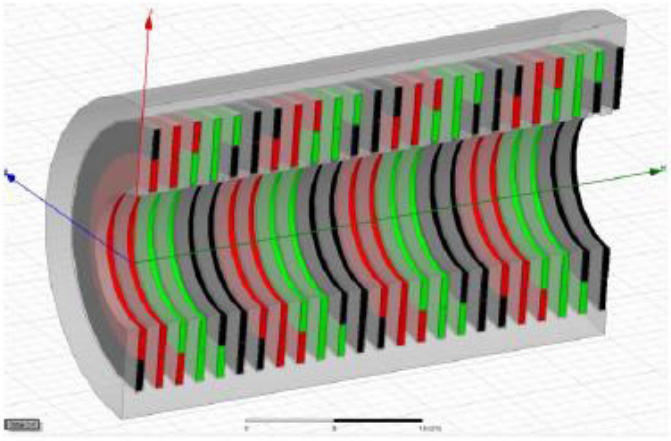

Figure 4.5 Stator core and windings

Table 4.1 reports the most relevant electrical and mechanical characteristics of the stator.

Number of coils	48
Number of turns for each coil	42
Length [m]	0.32
Number of slots	24
Slot depth [m]	0.04
Air-gap [mm]	0.8
Resistance at 20°C [Ω]	21.95
Linear weight	7

Table 4.1 Electrical Parametes of the stator

The translator of the tubular generator studied consists of iron core rings fixed on an aluminum shaft alternated with permanent magnet rings magnetized in radial directions, as shown in fig. 4.6.

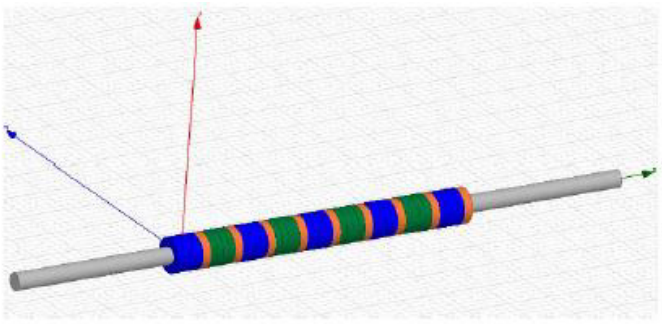

Figure 4.6 Iron core rings fixed on shaft alternated with 4PM

The 36 permanent magnets (green and blue) have alternated magnetization as shown in fig. 4.7. Hence, strong magnetic flux is generated outside the moving armature.

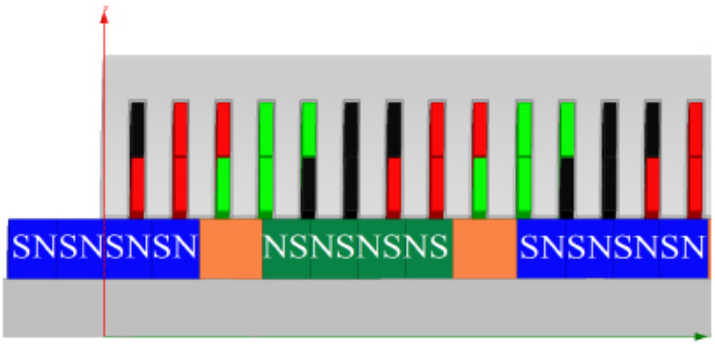

Figure 4.7 Permanent magnet rings with alternated magnetization

Table 4.2 reports the technical information of the magnets [20]; the 9 iron core rings (orange) have 80-40 mm diameters and a height of 20 mm. The alumina shaft (grey) is 148 cm long and has a diameter of 40 mm.

Outer diameter [mm]	80
Inner diameter [mm]	40
Height [mm]	15
Direction of magnetization	Axial (parallel to height)
Material	Ferrite
Type of coating	No coating
Strenght [N]	Approx. 93,2
Weight [g]	274,26
Manufacturing method	Sintered
Magnetization [grade]	Y35
Max working temperature [°C]	250°C (poss.lower)
Curie temperature [°C]	450°C
Residual magnetism Br [T]	0.4-0.41 T
Coercive field strength bHc [kA/m]	175-195
Coercive field strength iHc [kA/m]	180-200
Energy product (BxH)max [kJ/m^3]	30.0-32.0

Table 4.2 Technical information of the magnets

The stator and the translator of the FTLPMG are shown in fig.4.8.

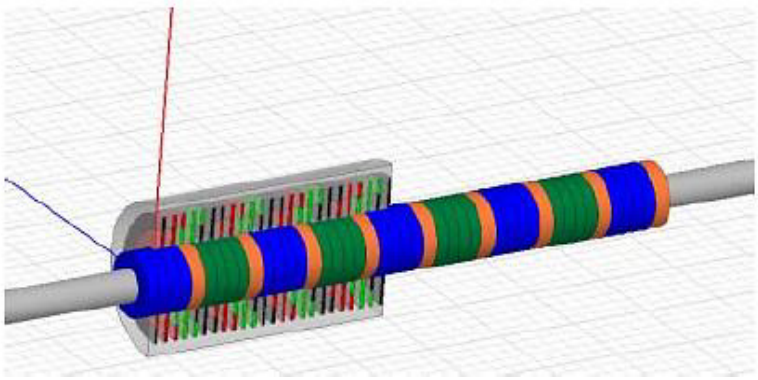

Figure 4.8 Stator and translator of the ferrite PM generator

4.1.2 Magnetic circuit analysis and FEM simulation

The first step in the analysis and design of a permanent magnet linear generator is the determination of the airgap field produced by the magnets. Whereas the fields may be precisely determined by finite-element analysis, a magnetic circuit approach yields approximate results acceptable for practical purposes.[25]

Thus, neglecting saturation and leakage, we have:

$$\boldsymbol{B_m = B_g = \mu_0 \cdot H_g} \tag{4.1}$$

Neglecting the reluctance of the core and the iron spacers, Ampere's law yields:

$$\boldsymbol{k_S H_g (2g) + H_m h_m = 0} \tag{4.2}$$

Assuming rare-earth magnets, their demagnetization characteristic can be written:

$$\boldsymbol{B_m = B_r + \mu_{rc} H_m} \tag{4.3}$$

The various symbols in equations above mentioned are defined as follows:

- B_m=PM operation flux density, T

- H_m=PM operation field intensity, A/m
- g = 1mm, Airgap
- ks = 1,1, Saturation factor
- B_r = 0,4T, Residual flux density [given from table II]
- $\mu_0 = 4\pi * 10^{-7}$ H/m, Vacuum permeability
- μ_{rc}= 1,01 μ_0 ,PM recoil permeability
- B_g = Airgap flux density, T
- H_g = Airgap magnet field intensity, A/m
- h_m= 6cm, four magnets thickness

Combining the equations, it's possible to obtain:

$$\boldsymbol{B_m = B_r \left[1 + \frac{\mu_{rc}}{\mu_0}\left(\frac{2k_S g}{h_m}\right)\right]^{-1} = 0.368T} \quad (4.4)$$

Having determined the maximum airgap flux density, we can obtain the total induced emf peak, E_p

$$\boldsymbol{E_p = \sqrt{2} \cdot 4{,}44 f B_m A_S N 2p = 20{,}3\ V} \quad (4.5)$$

Where:

- p = 2 number of pole pairs
- τ=0,08 m, pole pitch
- ν= 0,4 m/s, speed of the translator
- $f = \frac{\nu}{2\tau}$= 2,5Hz , frequency of motion
- r_s = 0,04m, radius of the iron spacer
- l_s = 0,02m, length of the iron spacer
- $A_S = 2\pi r_S l_S = 0.005\ m^2$,surface area of the iron spacer
- N_i= 42, total number of turns of the inner coils for one pole
- N_0= 42, total number of turns of the outer coils for one pole
- N_c= 2, total number of coils for one pole
- $N = (N_i + N_0) \cdot N_C = (42 + 42) \cdot 2 = 168$, total number of turns for one pole

The aim of the second part of the study is based on the FEM simulation of linear generator. For this

For this purpose, the ANSYS-Maxwell software was used; Maxwell uses the accurate finite element method to solve static, frequency-domain, and time varying electromagnetic and electric fields. Maxwell Transient is able to

evaluate interactions between transient electromagnetic fields and mechanical motion of objects. Derived quantities such as forces, induced voltage, flux linkage and core loss may be calculated from these basic field quantities and can be obtained by creating a[26] 2D report to find the parameter values as a function of time.

Three different simulations were carried out, with no electric load, and with two electric loads. In every simulation, the translator moves with a 0.4 m/s constant speed from his initial position (fig. 4.9) and completes his stroke in 1s (fig. 10). In order to simulate the no load and the load conditions the circuit editor, provided also by Ansys was used. The results are reported below

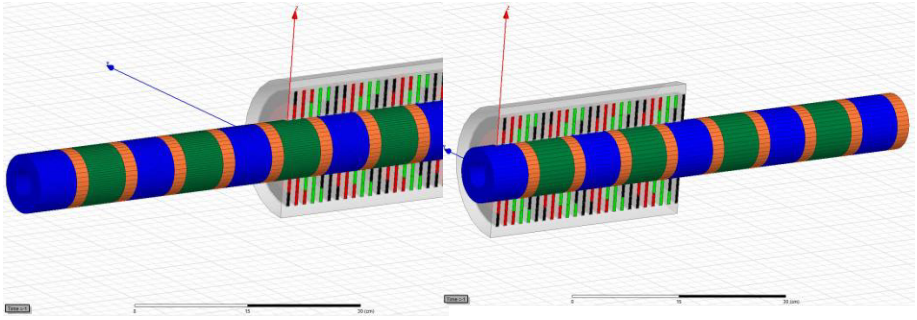

Figure 4.9 Inizial and final position of the translator

The computed induced voltage and the flux linkage in the winding for the no-load simulation are shown in Fig. 4.10 and Fig.4.11

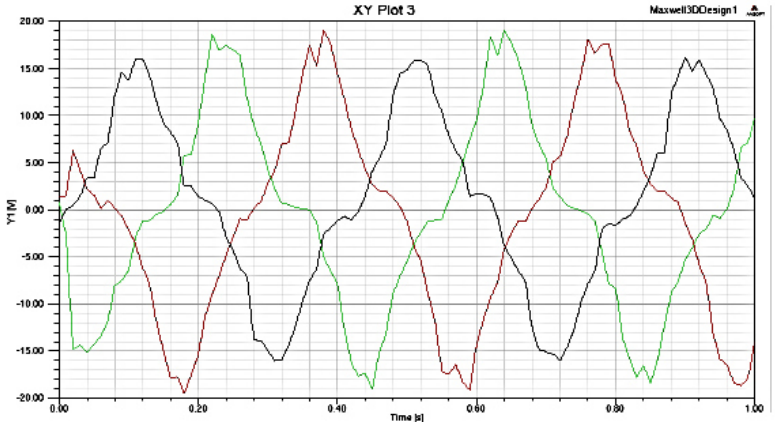

Figure 4.10 Induced voltages in the windings (no load condition)

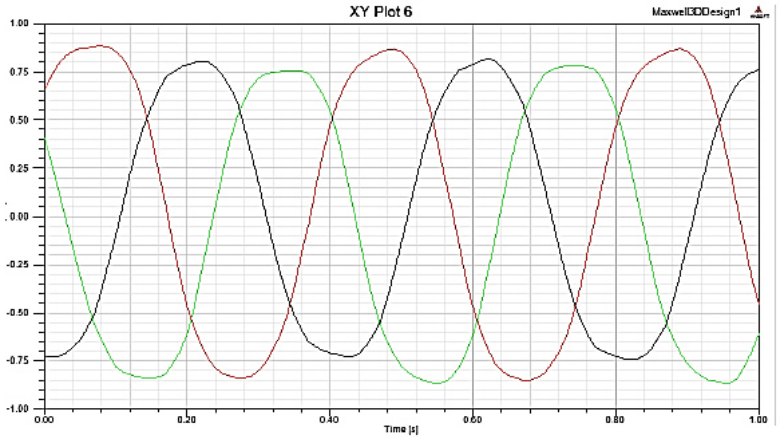

Figure 4.11 Flux linkages in the windings (no load condition)

The first electric load condition is obtained with a three-phase balanced resistive load of 10 ohms. The induced voltages and the currents in the windings are shown in fig. 4.12 and fig. 4.13.

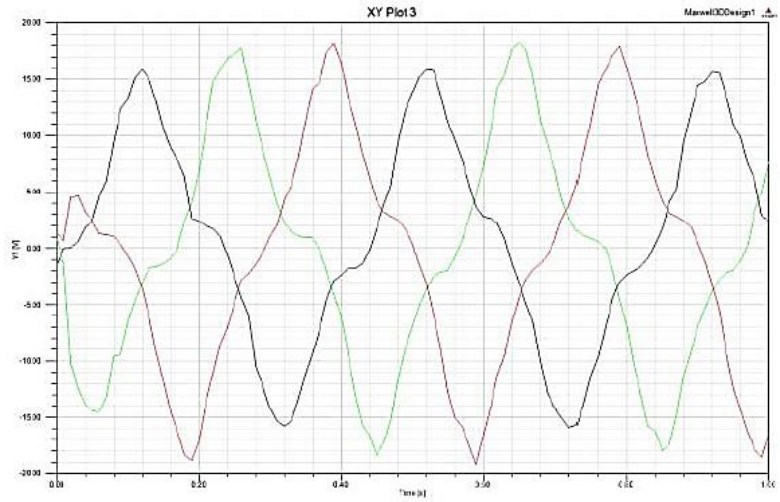

Figure 4.12 Induced voltages in the windings (ohmic load)

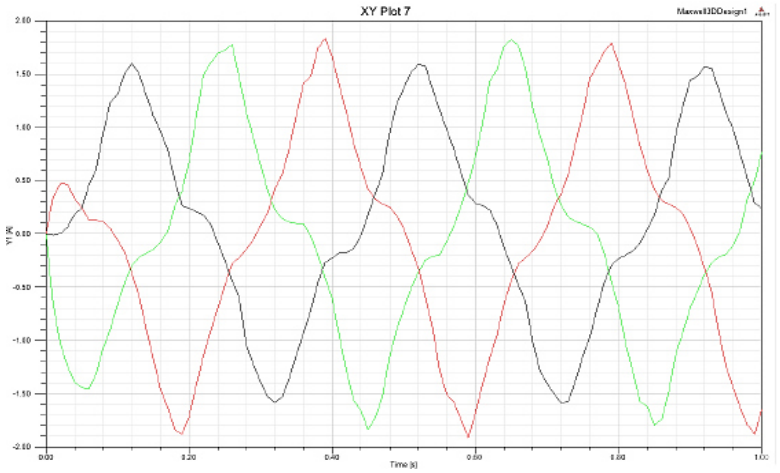

Figure 4.13 Currents in the windings (ohmic load)

The second load condition is obtained with a three-phase balanced ohmic-inductive load; the resistances are 10 ohms and the inductances are 0.65 mH. The induced voltages and the currents in the windings are shown in fig. 4.14 and fig. 4.15. This simulation is important since the majority of the electric loads are of this nature.

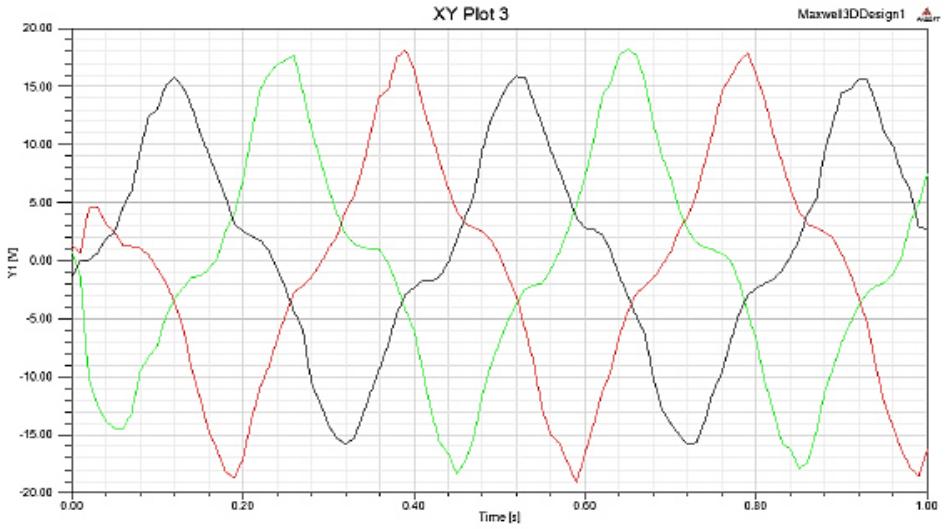

Figure 4.14 Induced voltages in the windings (ohmic-inductive load).

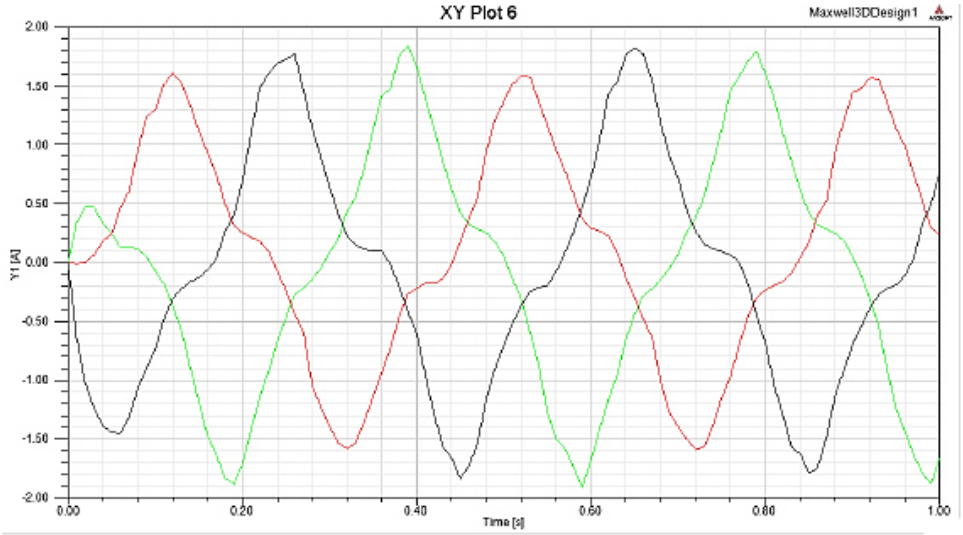

Figure 4.15 Currents in the windings (ohmic-inductive load)

The magnetic induction B in the machine is also reported in three different instances. The first instant is at 0s, when the translator is at the initial position (fig.4.16). It can be noticed that the magnetic field is provided by the translator and comes out from the iron spacers

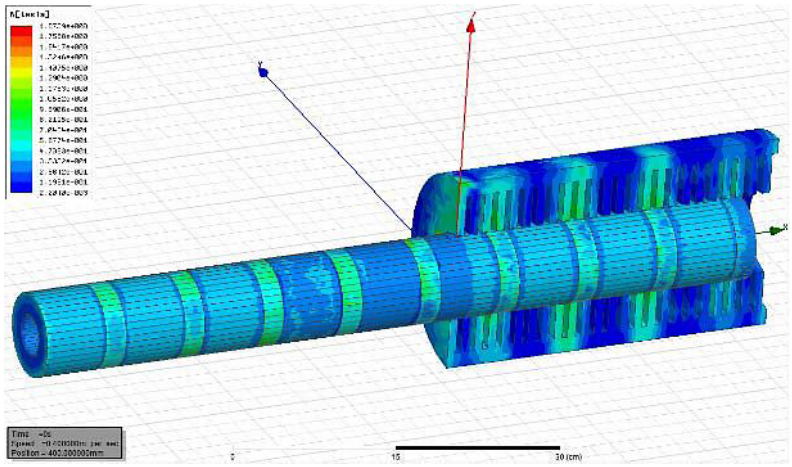

Figure 4.16 Stator magnet induction B at 0s.

The second instant is at 0.5s, when the translator reaches his central position (fig. 4.17).

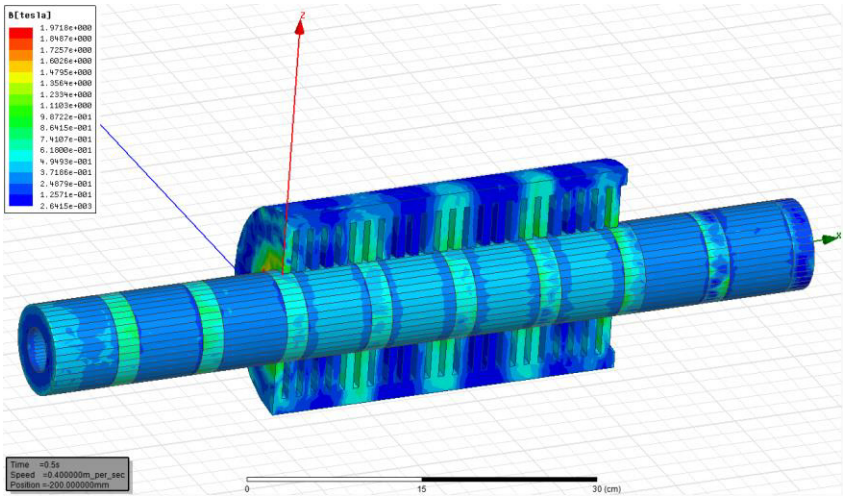

Figure 4.17 Stator magnet induction B at 0.5 s.

The third instant is at 1s, when the translator reaches his final position.

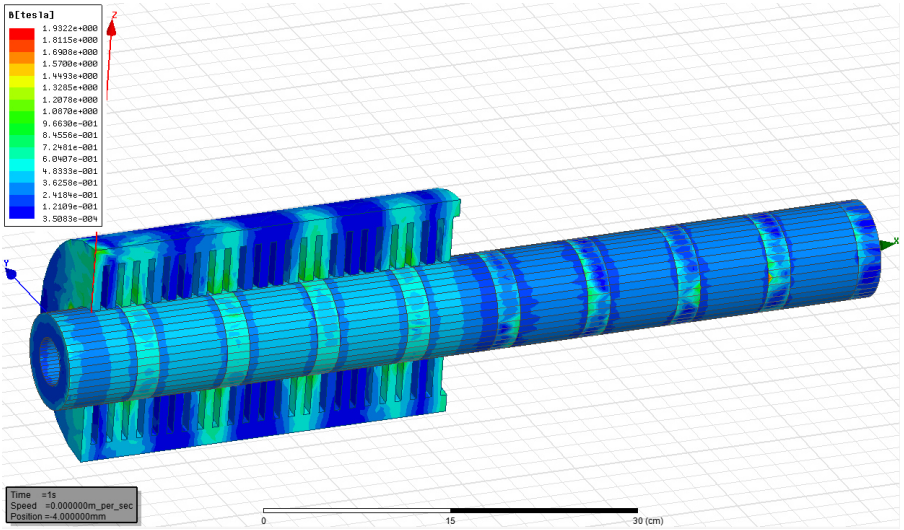

Figure 4.18 Stator magnet induction B at 1 s.

The machine was designed based on the simulations and the magnetic circuit analysis. The purpose of this study is to create an economic machine easy to make and assemble, that requires low maintenance for both the stator and the translator.

The simulation results confirm that this simple and economic device can be employed for the generation of electric energy from sea waves.

4.2 Design of a transverse flux machine for power generation from seawaves

The transverse flux technology is over one hundred years old and was first described by W. M. Morday, who applied for the first patent in 1895. Today several universities are researching this field.

In this section, we investigate the possibility to use a transverse flux linear generator (TFG)[27] because transverse flux technology presents the highest force density per volume index among the iron based electrical machines.

The stator of a machine with transverse flow is constituted by a series of magnetic cores in the shape of "C", in which the flow circulates mainly along lines perpendicular to the direction of motion: the conductors, therefore, must develop in the direction parallel to the movement of the translator.

The shifter can be constituted by permanent magnets mounted on a structure made of iron or non-ferromagnetic material, depending on the paths that have been established during the design for the circulation of the flow. The system therefore requires no excitation coils, and its operation as a generator is obtained by means of the magnetic cores will have alternate streams connected to alternating orientation of the magnets.[28]

The advantages of TFG topology [29]against the classical longitudinal concept are:(a) the magnetomotive force per pole is independent from the total pole numbers; (b) the magnetic flux geometry and the coil section are independent design parameters; (c) armature coils geometry is simple; and (d) phases are magnetically decoupled.

One of the main disadvantages of the machines TFM is given by the cost of production and realization: : the shape of these machines is responsible for a number of inconveniences; these machines must be laminated in the transverse

direction, which can create problems both of constructive type (sometimes difficult assembly) that of the magnetic type (additional losses for the flows which are closed again on the side face of the sheet).

4.2.1 Principle of Operation for the Generation of Electrical Energy from Seawaves

The moving part of the generator is driven from the sea waves and induces and emf on the winding mounted on the armature. The motion of the slider can be modelled as follows:[30]

$$\rho g S(y_s - y_g) - mg - kib - k_s(y_s - y_0) = m\frac{\partial^2 y_g}{\partial t^2} \quad (4.6)$$

$$e(t) = iR_i + L\frac{\partial i}{\partial t} + iR \quad (4.7)$$

$$e(t) = -\frac{\partial \varphi(t)}{\partial t} \quad (4.8)$$

where g is the acceleration gravity, q is the water density, *S* is the area of the buoyant, y_s is the vertical coordinate describing the sea level, y_g is the vertical coordinate describing the position of the slider, k_s is the spring constant, *m* is the total mass of the translator and of the buoyant, *k* is the electromagnetic constant, *i* the current B the magnetic induction, *e(t)* is the induced electromotive force (emf), R_i is the internal resistance of the machine, *L* is the inductance of the machine, *R* is the resistance of the external load, *f* is the linked flux, and y_0 is the rest position.[31]

The first equation models the dynamic behaviour of the device. On the left hand side there are the forces acting on the slider and on the right hand side there is the acceleration of the slider. No hydraulic friction is considered.

The second equation describes in terms of lumped parameters the generator connected to a resistive load. The third equation describes the emf.

In order to optimize the generator for the conversion of energy contained in seawaves, a detailed knowledge of the characteristics of the seawaves that will interact with the generator is needed. These characteristics strongly depend on geographical site as a result in order to acquire this knowledge a measurement system has been built and placed in the area of installation of the generator.

The main problem in order to perform the optimization is to model realistically the motion of the sea. However, the main features of seawave (maximum vertical speed and wave height and wave period) have been used for the preliminary design.

In order to have a usable numerical model, it has been assumed that the waves hitting the generator consisted of purely sinusoidal waves but each waves had different amplitude and period in comparison with the others.

As a result, in the proposed approach, each seawave has been modelled as follows:

$$y_s = Asin(\omega t) + y_0 \tag{4.9}$$

where A is the amplitude and x is the frequency. The use of such a driving force does not allow to use an analytical approach to the optimization, but a numerical approach which includes the main stochastic feature of the phenomenon must be followed.

4.2.2 Design of a Transverse Flux Generator

The seawave characteristics presented clearly show that the energy in seawaves is mostly "contained" in terms of high force density and low speed.

This form of energy is not very usual for electromagnetic devices that are more aimed to convert energy from relatively high speed and less intense force. As a result, the direct conversion of seawaves energy into electrical energy is a difficult task, which needs electromagnetic converters specifically conceived for this purpose.[27]

The main characteristic that such a converter should have is the capability to handle high force density. From this point of view, the most suitable electric machine able to deal with high density force is a transverse flux linear machine and as a result in this paper, we propose to use a Double Sided Transverse Flux Linear Synchronous Generator as the electromagnetic converter to be used to convert seawave energy into electric energy[32].

It is shown in Fig. 4.19. This kind of machine has been proposed recently as motor. Fig.4.20 shows the structure of the three phase unit and its parameter specifications. The machine consists of a moving armature and a standing excitation. The armature is composed of four coils and an iron core. The two coils on one side of the armature unit are wound in the opposite direction of the coils wound on the other side and are connected in series.

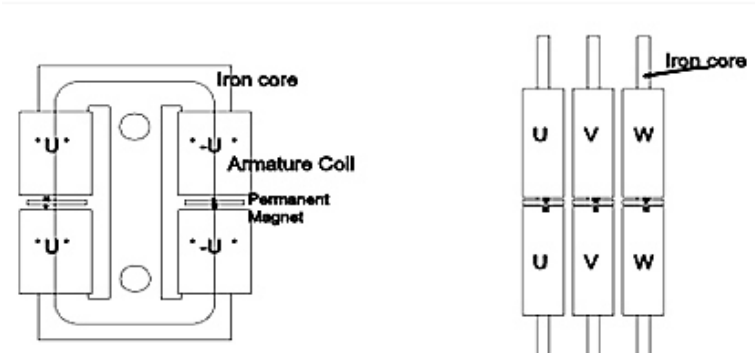

Figure 4.19 The basic configurations of the three phase unit.

(a) Armature and field inductor. *[32]*

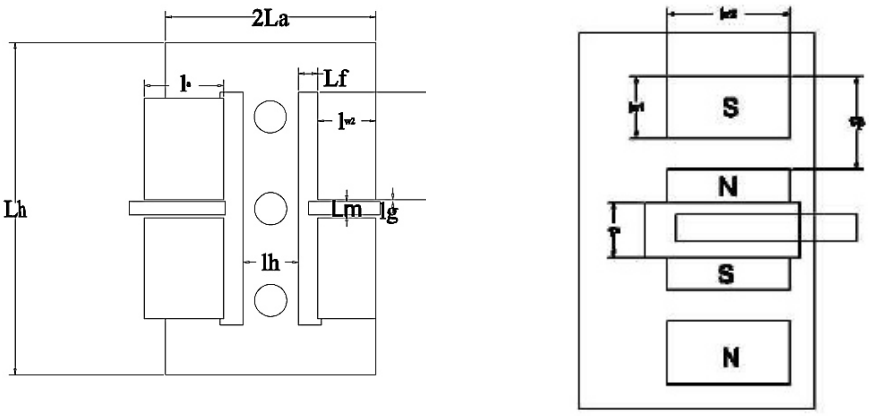

Figure 4.20 Specifications of geometrical parameters. *[32]*

The coils of different armature units are connected in parallel. Armature units and inductor magnets are installed along the moving direction. Magnets are made of NdFeB and are separated by 180 electrical degrees. Each armature unit is separated by the following one by 120 electrical degree. The main difference between this transverse machine and other transverse conventional solutions is that in this case the magnetic circuit is inherently 2D.

The 2-dimensionality of the magnetic circuit simplifies the following aspects of the manufacturing aspects of the TFG:

1) the iron core can be assembled from traditional laminated steel plates;
2) the structure is simple and can be fabricated in sub unit;
3) higher manufacturing tolerances which allows a simplification in the air gap design and fabrication.

The maximum force can be expressed as follows:

$$F_{t,max} = p\frac{E_{rms}}{v}I = \frac{\sqrt{2}(p\pi\varphi_{ml\_max}}{2t_p}N(l_a, l_c) \qquad (4.10)$$

where the geometric parameters l_a and l_c can be deducted from figures above inserted.

4.2.3 Optimization procedure and numerical simulation

Optimization procedures have been focused on the maximization of the annual production yield per unit of active (iron and magnets) material that has been used. This approach is equivalent to design the generator maximizing the tangential force and leads to an expression for force as in (4.11).

However, expression in (4.11) can been more exactly computed if a 3D analysis is performed and if some numerical simulation of the generator lead by seawaves can be performed.

In each simulation, parameters R_i, L, k, and / had values different from the ones used in the previous simulation. In each run of the simulation the water was let vary according to Eq. (4.9) and a wave train was generated. The wave train consisted of ten oscillations.

Each oscillation of the train wave had an amplitude and a frequency generated through a random number generator, whose statistic features were obtained from the experimental data above mentioned.

R_i, L, k, and Φ were let vary among some values that were compatible with the size of the linear generator, with the induced emf and with the linked flux.

The design specifications are reported in Table 4.3 from where it can be seen that the free parameters were l_a and l_c[30].

Symbol	*Quantity*	*Symbol*	*Quantity*	*Symbol*	*Quantity*
L_a [mm]	40	l_f[mm]	10	l_g[mm]	1
L_b[mm]	100	l_b[mm]	20	l_b[mm]	2
p[mm]	13.5	L_{w1}[mm]	11.5	l_a, l_m, l_c	Variables
s[mm]	9	L_{w2}[mm]	20		

Table 4.3 Preliminary design specifications

The objective function was the energy output that under the assumptions presented has the following form:

$$\boldsymbol{E_0 = \int_0^{T_{fin}} i^2 \cdot R dt} \qquad (4.11)$$

where E_o is the output energy and T_{fin} is the final time. The final T could vary from run to run and it was equal to the time needed to let the water complete 10 full oscillations.

The output of the optimization procedure was the values of the design parameters l_a and l_c; so this procedure led to compute this free parameters., which were equal to 2.5mm and 4mm.

In order to verify if the design procedure had led to satisfactorily results, we computed thrust at the optimal point by using Eq. (4.10) and computed the same quantity obtained by a 2D and 3D simulation.

In 2D case study, the principal phase of one correct simulation is to individuate an appropriate geometry.

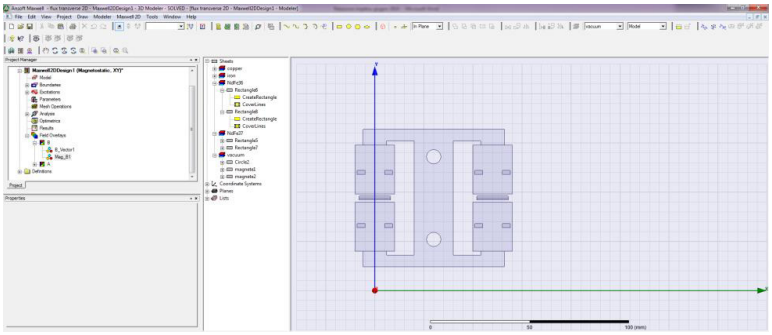

Figure 4.21 Early Image of FEM Software

The chosen materials are:

- Iron to the Stator;
- NdFe35 to the Magnets;
- Copper to the Windings.

Executed these simple steps has been possible to calculate the magnetic field B and the vector potential (defined as the potential that can also be defined as a function of position, normally, it uses this type of boundary condition to specify the external potential boundaries).

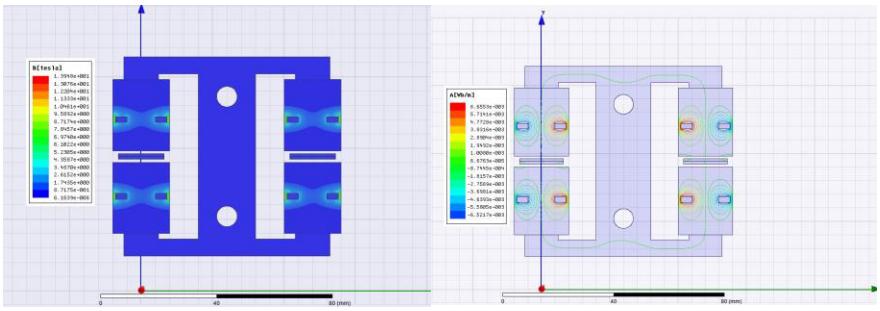

Figure 4.22 Report of Magnetic Field and Flux Lines

As for 3D simulation, it's adopted all identical geometrical considerations of 2D case study.

The theoretical value that was computed was 38.3 N, the value obtained in the 3D FEM analysis was 36.8N. From this value, we were able to compute the power density generation capability of the device that was equal (for the type of seawaves considered in the simulation) to 6.5 kW/m^2.

4.3 Design of a PM linear generator

The PM linear generator represents the most important device that is available to exploit energy from marine oscillation.

We find some advantages when permanent magnets are located in the moving part of the machine: the possibility to obtain a magnetic induction field without the use of current, it isn't necessary the presence of some conductors or sliding contacts and in particular we haven't Joule losses in the inductor.[33]

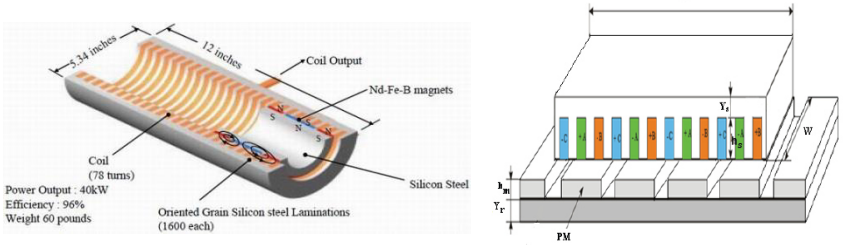

Figure 4.23 Examples of PM generator

The use of permanent magnets allows to reduce the mass of the translator so the magnetic flux flows among stator and translator of this device (in an exclusive way). The utilization of iron is connected to magnetic and electrical characteristic while you can take other materials to structural functions and mechanical strength.[34]

In spite of these advantages, the PM-LG's in generals have a high cogging force to deal with, The cogging force is produced by the interaction between the PM's and the slotted iron structure and the finite length of the stator core. The cogging force produces a pulsating force ripple resulting in vibrations and acoustic noise which is detrimental to the linear generators[35].

The principle drawback is the cost of magnets that are made using alloys based on rare earths as SmCo or NdFeB.

Material Type	First Introduced	Consumption (Product Value)	Use Trend
A. Principal Magnet Materials			
Alnico Alloys	1932	Medium	Slow decline
Ferrites (oxides)	1952	Largest	Medium growth
Rare Earth-Cobalt Alloys (Sm-Co Base)	1970	Medium	Slow growth
Rare Earth-Iron Alloys (Nd-Fe-B Base)	1983	Medium	Rapid growth
B. Materials of Minor Significance			
Co, Cr-Steels	1900	Very small	Declining
Fe-Co-Mo (Remalloy)	1934	Very small	Declining
Fe-Ni-Cu (Cunife)	1935	Very small	Steady
Pt-Co	1936	Extremely small	Steady
Co-Fe-V (Vicalloy)	1940	Very small	Steady
Fe-Co ESD (Lodex)	1954	Discontinued in 1988	
Fe-Cr-Co	1979	Small	Steady
Mn-Al-C (Almax)	1979	Very small	Steady

Figure 4.24 Permanent Magnet Materials in use today[36]

Shapes, size and manner of mounting of the magnets strongly influence the characteristics of the translator and then the whole machine. To obtain a machine with high performance and not excessive weight it is appropriate to use buried magnets.

The methods of installation depend on their orientation: if you want a highly variable flux over short lengths, then using small magnets placed one next to the other or to limit separated by a thin layer of iron or in one other case it' s possible install alternate polarities ,in a direction perpendicular to the motion, fixed on the supporting structure (anon-ferromagnetic material as titanium alloy or aluminium)[36].

Another possible configuration is the surface mounted magnets that presents an easy assembly.

In the end there's the layout called " Halbach," which allows for a more sinusoidal profile of induction in the gap.

A linear generator can have a circular cross-section or it can show a cross-section with the shape of regular polygon (square, hexagon, etc.). The most used configurations are those in which the cross-section is square or circular; in this case the motor is called cylindrical.

The most used configuration of a LPMG is a machine with short inductor, fixed to a basement, and with induced part, usually longer than the inductor, as moving part.

The magnetic core is realized with iron-laminated blocks (thin laminations generally wrapped up in an even number of blocks), needed to shorten the paths of the induced current. This lamination can be longitudinal or transverse with respect to the direction of motion[37].

In case of longitudinal lamination the magnetic core of the inductor is composed of more blocks in which each sheet present alternately teeth and slots.

For these two types of laminated iron-cores, the drawbacks are: for the former, the practical difficulty to precisely align the laminations of every core, bearing in mind their length; for the latter, the substantial total thickness of the insulations among the laminations that implies a considerable reluctance of the magnetic circuit.[38]

4.3.1 Procedure and 2D numerical simulation

As regards the numerical simulation of PM generator, we initially studied characteristics of monolater electric PM structure. In particular, all geometrical dimensions were be used to design the device in CAD and FEM simulation.

The PM generator is constituted by: a stator (structure comb) and two permanent magnets. The material of stator is iron and NdFe35 to magnets.

In table 4.4 we report data of material of software's libraries.

Name	Type	Value	Units
Relative Permittivity	Simple	1	
Relative Permeability	Simple	1.0997785406	
Bulk conductivity	Simple	625000	Siemens/m
-Magnitude	Vector Mag	-890000	A_per_meter
-X Component	Unit Vector	0	
-Y Component	Unit Vector	1	
-Z Component	Unit Vector	0	
Mass Density	Simple	7400	Kg/m^3

Figure 4.4 Magnetic Material

To optimize the design of generator we performed different parametric simulation.We identified three parameters that are analysed to perform the design of PM generator. The electrical structure is a bilater generator.

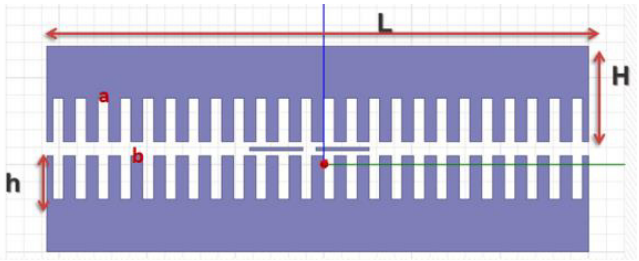

Figure 4.25 Generic 2D geometry of PMG

a	*parameter*
b	***1,35cm***
H	***11 cm***
H	***parameter***

Parameter a

The parameter a identifies the width of the stator slots. We introduced this variable in the design model. The parametric analyse is an interval from 0.01 cm to 1.2 cm with linear step of 0.05 cm. The results are intensity of magnetic flux density [tesla] and flux intensity [Wb/m].

In a magnetostatic solution, the magnetic field is produced by DC currents flowing in conductors/coils and by permanent magnets. The electric field is restricted to the objects modeled as real (non-ideal) conductors. The electric field existing inside the conductors as a consequence of the DC cur-rent flow is totally decoupled from the magnetic field. Thus, as far as magnetic material properties are concerned, the distribution of the magnetic field is influenced by the spatial distribution of the permeability. There are no time variation effects included in a magnetostatic solution, and objects are considered to be stationary. The energy transformation occurring in connection with a magnetostatic solution is only due to the ohmic losses associated with the currents flowing in real conduc-tors.

As for "Flux Intensity", the vector Potential A can also be defined as a function of position using math functions. Normally, this type of boundary condition is used to specify the potential of outer boundaries. It can also be used to set the interface between two objects to a potential, modelling the presence of a very thin conductor between the objects. They are sometimes called Dirichlet boundaries.

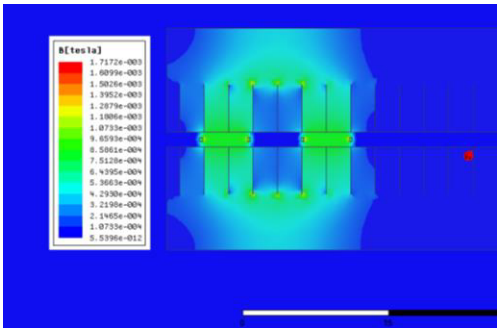

a=0.01cm

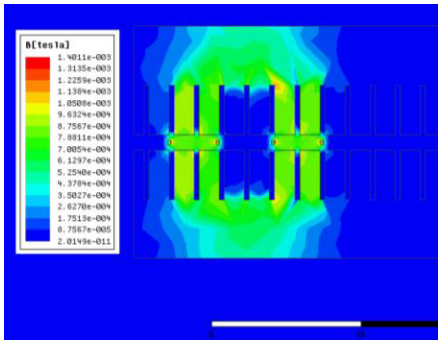

a=0.5cm

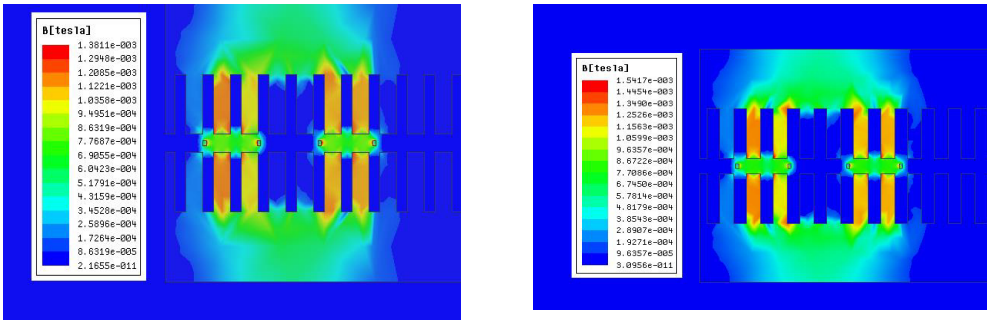

a=1cm a=1.2 cm

Figure 4.26 Plot of Magnetic Flux Density [Tesla] to optimization of a

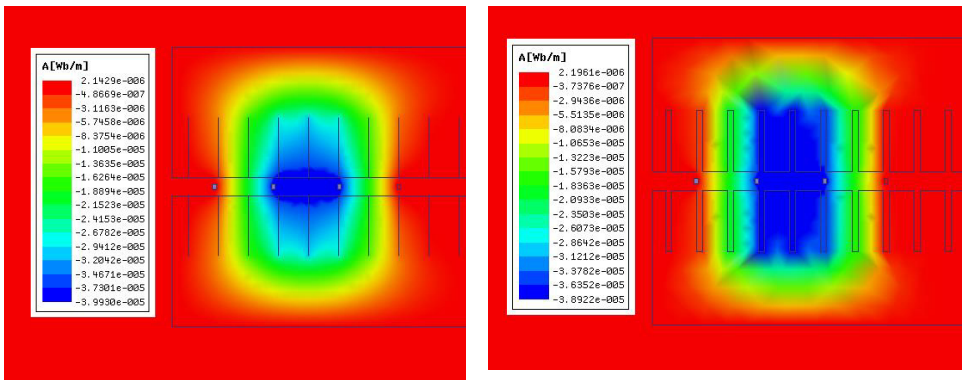

a=0.01cm ***a=0.5cm***

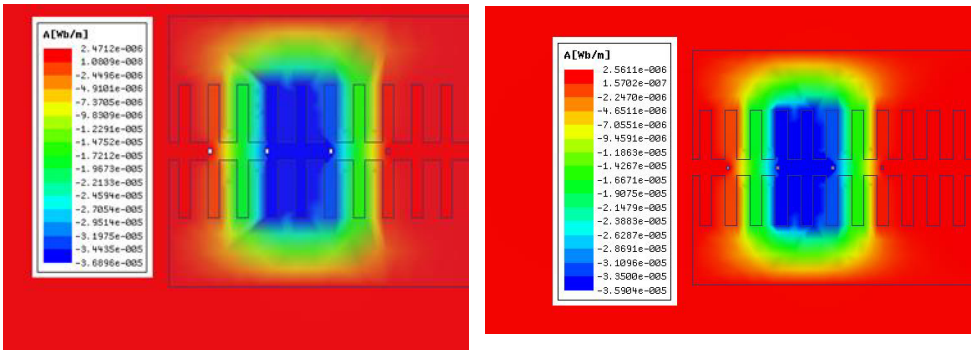

a=1 cm ***a=1.2 cm***

Figure 4.27 Plot of Flux Itensity [Wb/m] to optimization of a

Parameter h

The parameter h identifies the height of the stator slots. We introduced this variable in the design model. The parametric analyse is an interval from 2 cm to 4 cm with linear step of 0.2 cm. We calculated same magnetic output above described.

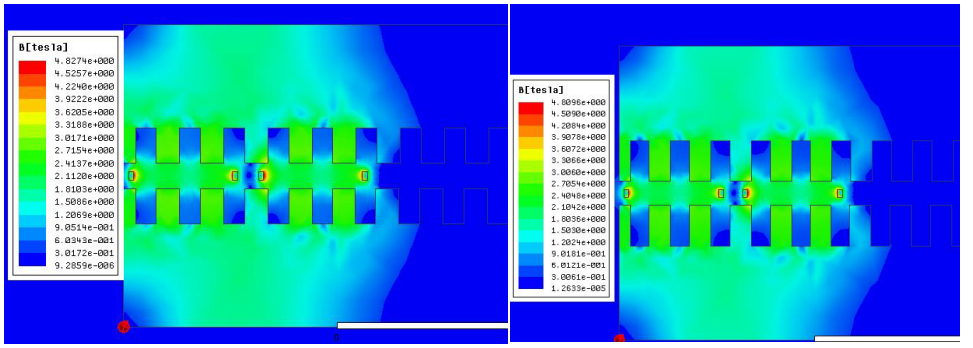

h=2 cm h=2.6 cm

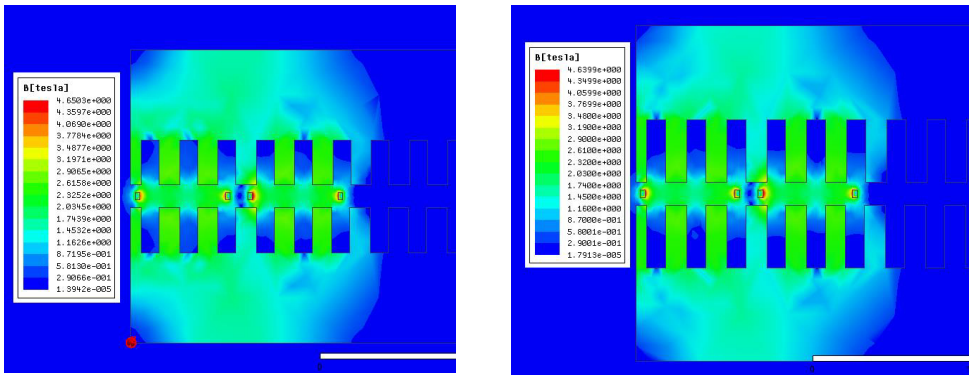

h=3 cm h=4 cm

Figure 4.28 Plot of Magnetic Flux Density [Tesla] to optimization of h

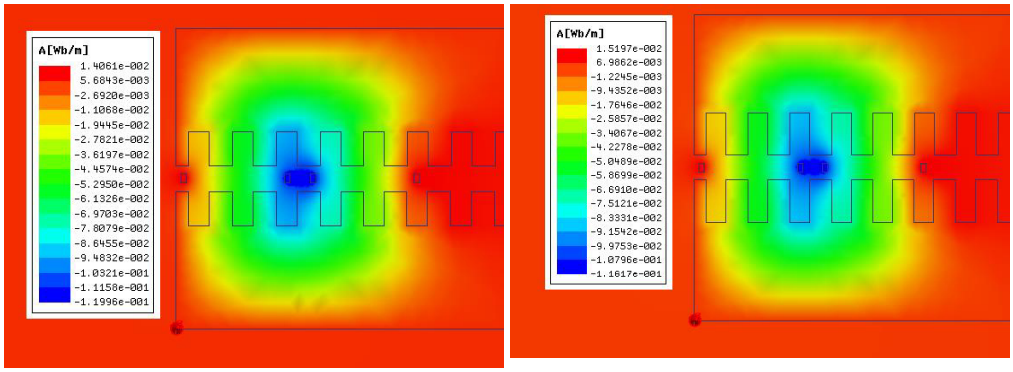

h=2 cm h=2.6 cm

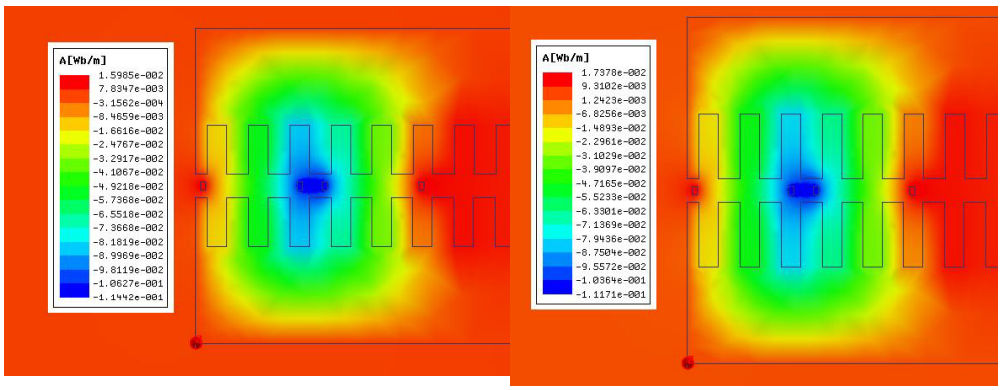

h=3 cm h=4 cm

Figure 4.29 Plot of Flux Itensity [Wb/m] to optimization of h

Parameter x_1

In the end, we studied the behaviour of PM generator when the permanent magnets change their position.

The variable which is introduced is x_1, and its value diversifies in a range of 0.5 cm- 48 cm with the linear step is 0.2 cm.

The results shown are: intensity of magnetic flux density [tesla], flux intensity [Wb/m] and the trend of "Force" on the position x_1.

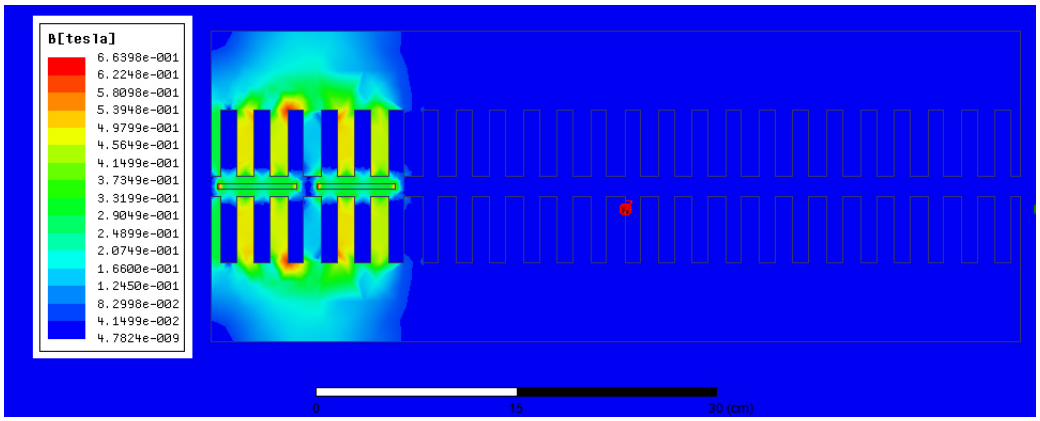

x_1=0.5 cm (initial position)

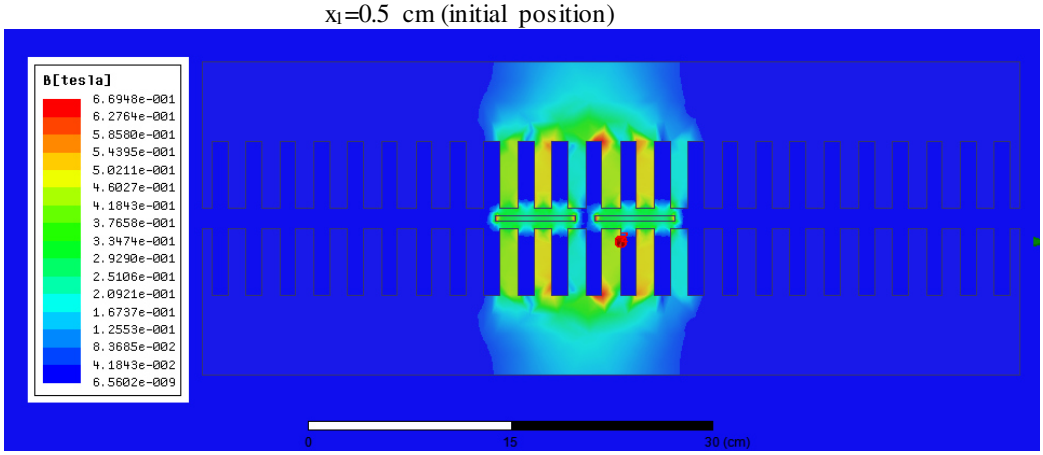

x_1=24 cm (central position)

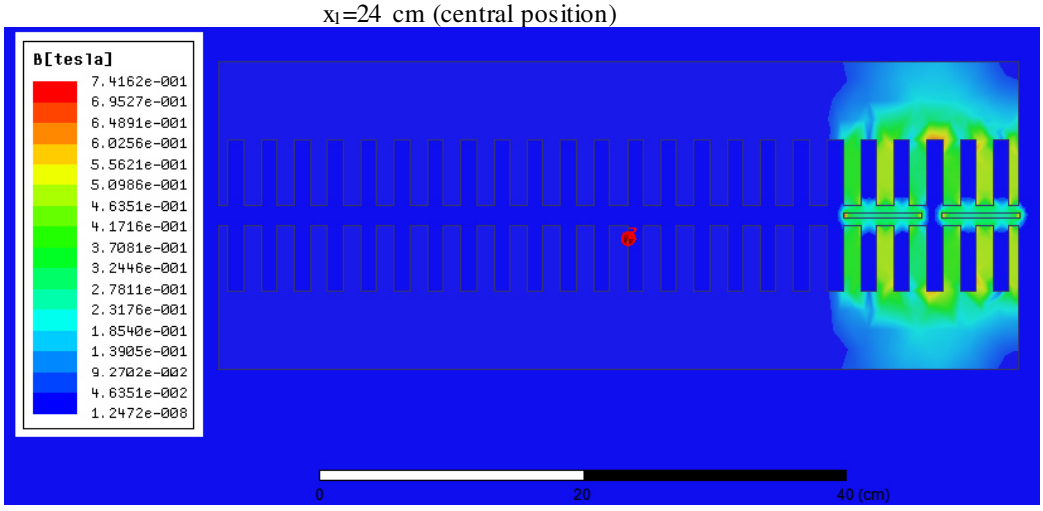

x_1=48 cm (final position)

Figure 4.30 Plot of Magnetic Flux Density [Tesla] to optimization of $\underline{x_1}$

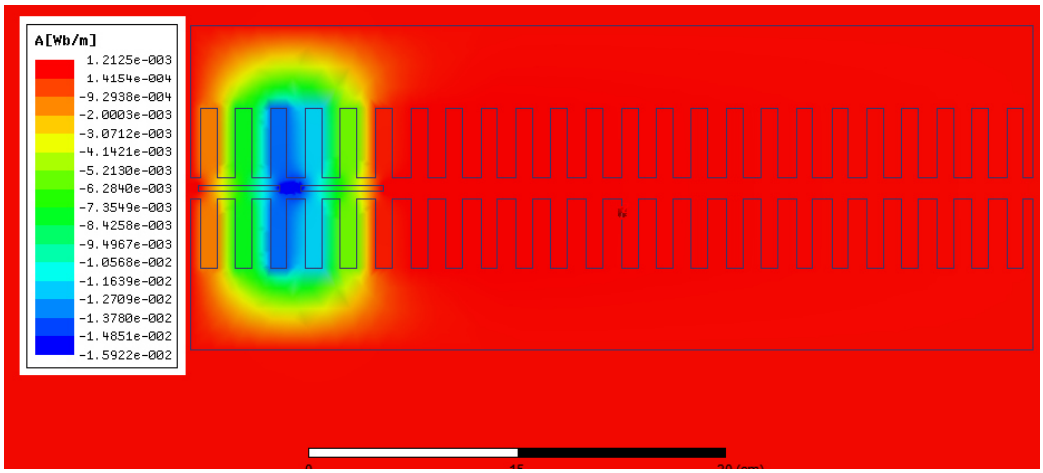

x_1=0.5 cm (initial position)

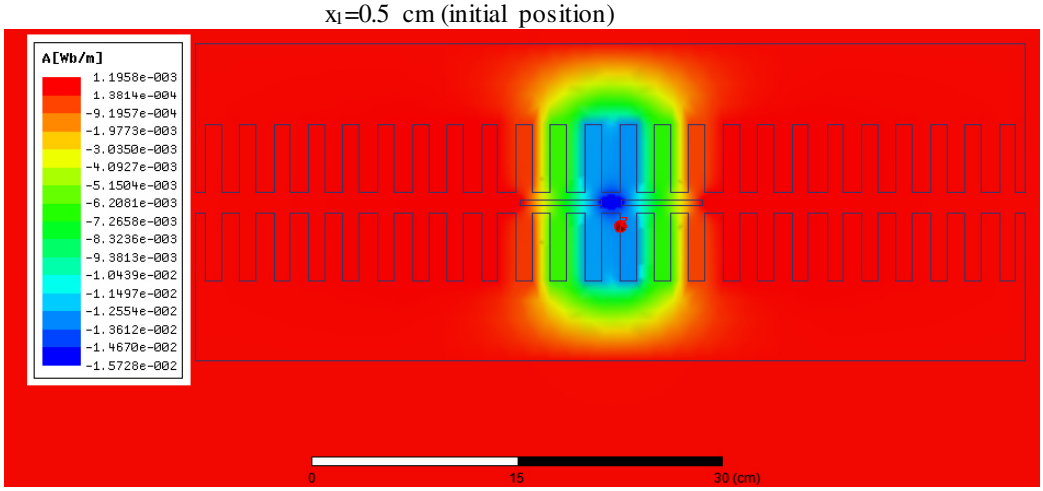

x_1=24 cm (central position)

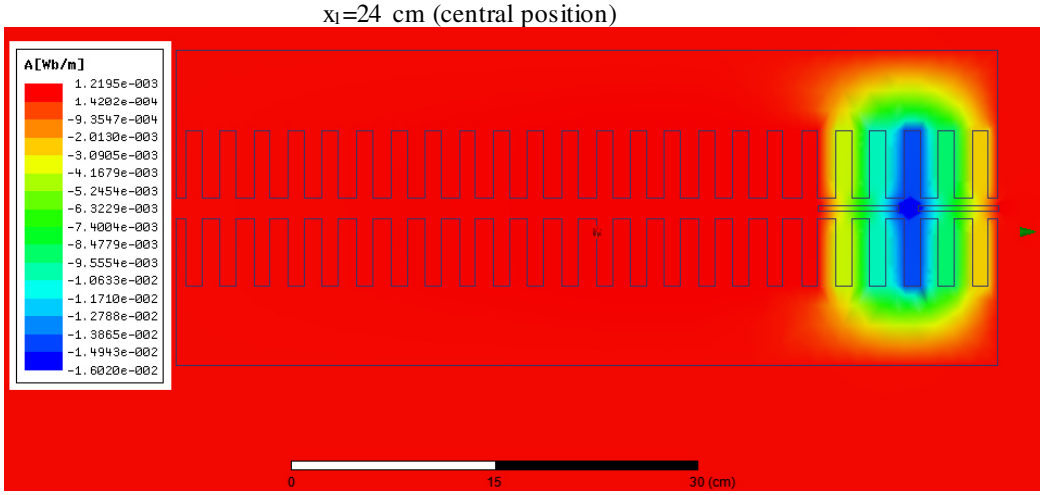

x_1=48 cm (final position)

Figure 4.31 Plot of Flux Itensity [Wb/m] to optimization of $\underline{x_1}$

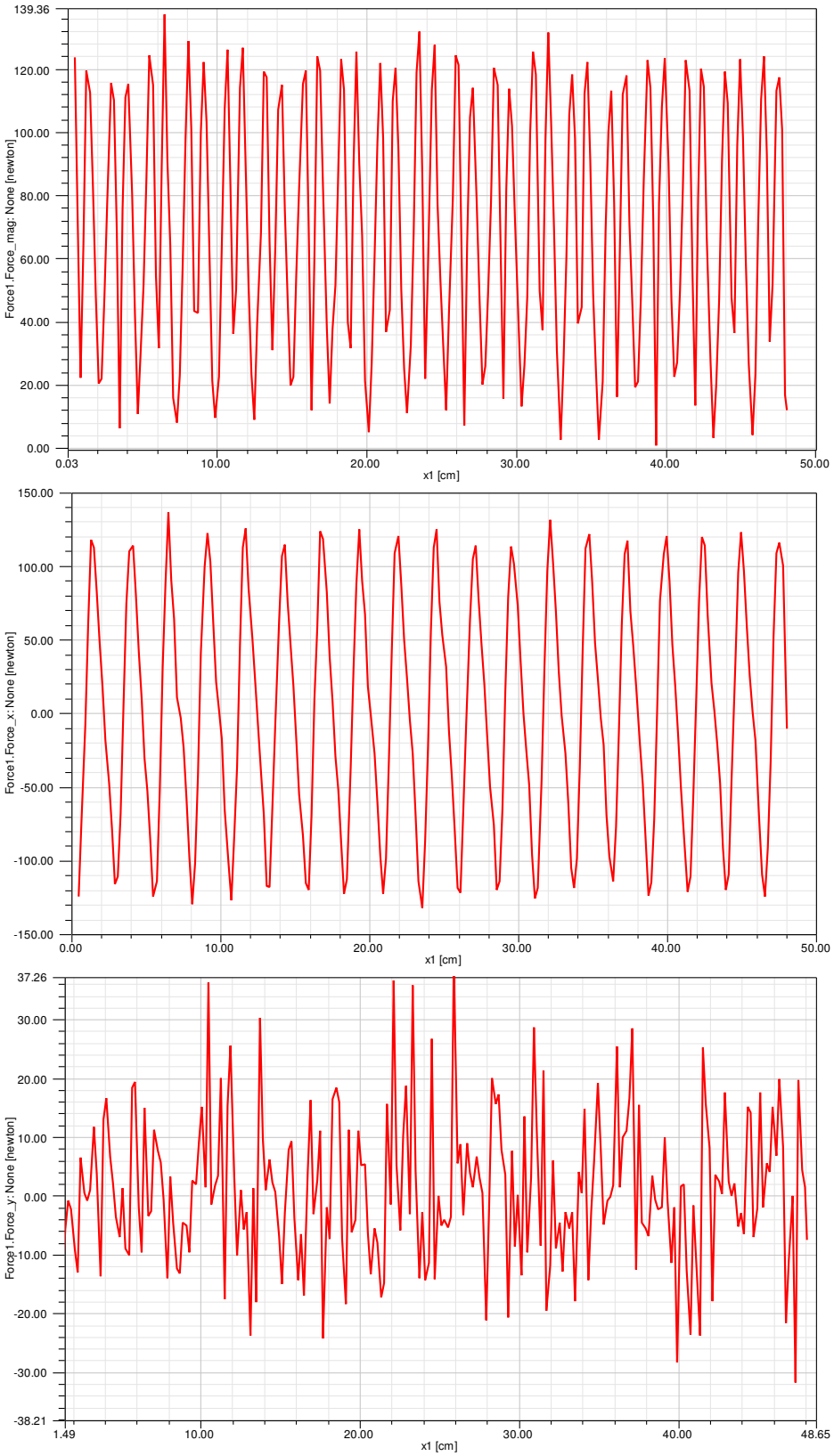

Figure 4.32 Trend of Parameter Force and x_1

4.3.2 Procedure and 3D numerical simulation

The next step to be carried out was run simulations in three-dimensional environment. The electric generator was initially designed through simple software CAD[26].

Similarly to the previous case, we studied the behaviour of the device in a magnetostatic case.

Using the already defined geometry was again simulated parametrically the position of the magnets, which constitute the shifter of the generator, compared to the fixed stator.

The variable that identifies the movement of the magnets is Z_1 (vertical movement) that was simulated in the range between -15 cm and 0 cm with a ΔZ_1 of 5 mm. The following images show the values of magnetic flux density [tesla], and the trend of "Force" on the position x_1.

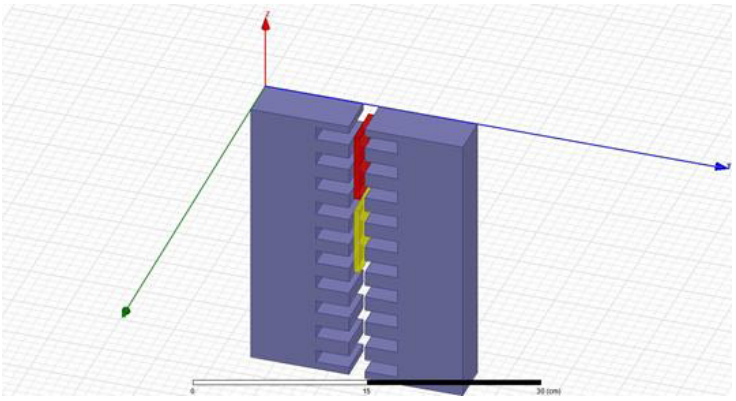

Figure 4.33 Design (3D) of PM generator

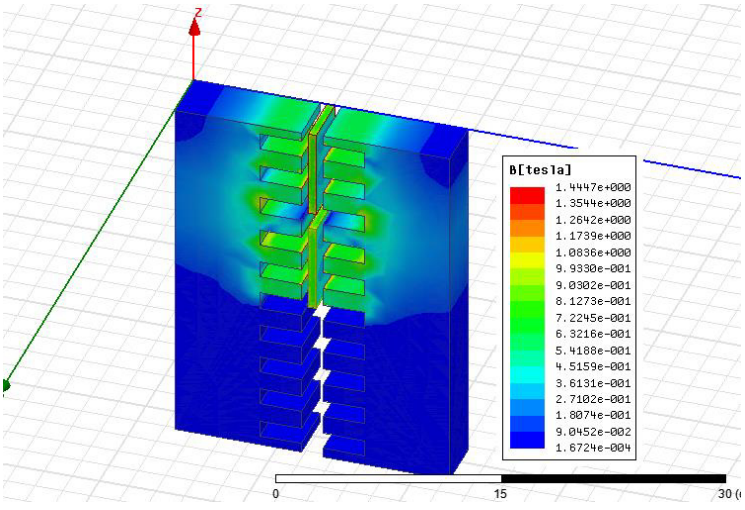

Z_1=0 cm

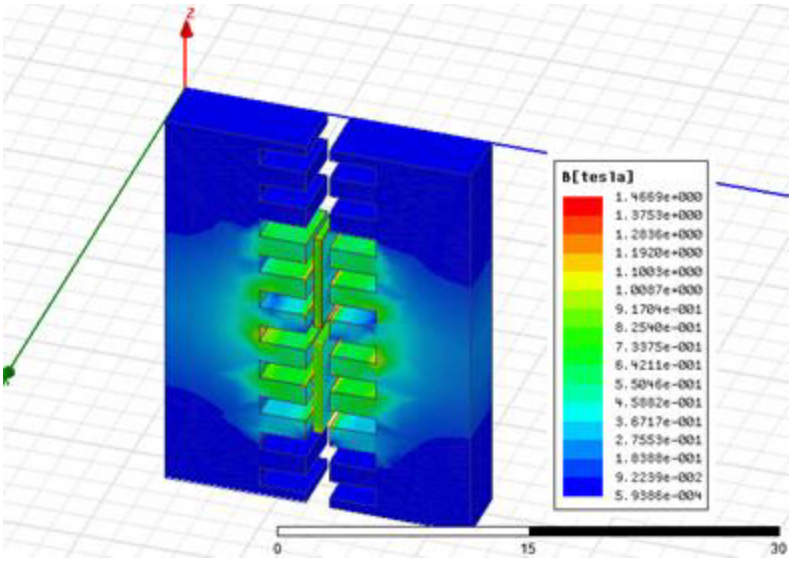

Z_1=-6.5 cm

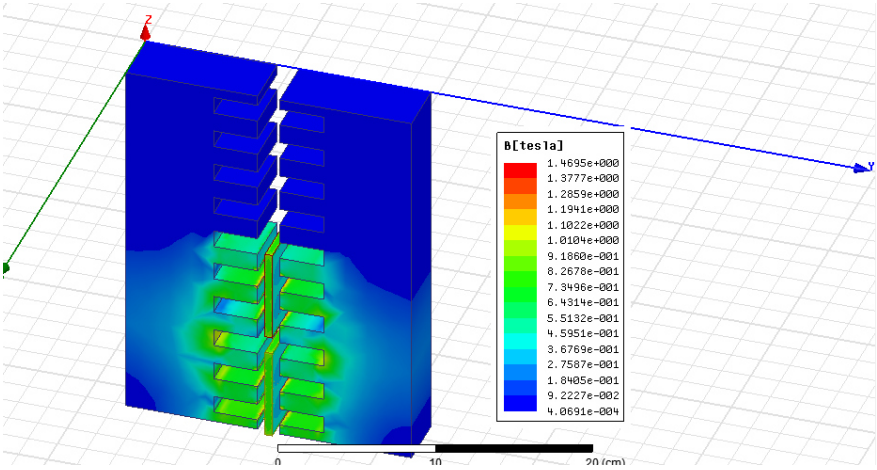

Z_1=-12 cm

Figure 4.34 Plot of Magnetic Flux Density [Tesla] to optimization of Z_1

The PM generator is been performed among various parametric simulation and the principle aim is been studied its electrical characteristics to exploit wave energy to electrical energy. The facility assembly and the simple geometry are the most important advantages of generator type.

4.4 Comparison of Conventional Generator Types

The following generator topologies are modelled, optimized and compared for application in wave energy.

The criterion to compare different generator types includes generator cost and losses[35]:

$$\boldsymbol{C = C_{gen} + PE_d C_{kWh}} \quad (4.12)$$

Where

- C_{gen} is active generator material cost;
- P is a period of five years;
- E_d is annual dissipation in the generator;
- C_{kWh} is price of energy.

As the basis of our calculations, we assume PM generator as electrical structure of WECs that will be built.

CHAPTER V

NEEMO: Design, Construction and Installation of Wave Energy Converter in Sicily

Introduction

In the final chapter of this work we describe the system ”WECs + electrolyzer” that is designed in Sicily.

In the previous chapter they were separately analysed the operation of wave buoy of DEIM and the numerical simulation of numerous electrical device. The Permanent Magnet Generator (PMG) was chosen as electrical system to be implemented.

A wave characterization of chosen site is the first step to an installation of wave converter; in fact the study of the site follow two approach: the first is only a statistical research using data of RON *(“Rete Ondametrica Nazionale”)*.

The next step presented in this chapter is a description of the generator. In particular, we introduce all electrical structure of PMG (stator and shifter), a FEM transient simulation of it that shams a sea wave condition and test bench of generator. So we obtain a real energy production. Its production in connected to the working of an electrolyzer.

Sea water electrolysis is a mechanism of production of Hydrogen; in fact we analysed the process, studying operative variable as Temperature and Pressure.

As for the conclusion of this work is based on the environmental valuation of the system realized: produce clean hydrogen from sea.

5.1 Wave characterization of chosen site

The definition of the potential energy of optimal coastal sites is one of the basic needs for the diffusion of new technologies and for their insertions. The determination of available wave energy potential of a given area is the basic requirement in any wave-energy program.

Mostly, it is difficult to find spectral measurements of wave heights and periods due to economic and technical restrictions. For the reason that basic wave statistics is needed for a wave energy study, one can invoke alternate means to estimate the available wave energy[39].

The installation of WEC occurred in a marine area of the north coast of Sicily, overlooking Sea Gulf of Castellammare in Tirren Sea. The mooring used is located within an area appointed to fish farming, shown in Figure 5.1, and that is not a problem for navigation as the bounding area appears to be well defined.

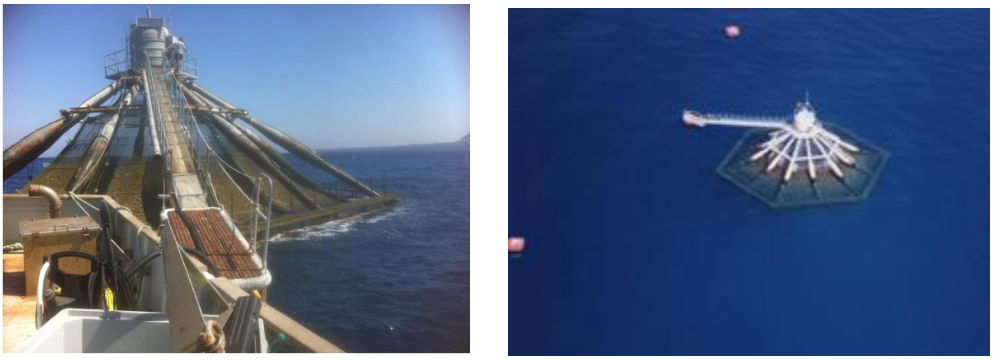

Figure 5.1 Site of WEC's installation

In terms of currents, the Gulf of Castellammare is affected by a surface current induced by the wind parallel to the coast from east to west or west-east direction. With a dominance of one in west-north / west

From data by the current meter placed at -10 meters, the average speed of the current is equal to 3.0 cm / s, the maximum speed of the current recorded was 39.6 cm / s towards the southeast. The predominant current goes to the north-northwest with an average speed of about 2.1 cm / s, with a frequency of 19.0% of total recorded data

Instead, at a depth of 30 meters, the average speed is equal to 3.1 cm / s, the maximum from the west-northwest reached 33.4 cm / s which represents the flow of current greater with an average speed of 5, 1 cm / s and a percentage of the total of 26.0%.

-10 m **-30 m**

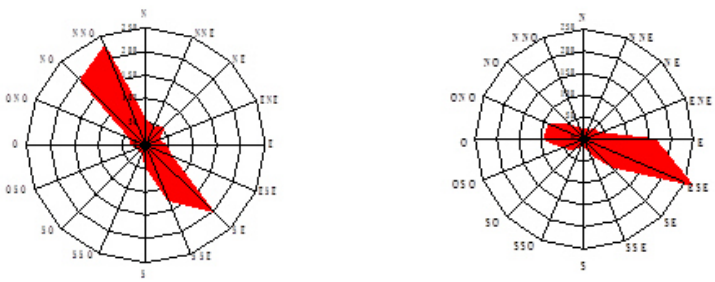

Figure 5.2 Distribution of sea current speed (direction and intensity)

The aim of this paragraph is to define the wave parameters and the potential energy in Sicilian coast using the wave data; in fact in the first section we analyse the statistical report provides the use of data of RON to evaluate the wave energy potential in the site of Castellammare del Golfo, while in the second section we report real data measured by buoy installed at that place.

5.1.1 Evaluation of the Potential Energy from statistical analysis

The measurements used to the simulation come from Rete Ondametrica Nazionale (RON), an Italian Wave measuring Network managed by Institute for Environmental Protection and Research (ISPRA).

RON was born in 1989 and it's made by 8 directional buoys "datawell-wavec". These are in operation since recording significant wave height Hs, peak period T_p, mean period T_m and mean wave direction θ_m. Until 2002 wave parameters were normally recorded every 3 h.[8]

The network consists of 15 oceanographic buoys located along the Italian coast. The buoys are moored in fixed positions shown on charts in areas off-limits to fishing and navigation typically with a radius of about 250 meters. Each buoy (Axys Watchkeeper) has a diameter of 1.7 meters and a height on the waterline of 2.8 meters. It contains a wave meter directional accelerometer solid state, high precision, TRIAXYS.[7]

Different wave measuring network can report on the status of the sea that is known sites where the buoys are installed.

Anyway the knowledge of the wave motion of big area outside of the measuring system is necessary to convert the mechanical energy in electric (energy). The aim of this work is to realize a mathematical tool .

The idea was born from the need to know the status of the sea of an unknown site where will be installed a new electric device.

The site is located within a geographical mesh note, that is surrounded by buoys measure for sites not too far away spatially. In particular the have some informations[9]:

- to know of long measurement sampling ;
- to find a geographical mesh;
- to calculate the distance among wave note site and our unknown.

In the first part of the experimental study is been necessary to validate the correlation of buoys of RON that are inside chose geographical mesh. The buoys are: Cetraro, Ponza, Mazara del Vallo, Siniscola (Capo Comino) e Capo Gallo (as showed in Fig.5.3).

Figure 5.3 Geographical mesh used and locations of 5 buoys.

The first step is to identify common interval working of all buoys. In particular, we study the climatic parameters as H_{0m} and T_m.

We chose a year of observations (01/01/2004 to 01/01/2005) and it was been necessary an operation of filtering namely to exclude invalid or missing data, or values outside the media (outsiders that are made by problems of sensor).

The next step is to choose the period that will be used to statistical simulation[9].

In general, available times of five buoys are:

- Cetraro, 01/01/1999 to 05/04/2008;
- Ponza, 01/07/1989 to 31/03/2008;
- Mazara del Vallo, 01/07/1989 to 04/07/2008;
- Siniscola, 01/01/2004 to 12/09/2005;
- Capo Gallo, 01/01/2004 to 31/12/2008.

As for the climatic conditions, they influence powerfully the state of wave motion, so in the study it's necessary to choose four different period (one for each season) of one significant year [14].

Based on the data, immediately after the filtering step (to eliminate hot spot), it is been decided therefore to analyse the following ranges:

- 21/03/2004 to 24/04/2004 for the Spring ;
- 20/07/2004 to 20/08/2004 for the Summer;

- 20/10/2004 to 20/11/2004 for the Autumn;
- 20/02/2004 to 20/03/2004 for the Winter.

After many simulations, setting a period occurred as the value of the wave of a single buoy is always proportional to the other.

In particular, there has been a certain constancy in the relationship between the value of the single H_{m0i} buoy at fixed period, and the summation of the values of H_{m0j} stations remaining the same period.

It is expressed by the parameter $P_i(t)$ given by:

$$\boldsymbol{P_i(t) = \frac{H(t)_{m0i}}{\sum_{j=1}^{n} H(t)_{m0j}}} \tag{5.1}$$

This parameter is a function of time of measure so we have a large sample of data and it's necessary doing arithmetical average for each individual season.

The second part of the study is addressed to obtain the value of Hm0 of the site "Castellammare del Golfo". A Sicilian town among Palermo and Trapani where will be installed the buoy projected by University of Palermo.

It was possible to calculate the wave height at the site in question while having no device of measuring placed there. It has in fact worked the following relationship:

$$\boldsymbol{H_{castellammare}(t) = M(t) \sum_{j=1}^{n} H(t)_{m0j}} \tag{5.2}$$

where M(t) is a parameter obtained by weighted harmonic mean expressed by:

$$\boldsymbol{M(t) = \frac{\sum_{j=1}^{n} d_j}{\sum_{j=1}^{n} \frac{d_j}{P(t)_j}}} \tag{5.3}$$

where d_j is the distance of the j-th buoy from the site in question and $P(t)_j$ is the parameter defined above (eq. 5.1).

The estimation of wave power transmitted per unit width is represented below (adopted in in deep water, when the depth is greater than half the wavelength):

$$P = \frac{\rho g^2}{64\pi} H_s^2 T_e \qquad (5.4)$$

where ρ is a seawater density and its value is, approximately, 1025 kg/m^3.

Using the eq.(5.4), it's possible to calculate the energy potential of the examined site. The wave period of this sampling doesn't suffer of a large variation so we choose as value 5 second and significant height is a mean value of previous analysis. In the table 5.1 we report the values.

Castellammare del Golfo		
Season of 2004	***Wave Height***	***SI***
Spring	2.7	[kW/m]
Summer	1.1	[kW/m]
Autumn	2.75	[kW/m]
Winter	5.1	[kW/m]

Table 5.1 Energy Potential of the chosen site

As regards the results, we obtain values of H_{mo} of Castellammare del Golfo that change in function of the season. As showed in the figure above.

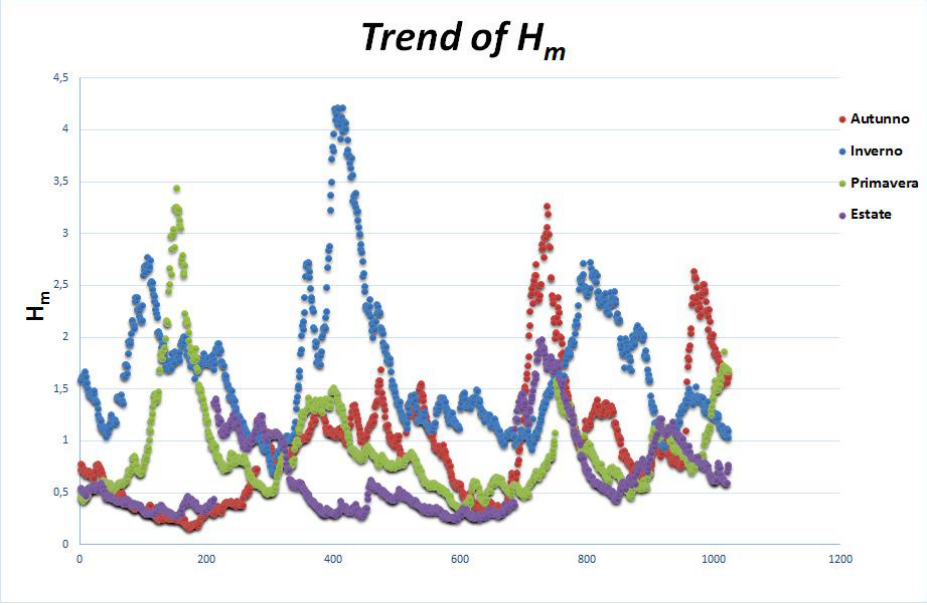

Figure 5.4 .Trend of average height of Castellammare del Golfo

This statistical approach validates the results obtained by other research. In particular, the most productive area, showing average values above 12 kW/m, is located in the western Mediterranean between the Balearic Islands and the western coast of Sardinia. Wave power in this area is most easily accessible from

the coasts of Sardinia, Balearic Islands and north Africa. The neighboring region located in the Sicily channel, off the north-western and southern Sicilian coasts, is also very productive with an average wave energy flux per unit crest that reaches 9 kW/m.[40].

The north-western and southern coasts of Sicily have a lower potential with average wave power ranging between 2.5 and 6.5 kW/m. On the northern coast west of Palermo average wave power flux is between 4 and 5 kW/m gradually increasing to values between 5 and 6 kW/m between San Vito Lo Capo and Trapani. The most productive area is located along the coastal stretch that lies north of Mazara del Vallo where average power is above 6 kW/m reaching values around 7 kW/m near Favignana Island. The rest of the southern coast is the least productive with average power flux below 4.5 and as low as 2.5 kW/m. The only exception is the area between Punta Secca and Capo Passero where values are almost everywhere near 5 kW/m. Similarly to what was previously observed on the Sardinia coast there is a sharp decline in average power east of Palermo and north of Capo Passero [40]

5.2 A case study of Permanent Magnet Generator (PMG)

In this section we describe a permanent magnet generator that is the "heart" of wave energy converter. In the chapter IV we studied different topologies of electrical devices that could be optimum solution for its aim, anyway after numerous FEM simulation, through an economic comparison we decided to realize a PMG. Below we will be described the principle parts of the machine.

- **Stator**

The PMG is defined as bilateral generator and we find two stators. The material used is iron and it is made by overlapping of 126 sheets, having a thickness of 0.5 mm, in order to minimize the eddy currents. The geometric dimensions of each single stator are: 60×972×65 [mm]. it consists of 39 slots and 8 holes with a diameter of 10.5 mm, according to the figure 5.5.

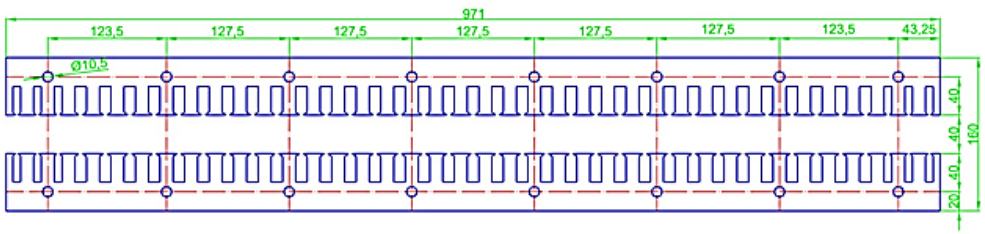

Figure 5.5 Plan of Stator of PMG

As you can see from the plan, the first and last three slots have a width of 8 mm while internal slots have a width of 12 mm because they must contain two winding. As for the teeth, they estimate 13.5 mm except the first and last tooth that measure 7 mm.

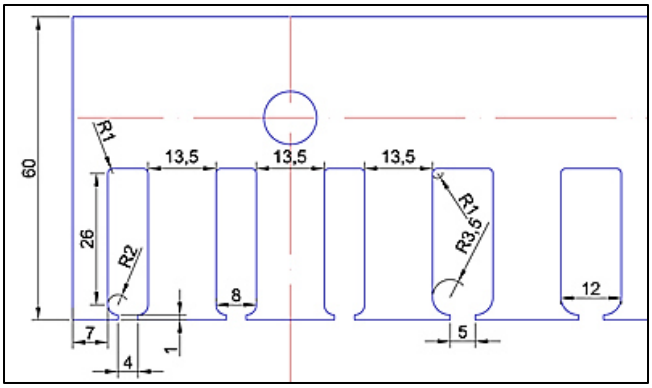

Figure 5.6 Slots and teeth of Stator

In the end, we find two tables of bakelite, used for assembling the stator block. In size 970x160x11mm. There are 32 holes to 10 mm, arranged according to the diagram shown in figure 5.7.

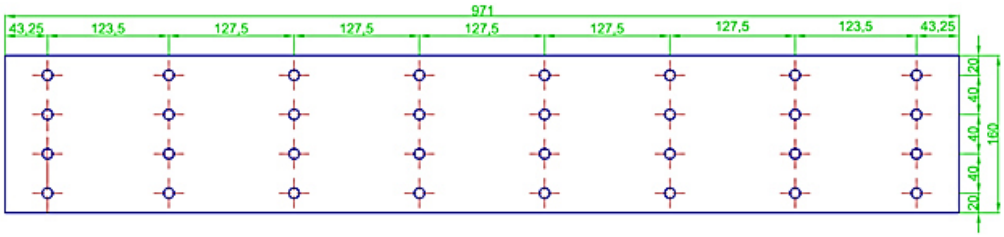

Figure 5.7 Support table of Stator

- **Translator**

The translator is made up of an alternating assembly of 40 *Neodymium–Iron–Boron (Nd–Fe–B*) permanent magnets, interspersed with soft iron pole pieces mounted on a bakelites sheet as shown in Fig. 5.8.

The magnets are stacked in pairs such that opposing magnetomotive forces (mmfs) drive the flux through the soft iron. Thus, the dimension of each magnet is 60 ×30×15 [mm] and it has a protective coating of nickel. Its weight is 205.2 g.

The sheet of bakelite is 1600×11×206 mm and it has 40 hallows to install each magnet.

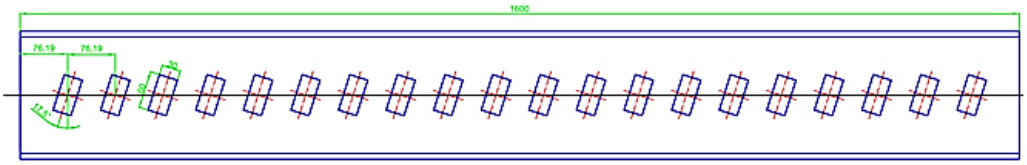

Figure 5.8 Schemes of shifter of PMG

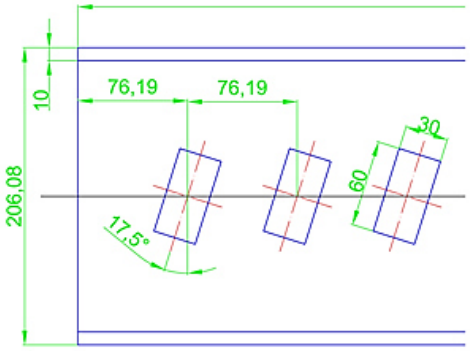

Figure 5.9 Permanent Magnets

- **Coils**

The material of coils is copper and in particular is enamelled copper wire of diameter 0.5 mm. The coils have 375 turns of rectangular shape with an average size of 85x135 mm. Each coil has a weight of 278 g.

We identify 72 coils that are arranged in 36 in each side of the armature (coils A and coils B).

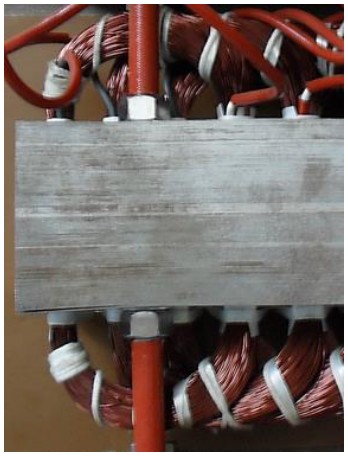

Figure 5.10 Image of Coil

As for the electrical device, we introduce below plan, real figure and summary tables of the PM generator.

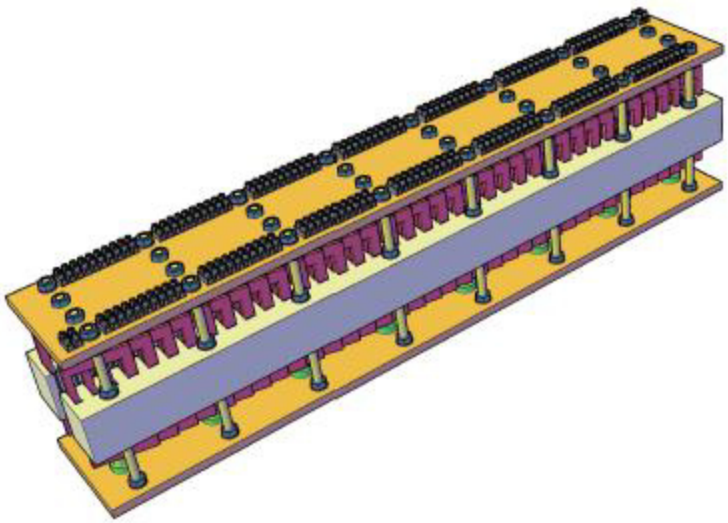

Figure 5.11 3D Design of PMG

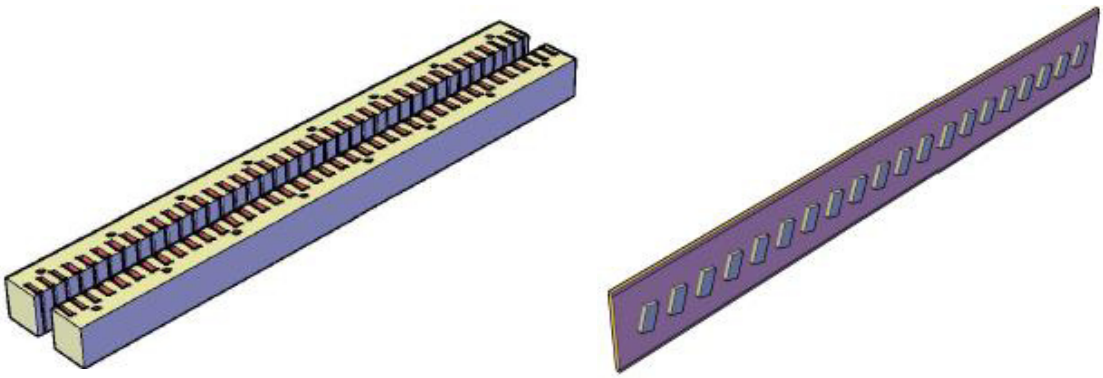

Figure 5.12 3D Design of Stator and Translator

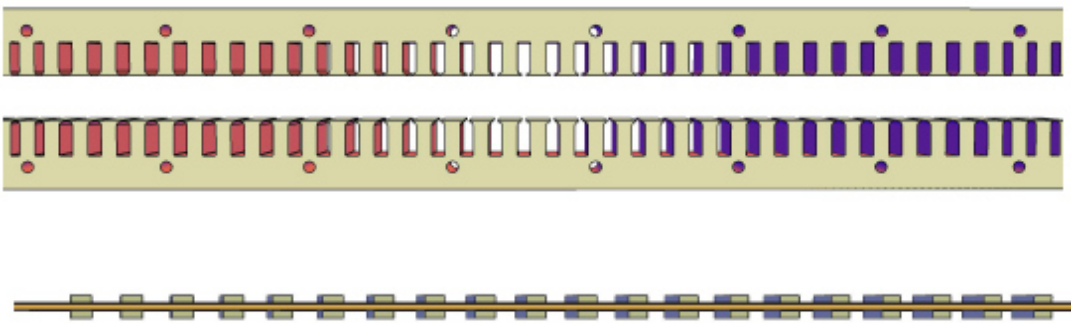

Figure 5.13 2D Design of Stator and Translator

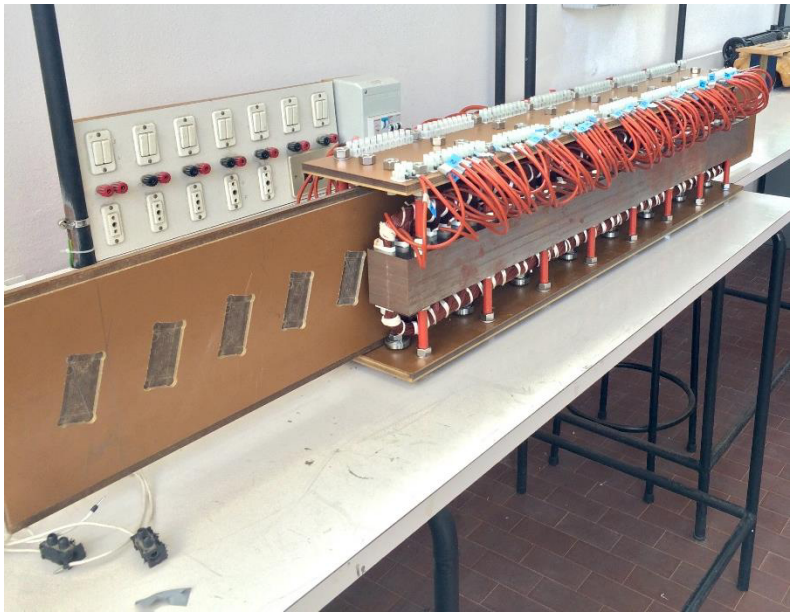

Figure 5.14 Photo of Permanent Magnet Generator

Figure 5.15 Photo of Assembly of Stator and Shifter

Permanent Magnet Generator	
STATOR	
Number of Coils	72
Number of Turns for each coil	375
Length	972 [mm]
Number of Slot	39
Slot Depth	8 [mm] (only 6) – 12 [mm]
Linear Weight	74.5 kg

TRANSLATOR	
Length	1600 [mm]
Material	Nd-Fe-B
Number of Magnets	40
PM Weight	205.2 [g]
Direction of Magnetization	Perpendicular direction to the face of greater extension
Linear Weight	13.1 [kg]

Table 5.2 Summary description of electrical device

5.3 Numerical simulation and experimental results

A 3D finite element model of linear PM generator was implemented, using Maxwell 3D from Ansoft Corporation. As for the FEM numerical simulation of Permanent Magnet Generator built[41], we calculated a transient simulation that could be representative of real operating principles. In particular, we simulated a translation of translator of PMG (where we located 12 magnets). The translate limit is from 0 [cm] to 54.4 [cm] with a velocity of magnets of 1 [m/s]. The simulation represents the load operation of the generator. The figure below shows a part of the electrical circuit inserted. The same scheme is been repeated for 72 coils.

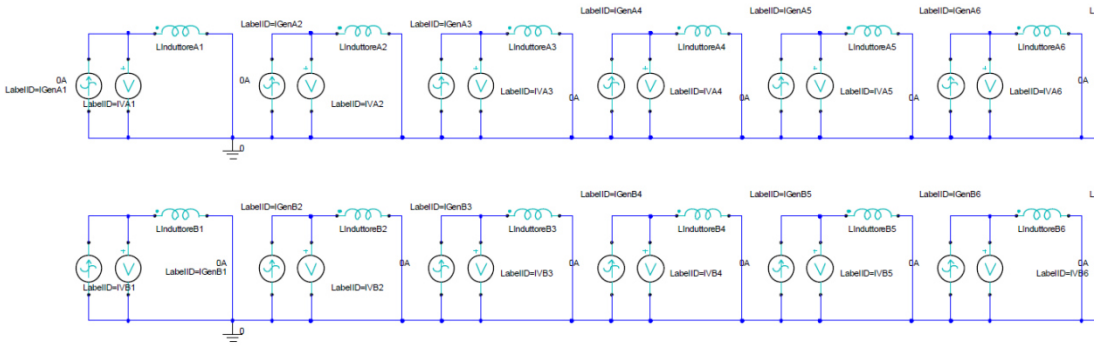

Figure 5.16 Electrical circuit of six coils A and B.

We report below results in terms evolution of Potential difference in all coils of the device. The mean value is 27 V.

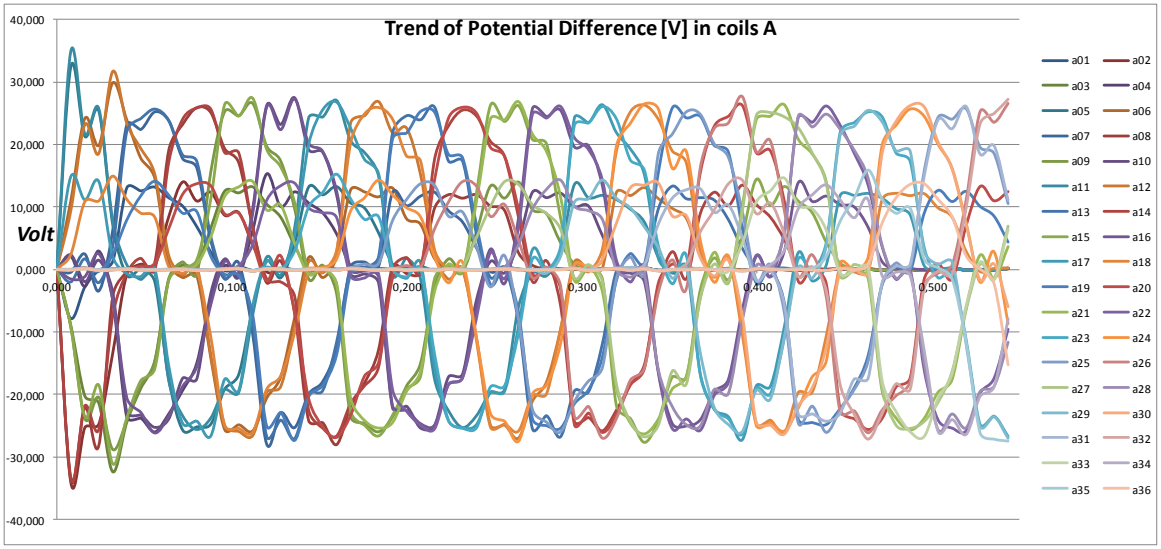

Figure 5.17 Trend of Potential Difference in coils A

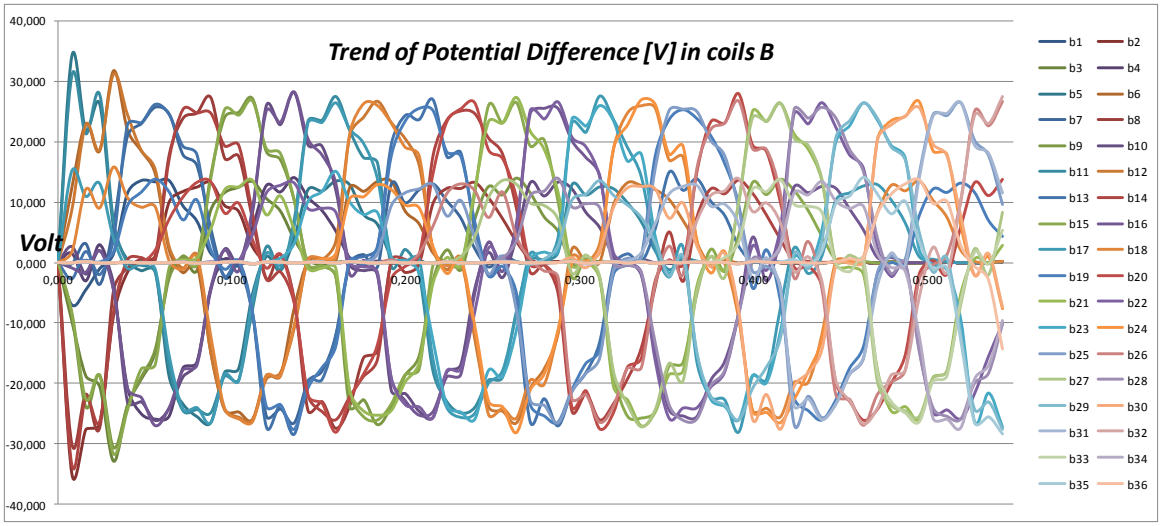

Figure 5.18 Trend of Potential Difference in coils B

Figure 5.19 shows a typical flux plot from FEM analysis of the generator for a given position of the translator and in particular it shows the magnitude of the magnetic flux density in the generator at a given time. The value varies among 0.58 T and 0.7 T.

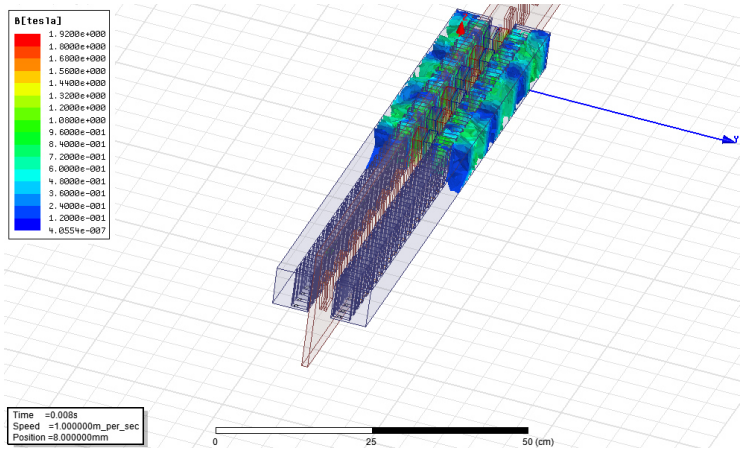

A) Initial Position magnets 8 mm

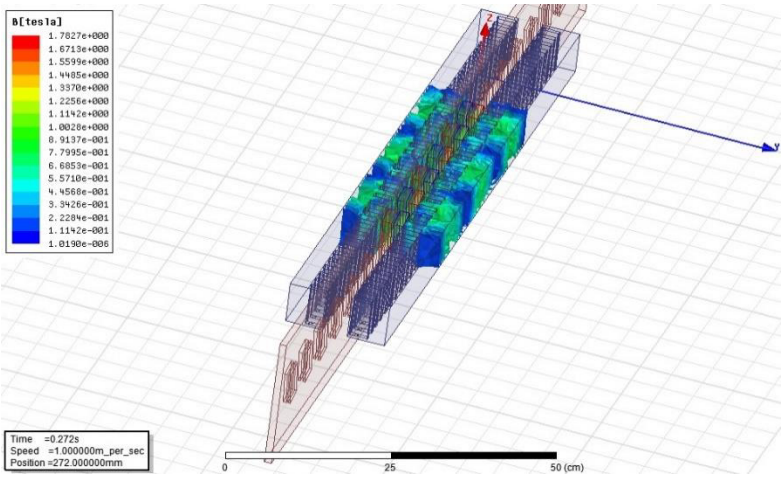

B) Position magnets 272 mm

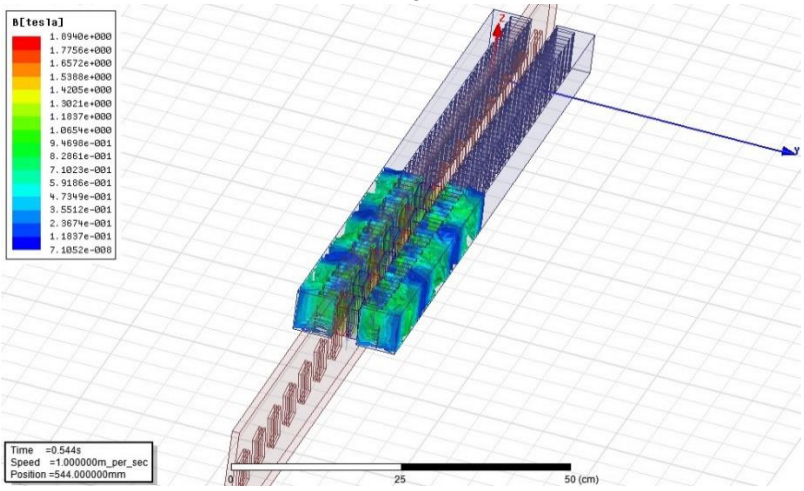

c) Final Position magnets 544 mm

Figure 5.19 Evaluation of Value of Magnetic Field

The testing of electrical generator was completed on December 2015. The aim was computed electrical characteristic of PMG. In the first laboratory experiment we measured resistance of the coils. The measure was carried out with a digital multimeter. The temperature observed is 24°C. The table 5.3 reports experimental results

RESISTANCE			
Coil A	***Resistance [Ω]***	***Coil B***	***Resistance [Ω]***
a36	12,637	b36	12,079
a35	12,6	b35	12,105
a34	12,616	b34	12,115
a33	12,577	b33	12,117
a32	12,687	b32	12,094
a31	12,628	b31	8,075
a30	12,642	b30	12,151
a29	12,617	b29	12,255
a28	12,613	b28	12,184
a27	12,54	b27	12,219
a26	12,624	b26	12,207
a25	12,618	b25	12,218
a24	12,587	b24	12,208
a23	12,635	b23	12,236
a22	12,586	b22	12,222
a21	12,583	b21	12,234
a20	12,581	b20	12,255
a19	12,641	b19	12,263
a18	12,558	b18	12,255
a17	12,627	b17	12,23
a16	12,671	b16	12,249
a15	12,635	b15	12,231
a14	12,7	b14	12,262
a13	12,586	b13	12,212
a12	12,686	b12	12,274
a11	12,62	b11	12,244
a10	12,65	b10	12,247
a9	12,645	b9	12,227
a8	12,651	b8	12,272
a7	12,769	b7	12,273
a6	12,697	b6	12,202
a5	12,61	b5	12,206
a4	12,653	b4	12,252
a3	12,672	b3	12,263
a2	12,678	b2	12,268
a1	12,666	b1	12,253

Table 5.3 Summary table of resistance measure

We noted a difference among two coils: the coils B present a mean value of resistance of 12.2 ohm while the value of coils A is 12.6 ohm.

5.4 Mechanical structure of the buoy - generator

The description of buoy-generator is the final step of the process of design of wave energy converter.

A lot of research has been carried out on the hydrodynamic behaviour of buoy based on the oscillation principle (first category) in an array. The hydrodynamic problem of wave power absorption is usually studied as a combination of two simpler problems: the diffraction problem (scattered incident wave field due to the presence of the WEC) and the radiation problem (wave field generated by the body).

The study of the generator buoy system was carried out by considering all the forces on the oscillating structure including the hydrodynamic forces. In simplified form, we consider two hypothesis:

a) The single degree of freedom motion of the buoy;
b) Simplified model of regular waves.[42]

The system is governed by equation (5.5)

$$\boldsymbol{m_t\ddot{z}(t) + b\dot{z} + cz + f = F_0 \cos(\omega t + \sigma)} \quad (5.5)$$

where:

- m_t is the virtual mass of the buoy including added mass;
- b is the hydrodynamic damping;
- c is the spring constant;
- f is the thrust from the linear generator;
- $F = F_0\, cos(\omega t + \sigma)$is the exciting wave force;
- z buoy vertical displacement.

The expression used in literature to identify the hydrodynamic damping for buoy is:

$$\boldsymbol{b = \frac{\pi^2 \rho g^2}{8\omega_n^3} \bar{A}^2 D} \quad (5.6)$$

where:

- ρ is density of sea water;
- $\omega_n = \sqrt{\frac{c}{m_T}}$ natural frequency of buoy in heave;
- D is the diameter of buoy
- $\bar{A}$ is a ratio of wave amplitude and amplitude of motion

The hydrodynamic forces, including excitation force, radiation impedance and hydrostatic force, are calculated by linear potential wave theory, and an analytical model is used for the linear generator. The buoys of different

dimensions are considered to explore the effect of buoy dimension on energy conversion and device efficiency.

When the wave generator is running, the buoy moves with the waves as longitudinal reciprocating motion. And it mainly affected by the three power: the buoyancy in seawater in, buoys' own gravity, and the generator's electromagnetic force. And buoys' own gravity includes generator's gravity and outer buoy's gravity. So the resultant force is :

$$\sum \boldsymbol{F} = \boldsymbol{F}_{\boldsymbol{buoyancy}} - \boldsymbol{G} - \boldsymbol{F}_{\boldsymbol{electromagnetic\ force}} \qquad (5.7)$$

where with G we consider the weight force of buoy and generator

The study of each part of equation above mentioned, it's primary to a correct size of system "Buoy+Generator".

In this thesis the choice of the excellent buoy is based on the comparison among two different layout: a vertical buoyant structure and a buoyant device with ellipse shape. In particular, it's possible underline that two floating structure could be used to exploit energy from sites with different sea conditions.

Power Buoy I	
Superior Floating	Ø= 3 [m]
	Thickness= 0.82 [m]
Inferior Floating	Ø= 3.22 [m]
Rigid Structural Part	L_P= 7.240 [m]
Total Length	L_T= 9.754 [m]
Length Submerged Section	L_S= 2.514 [m]

Table 5.4 Summary description of Power Buoy I

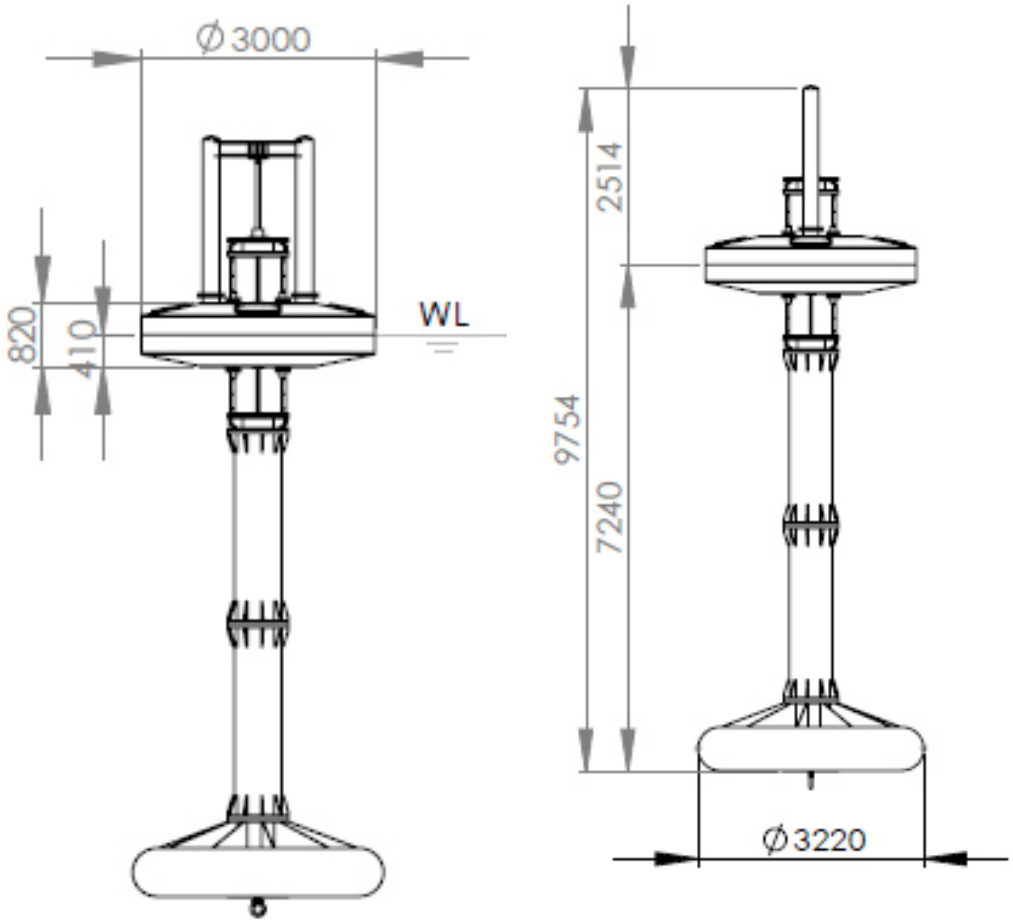

Figure 5.20 Plan and Design of Power Buoy I

Power Buoy 2	
Total Length	L_T= 4 [m]
Total Height	H_T= 5.3 [m]
Dimension Section A	D_A= 1.5 [m]

Table 5.5 Summary description of Power Buoy 2

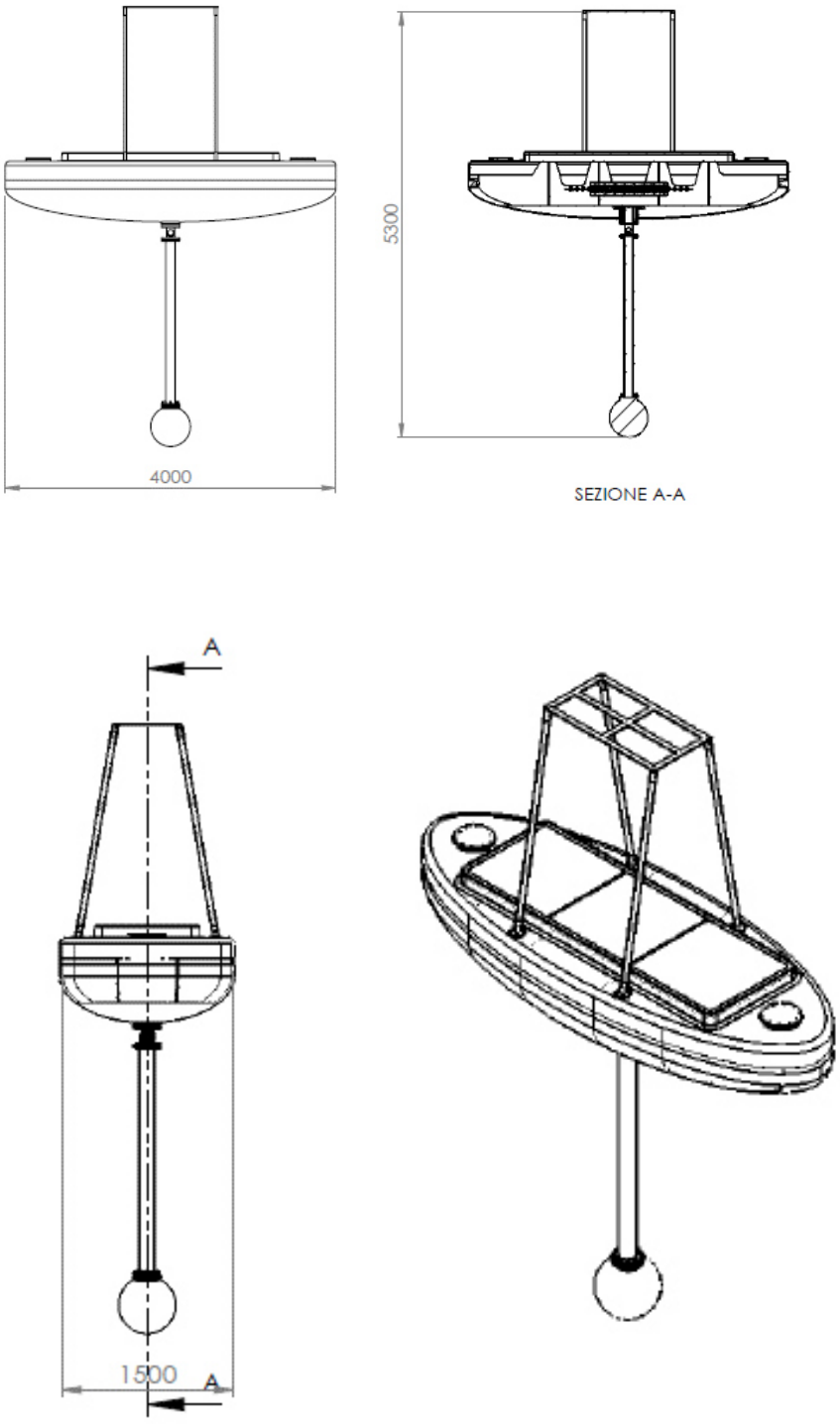

Figure 5.21 Plan and Design of Power Buoy 2

Considering the *Power Buoy 2*, the largest buoy can extract more energy at study location and the use of the submerged body allows the increase of the energy production; in addition the structure represents an innovative choice if we consider state of the art of buoyant WECs. The figure 5. 22 shows definitive design of it.

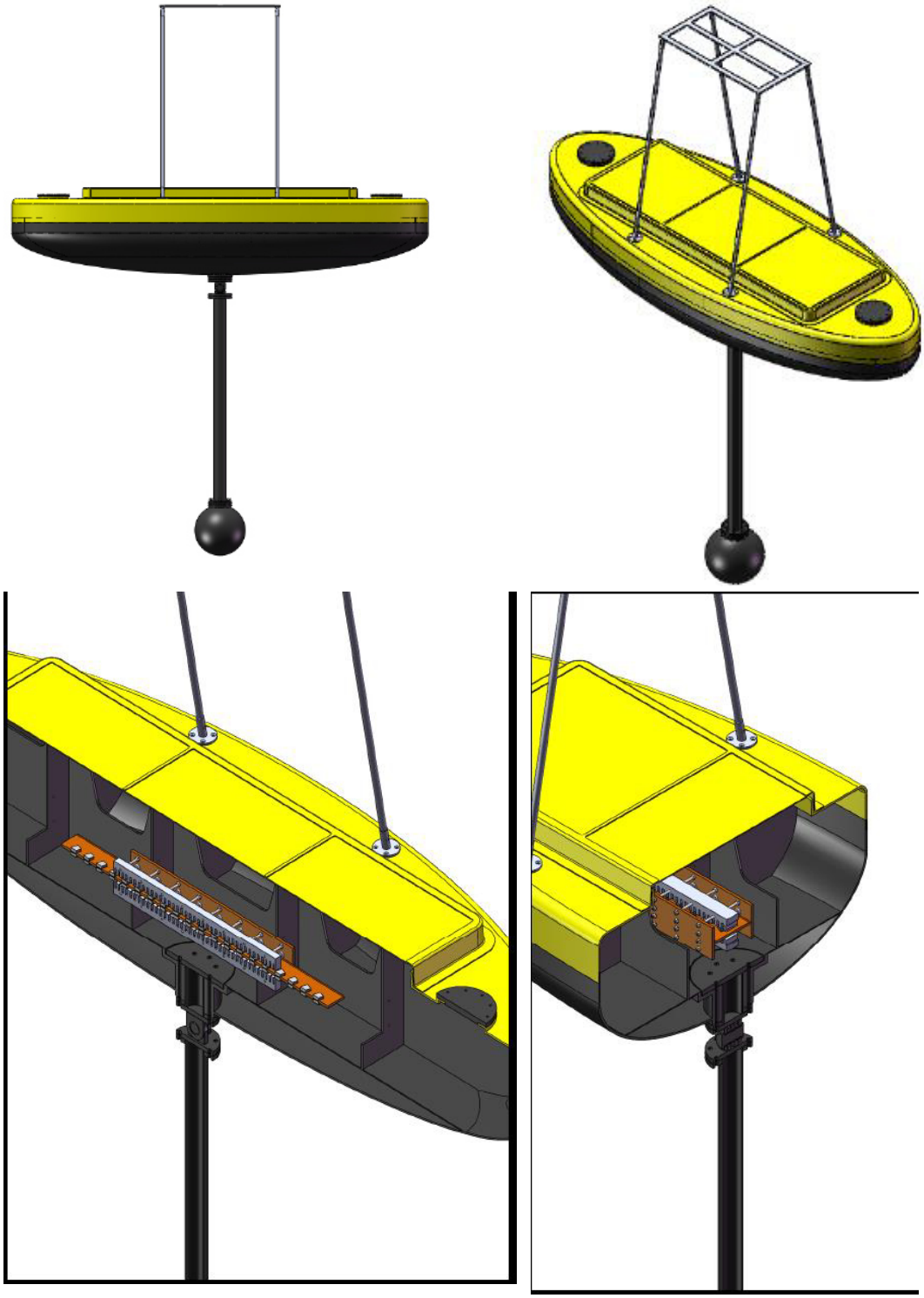

Figure 5.22 3D Definitive Model of Power Buoy Impetus

The installation and testing of the Power Buoy will be completed between March- April 2015 The system will be installed in two phases, with the buoy measure system being installed in March and the floating system in early April

5.5 *Hydrogen from The Sea: The Challenge of the Future*

Among the actions that the Kyoto Protocol innovative technologies are promoted, in particular the production of hydrogen. Different works create a system of production, storage and distribution of hydrogen.

For prevention of exhaustion of fossil fuels, renewable energy should supplied to meet the demand of the whole world. Intermittent electricity generated by solar cell or wind turbine or wave energy converts can be used as primary energy to create hydrogen using water. Hydrogen as an energy carrier has many advantages[43]:

- zero environmental impact, both globally and locally;
- producible from more primary energy sources, interchangeable and available on a large scale;
- distributed across a network.

Thus hydrogen is a clean, efficient and versatile energy carrier. Hydrogen exists on the earth only in combination with other elements and is produced from its compounds, using energy sources.

5.5.1 *Production of Hydrogen*

It can be obtained from a different variety of sources, such as fossil fuels or water, etc. In the figure below we propose a scheme of processing system of production of Hydrogen.

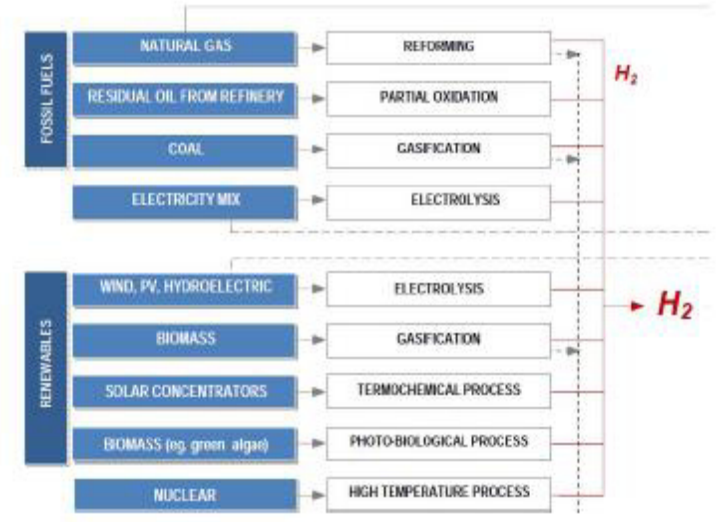

Figure 5.23 Scheme of Production Hydrogen[43]

Technologies for the production of hydrogen from fossil fuels (steam reforming, partial oxidation, gasification) are, as mentioned, mature and widely used (more than 95% of the hydrogen produced today comes from these processes).[44]

However, whatever the process and starting fuel used, production from fossil fuels, to be sustainable in the medium to long term, it must be coupled to CCS (Carbon Capture and Sequestration).

As for the production of it from renewable sources, can be identified:

- production from biomass;
- production from water.

Hydrogen can be produced from biomass through several thermochemical processes as gasification or pyrolysis and biological processes.

One of the possible renewable energy sources to be used to produce hydrogen is water, through electrolysis or thermochemical cycles In particular, the possible renewable energy sources used for the production of hydrogen is that wind through decentralized processes, can give life to produce both electricity and hydrogen.

In reality, wind turbines produce electricity, which in turn, through electrolyzer, hydrogen can be produced near to the wind turbines. The importance of these processes is related to the impossibility to control and may re ire the presence of wind electricity demand. We report a table of costs of hydrogen production processes.[43]

Tecnologia		**Stato Di Sviluppo**	**Emissioni CO_2**	**Tipologia Di Produzione**		**Costo Di Produzione**	
				Distribuita	**Centralizzata**	**Attuale**	**Futuro**
Natural Gas Steam Reforming	**No CCS**	Commercial Plants	Medium/ High		✓	5-9 €/GJ (GN 3-6 €/GJ) (20.000-250000 Nm^3/h)	
				✓	✓	19-22 €/GJ (<20.000 Nm^3/h)	21-25 €/GJ (2020)
	with CCS	Prototype in development	Low		✓	-	11-12 €/GJ (2020)
Coal Gasification	**No CCS**	Commercial Plants	High		✓	8-10 €/GJ (Carbone 1.5-2 €/GJ)	-
	with CCS	Prototype in development	Low		✓	-	10-12 €/GJ (2020)
Biomass Gasification		Pilot Plants	Low	✓	✓	10-25 €/GJ	10-20 €/GJ (2020)
Biological Processes		Lab stage	Low		✓	-	-
Electrolysis (electricity from electric grid		Commercial Units	*	✓	✓	25 €/GJ (E.E 0.0025 €/kWh) 200 €/GJ (E.E 0.20 €/kWh)	15-30 €/GJ (2030)
Thermochemical Cycles	**solar**	R&S stage	Zero		✓	-	20-30 €/GJ (2030
	nuclear	R&S stage	Zero		✓	-	10-20 €/GJ (2030

In this work we study the possibility of an integration among WEC converters that use wave motion to produce energy and electrolyzer that uses saline water. We use mathematical approaches and techniques developed and used in other field of science[45].

In figure 5. we report a scheme of this new integrated system.

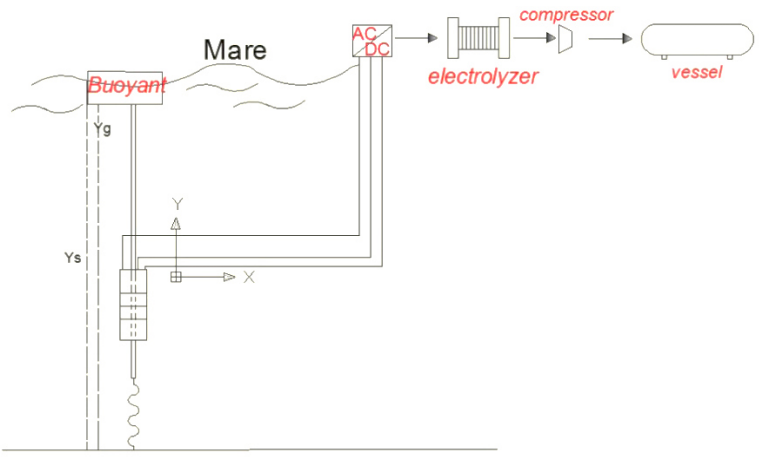

Figure 5.24 An integrated system of WEC plus Hydrogen

5.5.2 The electrolytic process for the production of hydrogen

Electrolysis is one of the most popular and simple methods used for the production of pure hydrogen. However, only a small percentage, about 4%, is manufactured by this process due to the high cost of the electrical energy.

It's governed by different parameters as thermodynamic and kinetic aspects that will be studied later.

A. Thermodynamic Analysis

The minimum value, or reversible, the cell voltage (E) is determined by the minimum value of the energy that must be supplied from the cell because the electrolysis takes place:[44]

$$\boldsymbol{E = -\frac{\Delta G}{nF}} \qquad (5.7)$$

where E is potential difference of balance, G is Gibbs free energy and F is Faraday's constant. So with appropriate modifications to the equation previously written:

$$E = -\frac{\Delta G}{nF} = \frac{RT}{2F}\ln\left(p_{H_2} \frac{p_{O_2}^{0.5}}{p_{H_2O}} \right) \tag{5.8}$$

Where p is the pressure. The equation shows that E increases with pressure. The potential is also dependent on temperature, mainly through the dependence of ΔG from temperature. The reaction is endothermic.

B. Kinetic Analysis

The reactions occur at the electrodes through a series of stages that involve the diffusion of the reagents towards the electrode. The presence of these various intermediate steps involves a dissipation of energy. In fact, you will have to take into account three contributions:[46]

- a cathodic overvoltage ηc and ηa an anodic overvoltage has to activate the electrolytic reactions and exceed the concentration gradients;
- E_Ω an ohmic drop due to the resistance to the electric current from the electrolyte, the electrode structure, the possible membrane or diaphragm.

So we can express the potential difference:

$$E = E_a + \eta_a - (E_c - \eta_c) + E_\Omega \tag{5.9}$$

$$E_\Omega = IR \tag{5.10}$$

$$\eta = \frac{RT}{\alpha_a nF}\ln\frac{i}{i°_a} + \frac{RT}{\alpha_c nF}\ln\frac{i}{i°_c} \tag{5.11}$$

where α is the coefficient of transfer of the electrolytic reaction ,i is the current density and i° is the density exchange current, which is proportional to the speed of exchange.

In conclusion, parameters as temperature or current density influence working of the electrolysis, an example current density determines the size of the electrodes and the price of the electrolyzer or an high operating temperature can be cause an increase of performance of it.

5.5.3 Case study

Alkaline water electrolysis is the technology used in present practice for large-scale electrolytic hydrogen production. Low efficiency, low current density and a lack of proper scale-up practice are the primary drawbacks of the

present technology. Significant improvements have been made, making it possible to reach improved cell efficiencies and higher current densities.

In this paper we proposed the use of saline water to product hydrogen. As far as using saline water, can be proposed two different scheme and technology. As regards the first option, is to subject the water to total desalination to remove all dissolved salts and produce distilled water. This distilled water can be subjected to electrolysis, alkaline electrolyte and electrolysis is cells.

In this case the most important disadvantage is the high cost caused by the process of osmosis or desalination.

The aim of this work is to design an electrolyze system capable of utilizing sea water for direct electrolysis. It is probable that these systems would operate at a low power density and electrolyze only a small portion of the water in contact with electrodes[47]

There are different disadvantages are: the rapid corrosion of electrodes or the production of undesirable products, anyway the realization of this new design could be possible lower capital cost and natural elimination of the waste brine. It may also be possible to recover economically significant quantities of the metals present in sea water, in particular magnesium in a form of magnesium hydroxide.

Sea water is a multicomponent natural electrolyte with sodium chloride as the main component. The process of electrolysis is a sum of space separated electrode reactions of cathodic hydrogen reduction and anodic oxygen evolving as a result of hydroxide-ion oxidation. The anodic chlorine evolution is also a possible reaction in sea water with NaCl as its main component.[48]

The reactions of the process of electrolysis are:

- the production of hydrogen at the cathode:

$$2H_2O + 2e^- \rightarrow H_2 + 2OH^- \qquad (5.12)$$

- the production of chlorine and oxygen at the anode:

$$6H_2O \rightarrow O_2 + 4H_3O^+ + 4e^- \qquad (5.13)$$

$$2Cl\_ \rightarrow Cl_2 + 2e^- \qquad (5.14)$$

The experimental set up is shown in figure 5.25 The power supply was able to emulate the voltage generated by a seawave power generator. Several tests were performed. The aim of the tests were:

1) to show that a seawave power generation system can produce hydrogen from sea water;
2) to quantify the hydrogen production under distorted regime;
3) to set up the optimum power electronics system to be used in order to maximize the hydrogen production in dependence of the type of electrodes to be used.

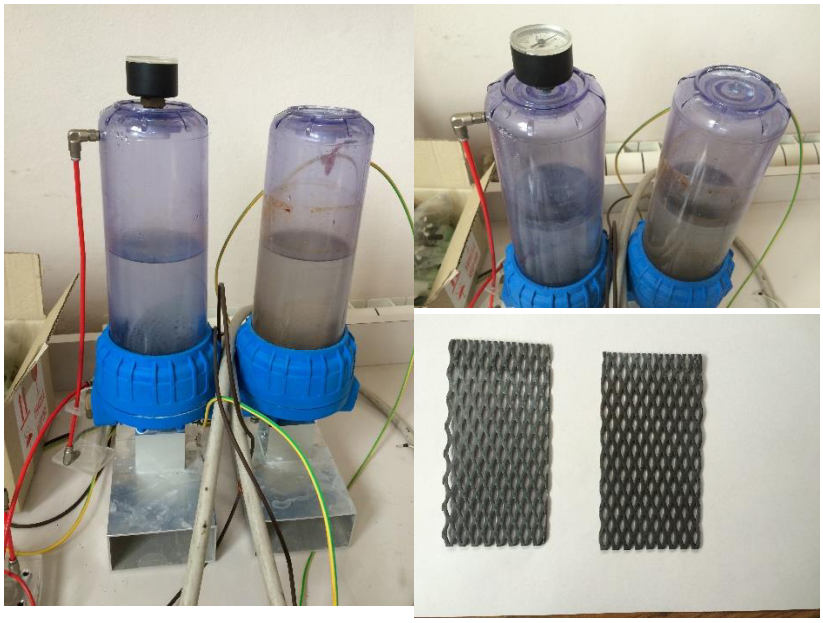

Figure 5.25 A prototype of sea water electrolyzer

In order to show that a seawave power generation system can produce hydrogen from sea water, we installed the electrolyzer in our generation buoy. The electrodes were supplied through the generator and a controlled rectifier. The system was able to produce hydrogen at a rate of 1/10 of mole per hour with a average height of wave of 55cm.

An exact quantification of the hydrogen production in terms of sea-condition was not possible. This was caused by the fact that in severe sea conditions the electrolyzer had severe hydrogen leakage and an exact quantification was not possible.

Several tests has been performed in order to optimize the type of electronics and to study the behavior of the system. We found that the structure of the system had to be composed by the generator, a controlled rectifier directly coupled to the electrodes. The rectifier had to be controlled by including in the control loop the wave height. As far as the type of electrodes to be used is concerned, we found that titanium electrodes had not a big advantage on steel electrodes.

5.6 Environmental Impact Assessment (EIA) of Wave Energy Converter

The evolution of WECs and the exploitation of sea to convert its energy in electrical energy influenced numerous studies in the analysis of environmental impact.

In its installation we should estimate impacts on the environmental components in chosen site. Another consideration regards the size of the device that could condition surrounding habitat. Moreover, take into consideration that different effects can be generated during the various phases of work: installation, operational phase and uninstall devices. So we consider this valuation as an essential step to create an eco-friendly electrical device.[49]

As for possible impact, we analysed:

- Noise Impact;
- Alteration of Magnetic Field;
- Visual Impact;
- Insertion of chemical pollution;
- Barrier of Marine Navigation.

The following assessments consider the environmental context in which it operates and the small size of the device being tested.

An aquaculture facility offshore is a place in itself can generate a number of effects on the environmental components which, however, will not analyse here. If you relate the area occupied by the device to the total area of the concession, this will be just the 0.0004%; also, the choice to use of a pre-existing mooring system allows to reduce to the minimum the operations at sea. The following table put in evidence the correlation among disturbances produce by the generator and environmental receptors.[50]

	Disturbances							
	Installation		Testing			Uninstallation		
Receptors	*Navigation*	*Mooring system*	*Mooring System*	*WEC*	*Chemical Covering*	*Navigation*	*Removal of WEC*	*Removal of mooring*
Wave Motion	-	-	-	L	-		-	-
Current	-	-	L	L	-		-	-
Sediments	-	-	-	-	-		-	-
Plancton	-	-	L?	L?	-		-	-
Comunity Fouling	-	M	M	M	-		M	M
Pelagic fish species	L	L	L	L	-		L	L
Demersal fish species	-	-	-	-	-		-	-
Invertebrates	L	L	L	L	-		L	L
Benthic macroinvertebrates	-	-	-	-	-		-	-
Infauna	-	-	-	-	-		-	-
Ornithological species	-	-	-	L	-		-	-
Cetaceans	-	-	-	-	-		-	-

Table 5.6 Correlation matrix disturbances-receptors. Legend: L = Light, Medium, H = high, L? = Difficult to quantify

Wave climates (wave motion and currents: it is reasonable to think that the generator will not lead to reduction of wave phenomena or variation of currents, since the installation of device is far away from the coastline.

Sediments: the use of pre-existing mooring system will not influence sediments.

Plankton: the generator and the mooring. system, as foreign bodies, may alter the natural movement of water masses generating effects on organisms in the plankton. However, this is a phenomenon difficult to quantify and, given the size of the device to be small. The device, addition, to generate energy does not require water to flow inside of circuits thereby avoiding accidental entrapment organisms.

Pelagic fish species: in literature we find as buoyant structure becomes attractor of a large number of species, both benthic (phytobenthos, zoobenthos), which are a useful substrate attack, and, above all, pelagic (grazers and predators), providing them with shelter from predators and food resources. These structures are known by the acronym FADS (*fish aggregating devices).*

Invertebrates: the only negative interactions could be established among the device, the mooring system and some invertebrates belonging to the *Phylum Cnidaria* that because of long filaments stinging bumping structures may remain adherent. It may still be a minor phenomenon.

Ornithological species: the emerged part of the generator may have an attractive effect with the bird species are able to take advantage of the floating structure as a roost. Exclude other forms of interaction.

5.6.1 Visual Impact

As for the evaluation of possible impacts, the visual impact represents the great among all. The impact is greater for WEC installed directly on the coast and for devices that have a considerable portion emerged. An additional source of impact of offshore WECS, can be linked to warning devices such for navigation, as lights, sound signals, radar reflectors and day markers. In the case study, the visual impact of the mark-generating as well as the visual signaling system, which is managed to minimize, is practically zero being the buoy installed about 1.5 km from the coast.

5.6.2 Noise Impact and Alteration of Magnetic Field

The noise impact is specific to device and it' s generated by noise above and below the free marine surface. In general, the noise s above the free marine surface is linked to devices such as the OWC, where the air processing fee is retained and then expelled, and this system generates noise. Noise below the free surface, instead, can be caused by devices that employ turbines, hydraulic pumps and moving parts. Our system does not present any of the characteristics enumerated above.

As for electromagnetic pollution, this is intrinsic in the mechanism of power generation but the emissions produced are minimal, as observed in the laboratory, and absolutely not create any impact on the surrounding environment and on marine life

5.6.3 Toxic Emissions

The main cause of toxic releases are leaks or accidental spills of liquids used by the systems that work with hydraulic fluids, or because of some materials, such as paint for ships which is often mixed with poison TBT to reduce marine growth. Each impact can be minimized by choosing non-toxic fluids,

through careful monitoring. In our case there are no oils or other fluids for generator operation and to protect the hull from the attack of microorganisms were normal antifouling paints normally used in yachting.

In conclusion, the device case study doesn't represent a great source of disruption to the environment because:

- Small size;
- Pre-existing mooring;
- The anthropic environment in which it operates
- Reduction in the hours of navigation to installation.

Conclusion

Word Energy Council has evaluated that 15% of the world's annual electricity needs could be met by systems that exploit the wave and that the annual demand of electricity in the world is about 15,000 TWh. So the energy obtainable globally, wave and in the order of 8^6 - 8^7KWh / year.

One of the main attractions of wave energy capture over tidal stream technology is the size of the resource. It is at least an order of magnitude greater than tidal stream. Despite this, it is not an easy technology to commercialise and a number of failures over the past decade have shown just how easy it is to underestimate the difficulties associated with designing a robust wave energy converter (WEC) given the extreme conditions to which it may be exposed.

It' s possible identify main detriments of wave energy converters:

- the modest efficiency of conversion achievable by generating systems;
- the unreliability of the mooring systems;
- problems on energy storage in situ.

The most critical aspect for the development of a system WEC is represented by the economical optimization: its costs must be compared to the stability, the hydraulic performance and energy efficiency of the device.

The prototype made in Sicily (principal subject of this work) presents characteristics that exceed some of the problems previously exposed.

Numerous experimental tests have shown as the system has a nominal power of 1 kW and that the site chosen for the installation of our device shows of equivalent hours of working of 1920 hours.

So it is possible to obtain for the conversion of hydrogen 1920 kWh annually for wave energy converter installed that through the electrolytic conversion leads to the production of 35 kg of hydrogen. The use of a fleet for public transport powered by hydrogen would need then assuming an electromechanical conversion efficiency of the order of 50% to 25 devices for each vehicle in the fleet. In conclusion the use of 150 m^2 of the sea would power a transport vehicle for a year.

It' possible to underline some of the main aspects of Power Buoy:

- low environmental and visual impact;
- possible integration in port facilities, in offshore installation and / or marine installations as fish farming;

- integration with other renewable sources (wind or photovoltaic system).

As for the further moves will directed to optimization of electrical generator and a new site of installation of wave energy converter.

In fact, the western Sardinia coast and the Sicily Channel are found to be among the most productive areas in the whole Mediterranean. Simulation results show the presence of significant spatial variations of wave power availability even on relatively small spatial scales along these two coastlines.

Another improvement regards buoy data that will implemented with a new measure system (pressure sensors) of height of sea wave and PV cells will assembled in all external surface of buoy.

As regards permanent magnet linear generator, an optimization procedure will adopted. The principal aim of it will be a reduction of cogging force among translator and iron stator and an increase of voltage.

Recent FEM simulations of its generator have shown as a change of inclination of magnets could satisfy aims (above mentioned). The parameters of the machines that has built are in good accordance to the ones that has been computed by the design approach chosen. The machine can be used to produce direct current to be used for hydrogen production.

So in this work I designed a prototype of new type of energy conversion: wave energy could become a valid energy alternative for islands that could convert the sea a source of prosperity.

References

[1] B. Sørensen, *Renewable energy: its physics, engineering, use, environmental impacts, economy, and planning aspects*, 3rd ed. Amsterdam ; Boston: Elsevier Academic Press, 2004.

[2] A. F. de O. Falcão, «Wave energy utilization: A review of the technologies», *Renew. Sustain. Energy Rev.*, vol. 14, n. 3, pagg. 899–918, apr. 2010.

[3] W. Sheng, R. Alcorn, e A. Lewis, «On improving wave energy conversion, part I: Optimal and control technologies», *Renew. Energy*, vol. 75, pagg. 922–934, mar. 2015.

[4] World Meteorological Organization, *Guide to wave analysis and forecasting*, 2nd ed. Geneva, Switzerland: Secretariat of the World Meteorological Organization, 1998.

[5] M. E. McCormick, *Ocean wave energy conversion*, Dover ed. Mineola, N.Y: Dover Publications, 2007.

[6] APAT, *Italian Wave Atlas*. .

[7] D. Vicinanza, P. Contestabile, e V. Ferrante, «Wave energy potential in the north-west of Sardinia (Italy)», *Renew. Energy*, vol. 50, pagg. 506–521, feb. 2013.

[8] L. Liberti, A. Carillo, e G. Sannino, «Wave energy resource assessment in the Mediterranean, the Italian perspective», *Renew. Energy*, vol. 50, pagg. 938–949, feb. 2013.

[9] A. Viola, M. Trapanese, e V. Franzitta, «Evaluation of the potential energy from wave motion on the Sicilian coast», 2013, pagg. 1–5.

[10] T. Ching-Piao, H. Ching-Her, H. Chien, e C. Hao-Yuan, «Study on the wave climate variation to the renewable wave energy assessment», *Renew. Energy*, vol. 38, n. 1, pagg. 50–61, feb. 2012.

[11] V. Franzitta, M. Trapanese, C. Giaconia, P. Ferrara, e A. Viola, «Design and experimental test of a low costweather buoy», 2013, pagg. 1–5.

[12] Franzitta V., Di Dio V., Viola A., Giaconia C., Ferrara P., e Trapanese M., «Experimental results of a low cost weather buoy», presentato al OCEANS 2013 MTS/IEEE - San Diego: An Ocean in Common, San Diego.

[13] Kashino Ranolph, «Curent State of Wave Measuring Technology from Buoys», presentato al Recent adavances and issues in wave buoy technologies.

[14] Johan Kuperus, «Wave Monitoring using Wireless Sensor Nodes», The University of Melbourne, Australian Insititute of Marine Science.

[15] SI OCEAN, «Ocean Energy: State of the Art». .

[16] B. Zanuttigh e E. Angelelli, «Experimental investigation of floating wave energy converters for coastal protection purpose», *Coast. Eng.*, vol. 80, pagg. 148–159, ott. 2013.

[17] M. S. Lagoun, A. Benalia, e M. E. H. Benbouzid, «Ocean wave converters: State of the art and current status», 2010, pagg. 636–641.

[18] Waveplam, «State of the Art Analysis: A Cautiously Optimistic Review of the Technical Status of Wave Energy Technology». 2009.

[19] Waveplam, «Report on the State of the art, non-technological barriers and best practices». .

[20] L. Szabo, C. Oprea, I.-A. Viorel, e K. A. Biro, «Novel Permanent Magnet Tubular Linear Generator for Wave Energy Converters», 2007, pagg. 983–987.

[21] J. Prudell, M. Stoddard, E. Amon, T. K. A. Brekken, e A. von Jouanne, «A Permanent-Magnet Tubular Linear Generator for Ocean Wave Energy Conversion», *IEEE Trans. Ind. Appl.*, vol. 46, n. 6, pagg. 2392–2400, nov. 2010.

[22] Jiabin Wang, G. W. Jewell, e D. Howe, «A general framework for the analysis and design of tubular linear permanent magnet machines», *IEEE Trans. Magn.*, vol. 35, n. 3, pagg. 1986–2000, mag. 1999.

[23] G. Cipriani, V. Di Dio, V. Franzitta, A. Russo, M. Trapanese, A. Viola, «A Ferrite Tubular Linear Permanent Magnet Generator (FTLPMG) analysis and design», 2014.

[24] J. Wang, D. Howe, e G. W. Jewell, «Analysis and Design Optimization of an Improved Axially Magnetized Tubular Permanent-Magnet Machine», *IEEE Trans. Energy Convers.*, vol. 19, n. 2, pagg. 289–295, giu. 2004.

[25] Vincenzo di Dio, Giovanni CIPRIANI1, Rosario MICELI, e Renato Rizzo, «Design Criteria of Tubular Linear Induction Motors and Generators: a Prototype Realization and its Characterization», *Leonardo Electronici Journal of Pratices and Technologies*.

[26] «Ansoft HFSS Fundamentals - Maxwell3D.pdf». .

[27] H. Polinder, B. C. Mecrow, A. G. Jack, P. G. Dickinson, e M. A. Mueller, «Conventional and TFPM Linear Generators for Direct-Drive Wave Energy Conversion», *IEEE Trans. Energy Convers.*, vol. 20, n. 2, pagg. 260–267, giu. 2005.

[28] J. Lima, A. Pronto, e M. V. Neves, «Transverse Flux Permanent Magnet Generator for Ocean Wave Energy Conversion», in *Technological Innovation for Sustainability*, vol. 349, L. M. Camarinha-Matos, A c. di Berlin, Heidelberg: Springer Berlin Heidelberg, 2011, pagg. 537–544.

[29] W. M. Arshad, P. Thelin, T. Backstrom, e C. Sadarangani, «Use of Transverse-Flux Machines in a Free-Piston Generator», *IEEE Trans. Ind. Appl.*, vol. 40, n. 4, pagg. 1092–1100, lug. 2004.

[30] V. Franzitta, A. Viola, e M. Trapanese, «Design of a transverse flux machine for power generation from seawaves», *J. Appl. Phys.*, vol. 115, n. 17, pag. 17E712, mag. 2014.

[31] M. Trapanese, «Optimization of a Sea Wave Energy Harvesting Electromagnetic Device», *IEEE Trans. Magn.*, vol. 44, n. 11, pagg. 4365–4368, nov. 2008.

[32] J.-S. Shin, T. Koseki, e H.-J. Kim, «Proposal of Double-Sided Transverse Flux Linear Synchronous Motor and a Simplified Design for Maximum Thrust in Nonsaturation Region», *IEEE Trans. Magn.*, vol. 49, n. 7, pagg. 4104–4108, lug. 2013.

[33] H. Arof, W. Nor, e K. M. Nor, «Linear generator: design and simulation», 2003, pagg. 306–311.

[34] D. Elwood, S. C. Yim, J. Prudell, C. Stillinger, A. von Jouanne, T. Brekken, A. Brown, e R. Paasch, «Design, construction, and ocean testing of a taut-moored dual-body wave energy converter with a linear generator power take-off», *Renew. Energy*, vol. 35, n. 2, pagg. 348–354, feb. 2010.

[35] B. Li, D. E. Macpherson, e J. K. H. Shek, «Direct drive wave energy converter control in irregular waves», 2011, pagg. 64–64.

[36] K. J. Strnat, «Modern permanent magnets for applications in electro-technology», *Proc. IEEE*, vol. 78, n. 6, pagg. 923–946, giu. 1990.

[37] International Conference on Electrical, Electronic and Computer Engineering, Jāmiʿat ʻAyn Shams, e Institute of Electrical and Electronics Engineers, *ICEEC'04: 2004 International Conference on Electrical, Electronic and Computer Engineering: proceedings: 5-7 September, 2004, Cairo, Egypt PERMANENT MAGNET LINEAR GENERATOR DESIGN USING FINITE ELEMENT METHOD*. Piscataway, N.J: IEEE, 2004.

[38] International Conference on Electrical Machines, *ICEM 2010 proceedings - Linear Generator for Direct Drive Wave Energy Applications*. [S. l.]: IEEE, 2010.

[39] R. P. G. Mendes, M. R. A. Calado, e S. J. P. S. Mariano, «Wave energy potential in Portugal–Assessment based on probabilistic description of ocean waves parameters», *Renew. Energy*, vol. 47, pagg. 1–8, nov. 2012.

[40] L. Liberti, A. Carillo, e G. Sannino, «Wave energy resource assessment in the Mediterranean, the Italian perspective», *Renew. Energy*, vol. 50, pagg. 938–949, feb. 2013.

[41] P. P. Silvester, e Ferrari, R. L., *Finite elements for electrical engineers*. New York: Cambridge University Press, 1996.

[42] S. Bozzi, A. Miquel, A. Antonini, G. Passoni, e R. Archetti, «Modeling of a Point Absorber for Energy Conversion in Italian Seas», *Energies*, vol. 6, n. 6, pagg. 3033–3051, giu. 2013.

[43] Mattucci A. e Calisi M., «MODELLO IDROGENO TIMES». ENEA, 2010.

[44] Abdel-Aal H.K., Zohdy K.M., e Kareem Abdel, «Hydrogen Production Using Sea Water Electrolysis», *The Open Fuel Cells Journal*, vol. 3, pagg. 1–7, 2010.

[45] Di Dio V., Franzitta V., Muzio F., Scaccianoce G., e Trapanese M., «The use of sea waves for generation of electrical energy and Hydrogen», [Piscataway, N.J.], 2009.

[46] V. Franzitta, A. Viola, e M. Trapanese, «Hydrogen from the sea: The challenge of the future. Present and future developments», 2014, pagg. 1–4.

[47] Z. Kato, K. Izumiya, N. Kumagai, e K. Hashimoto, «Energy-saving seawater electrolysis for hydrogen production», *J. Solid State Electrochem.*, vol. 13, n. 2, pagg. 219–224, feb. 2009.

[48] J. Bennett, «Electrodes for generation of hydrogen and oxygen from seawater», *Int. J. Hydrog. Energy*, vol. 5, n. 4, pagg. 401–408, 1980.

[49] A. Copping, H. Battey, J. Brown-Saracino, M. Massaua, e C. Smith, «An international assessment of the environmental effects of marine energy development», *Ocean Coast. Manag.*, vol. 99, pagg. 3–13, ott. 2014.

[50] R. H. Leeney, D. Greaves, D. Conley, e A. M. O'Hagan, «Environmental Impact Assessments for wave energy developments – Learning from existing activities and informing future research priorities», *Ocean Coast. Manag.*, vol. 99, pagg. 14–22, ott. 2014.

[51] «IEA_ocean05 - Poster_Ocean_Energy.pdf». .

[52] V. Sanil Kumar e T. R. Anoop, «Wave energy resource assessment for the Indian shelf seas», *Renew. Energy*, vol. 76, pagg. 212–219, apr. 2015.

[53] Baodong Bai, Jin Lu, e Bing Xu, «The research of external buoy wave permanent magnet linear generator's design». Electrical Machines and Systems (ICEMS), 2011.

[54] N. Jiang, H.-M. Meng, L.-J. Song, e H.-Y. Yu, «Study on Ni–Fe–C cathode for hydrogen evolution from seawater electrolysis», *Int. J. Hydrog. Energy*, vol. 35, n. 15, pagg. 8056–8062, ago. 2010.

[55] *Policy Report, IEA-OES, 2006 IEA Statistics for 2004, FORM OF OCEAN ENERGY, ESTIMATED GLOBAL RESOURCES*,

[56] I. K. Igumenov, N. V. Gelfond, P. S. Galkin, N. B. Morozova, N. E. Fedotova, G. I. Zharkova, V. I. Shipachev, E. F. Reznikova, A. D. Ryabtsev, N. P. Kotsupalo, V. I. Titarenko, Y. P. Dikov, V. V. Distler, e M. I. Buleev, «Corrosion testing of platinum metals CVD coated titanium anodes in seawater-simulated solutions», *Desalination*, vol. 136, n. 1–3, pagg. 273–280, mag. 2001.

[57] G. Scrivano, A. Piacentino, e F. Cardona, «Experimental characterization of PEM fuel cells by micro-models for the prediction of on-site performance», *Renew. Energy*, vol. 34, n. 3, pagg. 634–639, mar. 2009.

[58] K. Rhinefrank, E. B. Agamloh, A. von Jouanne, A. K. Wallace, J. Prudell, K. Kimble, J. Aills, E. Schmidt, P. Chan, B. Sweeny, e A. Schacher, «Novel ocean energy permanent magnet linear generator buoy», *Renew. Energy*, vol. 31, n. 9, pagg. 1279–1298, lug. 2006.

[59] R. Balaji, B. S. Kannan, J. Lakshmi, N. Senthil, S. Vasudevan, G. Sozhan, A. K. Shukla, e S. Ravichandran, «An alternative approach to selective sea water oxidation for hydrogen production», *Electrochem. Commun.*, vol. 11, n. 8, pagg. 1700–1702, ago. 2009.

[60] K. Meier, «Hydrogen production with sea water electrolysis using Norwegian offshore wind energy potentials: Techno-economic assessment for an offshore-based hydrogen production approach with state-of-the-art technology», *Int. J. Energy Environ. Eng.*, vol. 5, n. 2–3, pagg. 1–12, lug. 2014.

[61] E. E. Bachynski, Y. L. Young, e R. W. Yeung, «Analysis and optimization of a tethered wave energy converter in irregular waves», *Renew. Energy*, vol. 48, pagg. 133–145, dic. 2012.

[62] K. K. Ahn, D. Q. Truong, H. H. Tien, e J. I. Yoon, «An innovative design of wave energy converter», *Renew. Energy*, vol. 42, pagg. 186–194, giu. 2012.

[63] L. Margheritini, D. Vicinanza, e P. Frigaard, «SSG wave energy converter: Design, reliability and hydraulic performance of an innovative overtopping device», *Renew. Energy*, vol. 34, n. 5, pagg. 1371–1380, mag. 2009.

Annex I

Design and Optimization of a Thermomagnetic Motor

Introduction

The use of new forms of energy can strongly help to satisfy the constantly increasing demand of energy. The purpose of this work is to show that a Thermomagnetic Motor which can rotate continously and has useful mechanical characteristics is feasible. Such a motor could be coupled to an electric generator to produce electrical energy. A thermomagnetic motor is a motor that directly converts thermal energy into kinetic energy. This kind of motor is also named Curie motor

In this type of motor the driving force is generated by a thermally induced permeability difference in two areas of the rotor. More precisely, the heating of one side of the rotor modifies locally the permeability of the soft magnetic material in comparison with the cool area of the rotor and this permeability difference can generate a force if the rotor is placed in a magnetic field. This force can be enhanced if the hot side temperature of the rotor is above the Curie's temperature of the magnetic material and the cold side under this temperature. If the geometry and the cooling/heating system of the motor allows to continuously keep the temperature, a continuous driving force is generated[1]

Unfortunately. traditional ferromagnetic materials have very high Curie's temperature and therefore their ferromagnetic phase transition cannot be used. As the result Curie motors built by using traditional materials have very poor performances. Experimental realization of the motor has been shown several times most of the applications presents a reciprocating motion and in all the experimental applications a relatively low speed and a very low torque have been obtained. The objective of this study is to show that a rotating Curie motor which presents useful mechanical characteristics is feasible.

Thermal Energy can be directly converted into kinetic energy in a Curie motor [2].In this type of motor the torque is produced by a permeability difference due to a temperature gradient in two areas of the rotor. This force can be enhanced if in the hot side the temperature of the rotor is above the Curie point of the magnetic material. If the geometry and the cooling/heating system of the motor allow to continuously keep the temperature, a continuous toque can be generated.

Several experimental realizations of the motor have been reported [3] but in all the experimental applications only a relative low speed, a very low torque and a discontinuous pulsed regime have been obtained. These poor features have been caused by the fact that in the force generation process two physical phenomena (thermalization and magnetization) characterized by two different time scale are involved. Because of that, no application (but some simple toys) has been found for Curie motors.

This study presents an optimization procedure based on a mathematical model which uses the d-q axis general theory of electric machines. This models shows on one hand how a Curie motor is equivalent to a d.c. machine and on the other hand it is able to describe the thermal processes that influences the motor working condition. These features allowed to optimize and build a motor which is able to rotate continuosly.

The annex is divided as follows: after the introduction in section I the principle of operation of the proposed motor is explained, in section II the dq axis theory of the Curie motor is briefly recalled, in section III the developed theory is used to discuss the design of the motor, and its structure in section IV the description of optimization procedure while in V section some experimental results are shown and finally in section VI some conclusions are drawn.

I Principle of Operation of Curie Motor

The principle of operation of the Curie-motor can be explained by fig. 1. The excitation magnetic field is obtained by a fixed permanent magnet and in order to generate a torque, one part of the rotor is heated and the other part is cooled. If the warm side of the armature is heated above Curie temperature, it behaves magnetically like air or vacuum. Thus the energy density of the magnetic field at the hot side increases and the permeability decreases, on the contrary, at the cold side of the armature, the energy density remains low and the magnetic permeability high.

As a result, a torque is generated and the rotor can start moving. Under the mentioned conditions the Curie-motor performs like a conventional magnetic device. In reality however, the Curie-motor will not produce a sharp boundary surface between warm and cold side. However, a sharp difference in the magnetic properties of the rotor are induced in the area at Curie Temperature. This effect allows to define a line of the rotor where the phase transitions takes place. This line is called Phase Transition Line.

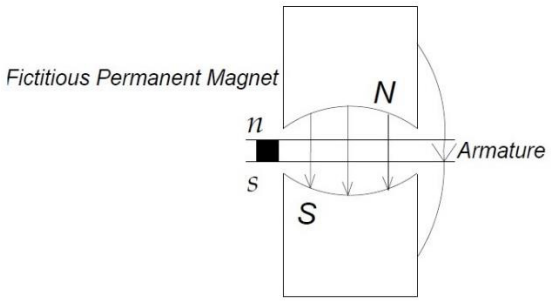

Figure.1. A Curie linear motor, with a soft magnetic, movable armature. The magnetization and temperature varies between the hot and the cold side [4].

II The Dq Axis Theory of the Curie Motor

The use of d-q axis theory of electric machines to describe Curie motor faces a fundamental difficulty: in Curie motor nor currents neither voltages are involved. As a result, one could think that d-q theory is not applicable to Curie motor. However in [4] it has been shown how this difficulty can be overcome by comparing field distribution of a Curie motor to the field distribution of a d.c. machine.

Accordingly to what said above, the set of dynamic equations that describe a Curie motor, in stationary conditions and under the hypothesis of a constant excitation field, reads as follows:

$$\begin{aligned} \varphi &= kI_d = const \\ C &= M_{dq} I_d I_q \\ V_q &= R_q I_q + \omega M_{dq} I_d \end{aligned} \qquad (1)$$

Where ϕ is the excitation flux, k is a constant, Id is a fictious current along the direct axis that is able to generate the excitation flux, V_q is the voltage on the quadrature axis circuit, R_q is the resistance of the armature, I_q is a fictious current along the quadrature axis that describes the magnetic poles needed to generate the field distribution induced by the temperature gradient, ω is the rotational speed, M_{dq} describes the magnetic coupling between d and q axis, C is the electromagnetic torque.

The physical meaning of the electrical quantities used in eqs 1 have been clarified in [4] and are briefly recalled below

Equation 1a describes the excitation flux. Because of the fact that excitation is generated by a permanent magnet., eq. 1 is absolutely identical to

the equation used to describe the excitation of a traditional dc machine and no novelty is found in this case. As a result Id is a current that the describe the excitation flux and, in a first approximation, is constant and does not depend on the armature temperature.

Equation 1b describes the torque generated by the curie motor and contains the novelties related to the description of a Curie motor. In a Curie motor the torque is generated by the permeability difference between hot and cold spot. As already said, I_d describes the excitation and, therefore, I_q is related to the permeability difference induced by the temperature gradient. At stand still T_h and T_c are governed by the convection heat exchange with the cooling and heating system and the thermal conduction between the hot and cold spots inside the rotor. By using lumped parameters the temperature difference can be expressed as follows:

$$T_c - T_h = \frac{L}{kS} \cdot \frac{dq}{dt} \tag{2}$$

where T_c is the temperature at the cold spot, T_h is the temperature at hot spot, L is the distance, k is the thermal conductivity, S is the surface normal to the heat flow and dq/dt the heat rate. At stand still heat flows from the hot spot to the cold spot and a constant temperature gradient is established. The maximum and minimum temperature T_h and T_c can be adjusted by adjusting the heat rate that is imposed by the temperature of the cooling and heating fluids.[3] These temperature imposes (through the magnetic characteristics of the material) the permeability difference and therefore determines I_q. If one assumes that T_h and T_c are respectively above and below the Curie temperature of the material and that permeability difference around the ferromagnetic critical point is proportional to a power of this temperature difference, one can express I_q as follows:

$$I_q = k_1 \Delta T^{\nu} = k_1 \left(\frac{L}{kS} \frac{dq}{dt} \right)^{\nu} \tag{3}$$

Where ν is the exponent that describes the dependence of the permeability difference on the temperature difference, and k_1 is a constant that allows to match the lumped parameter to the real values. If eq. (3) is compared to eq. (1c), one can see that voltage in dq theory is played by the heat rate (in a non linear way if ν is different from 1).

If eq (3) is used to express in Iq in (1b), one obtains:

$$C = \frac{M_{dq} k_1 L^{\nu}}{k^{\nu} S^{\nu}} I_d \cdot \left(\frac{dq}{dt} \right)^{\nu} \tag{4}$$

If the rotor is moving the physical phenomenon involved does not remain the same but one must also include the advection (the change in the thermal energy of a mass as it moves through space). As a result, one can show that the temperature difference can be roughly expressed (at least in the regimes feasible for a Curie motor) as

$$\Delta T = k_2 e^{-d\omega} \tag{5}$$

Where d is the distance between hot and cold spots and □ is the angular speed, k2 is an angular constant that takes into account the geometrical details. In [4] it is shown how, this mathematical model is able to describe experimental results published by other authors [3]

III Design of a thermomagnetic motor and Structure of the machine

In order to obtain the first design of the thermomagnetic motor the mathematical model above outlined has been used. More particularly, it is combined the required performances with the magnetic characteristics of the material in order to obtain a preliminary design. In particular, must be satisfied:

a) a high torque is related to a high heat flow;

b) the higher the temperature difference between hot and cold spot, the higher the achievable speed;

c)the higher the permeability difference between hot and cold spot, the higher the achievable torque;

d)the temperature difference is inversely proportional to the surface perpendicular to heat flow between hot and cold spot

The above said considerations implies that the structure of the machine should be as sketched in fig. 2.

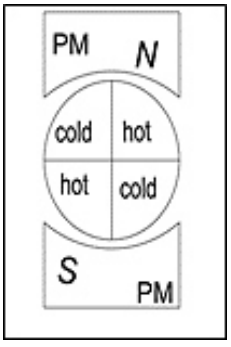

Figure.2 The structure of the rotor of a thermomagnetic machine.

It can be seen from the equations above presented and from fig. 2 the following facts:

1)A hot and a cold side is needed for each pole;

2)The angle between the line which divides the hot and cold sides (i.e. the transition line) and the direct magnetic axis influences the torque;

3)The transition line position does not depend on the rotational speed but does depend on the position of the cold and hot heat source;

4)Torque depends on the permeability difference induced by the temperature difference between hot and cold side and on the position of the heat sources;

5)Temperature difference depends on rotational speed and on the thermal coupling between the heat and cold sources.

The above outlined consideration together with some analytical consideration have produced a preliminary design that has been refined trough a numerical multiphysics analysis.

The main characteristics of this design is that the thermal coupling between the rotor and the heat sources has been maximized, by maximizing the coupling surfaces. As a result, the structure of the rotor is obtained by using several tubes installed along a circumference. The tubes perform to task: they contain the ferromagnetic material which undergoes to the ferromagnetic transition and they allow to maximize the heat exchange.

The machine obtained is shown in fig.3.

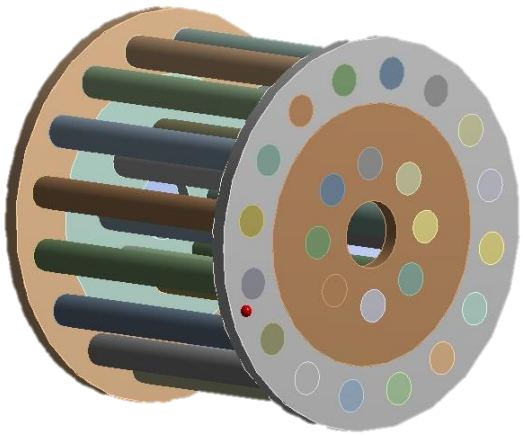

Figure.3 The structure of the rotor of a thermomagnetic machine.

As already said the structure of the rotor has been designed by using a numerical multiphysics approach. The stator of the machine is obtained by using the stator of a single pole of a dc machine. The field generated by the stator was equal to 0.9T.

The heat source is guaranteed by an electromagnetic source which emits infrared rays. The heat sink is obtained by using cool water. The rotor consists of an array of tubes circularly placed (fig.4). The radius of the rotor is 11 cm.

Each tube is able to contain the ferromagnetic material and to guarantee the correct flow of the heat. The external diameter of the tube is 20mm.

The tube consists of two regions separated by two layers: in the inner region is contained the cooling fluid, in the external region the ferromagnetic material, the inner layer is made of aluminum and the external layer of plastic material. The function of the aluminum is to shield the fluid from infrared rays and to let the ferromagnetic material follow the optimum temperature cycle by maximizing the heat exchange and therefore the torque production. In fig. 4 the section of the tube is shown.

Figure.4 Section of a tube.

Inside the tube is placed the ferromagnetic material, which guarantees the torque production. In order to maximize the torque production the ferromagnetic material must undergo to the ferromagnetic phase transition between the hot and the cold side, as a result the choice of the ferromagnetic material sets the operating point of the machine.

Unfortunately, the traditional ferromagnetic materials (iron, nickel, etc) have very high Curie temperatures and are not suitable to maximize the torque production. Only one ferromagnetic material, Gadolinium, has a Curie temperature which allows to obtain an easily usable Curie temperature. As a result, Gadolinium has been used as the ferromagnetic material of this motor. Gadolinium powder, was inserted inside the external area of the tube. The Curie's temperature of Gadolinium powder is 293 K.

IV Optimization of a Thermomagnetic Motor

The optimization procedure that has been followed had as main objective the maximization of the power under a continuous rotational regime and a constant use of active magnetic material. We choose to set as constant speed a target of 1/10 rad/sec (equivalent to a revolution per minute) by using 0.5 Kg of gadolinium

From a mathematical point of view this is equivalent under the assumptions above said, the optimization problem is equivalent to maximize the torque with the constraints to use 0.5 Kg of Gadolinium. The optimization function is therefore:

$$Max(C = \frac{M_{dq} k_1 L^{\nu}}{k^{\nu} S^{\nu}} I_d \cdot \left(\frac{dq}{dt}\right)^{\nu}) \qquad (6)$$

With a constraints on the volume of active material used in the rotor.

In order to obtain the draft design of a thermomagnetic motor the mathematical model above outlined has been used as. More particularly eq.4, 5 and 2 can be combined together with the magnetic characteristics of the magnetic material in order to obtain a preliminary design. Eqs. 2, 4 and 5 show that in order to obtain the required performances the following points must be satisfied:

a) a high torque is related to a high heat flow (eq2);

b) the higher the temperature difference between hot and cold spot, the higher the achievable speed (eq.5);

c)the higher the permeability difference between hot and cold spot, the higher the achievable torque(eq. 4);

d)the temperature difference is inversely proportional to the surface perpendicular to heat flow between hot and cold spot (eq.2).

The above outlined consideration together with some analytical consideration have produced a preliminary design that has been refined trough a numerical multiphysics analysis. More particularly, a 3D FEM has been used to calculate the temperature field in various working condition. The temperature field was used to compute the permeability distribution in a 2D FEM solver which was able to calculated the torque.

The fact that heat exchange rate is directly related to the obtainable torque led to the rotor structure shown in fig.2. This structure maximize the heat exchange and therefore the obtainable torque. The machine consists of an array of ferromagnetic tube circularly placed. The tube are made of Gadolinium

material and the hot and cold spot are marked in the figure 3. Somehow, it resembles a vapor heat exchanger.

Each tube is supposed to be connected to the hot and cold source on the basis of the position it assumes. The temperature field is calculated by using a 3D FEM.

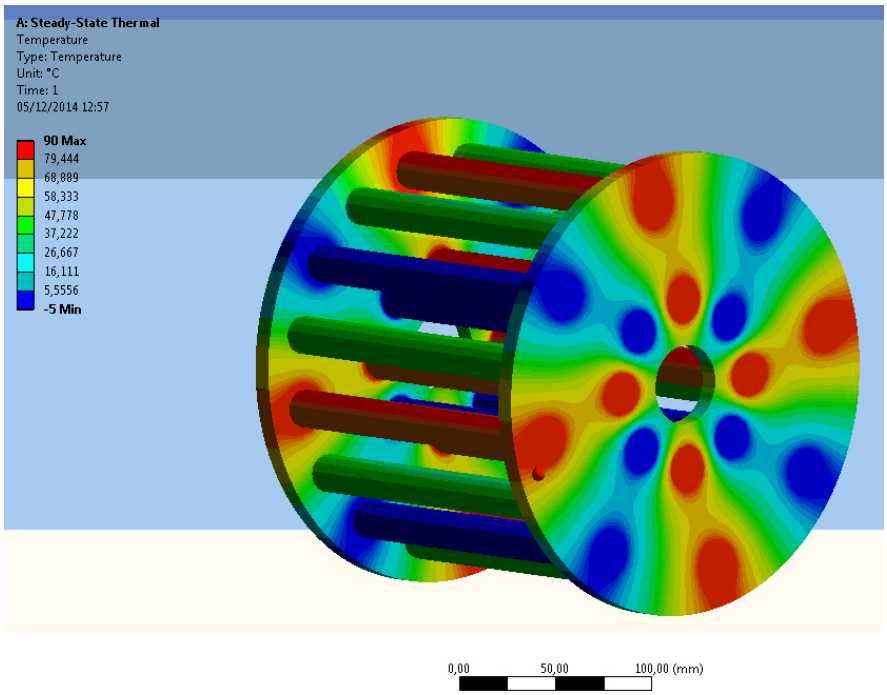

Figure.5 Temperature field (90;-5 °C) of the machine

When the machine is rotating the temperature field assumes the same qualitative distribution, but because of the advection, the temperature difference is reduced.

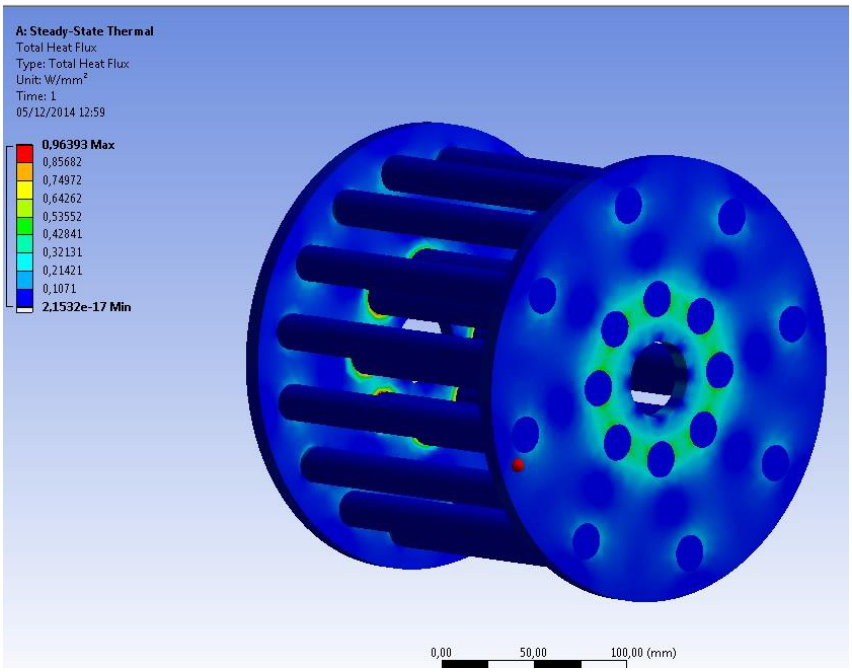

Figure.6 Total Heat Flux [W/mm^2] of the machine

At a critical rotational speed the temperature difference reaches a value where no ferromagnetic area are present. At this speed the obtainable torque vanishes. The optimization procedure was performed by choosing the structure of the rotor that maximize the heat exchange.

IV. Numerical and Experimental Results

The thermal computation allowed to design an actual machine and to manufacture part of the rotor. The rotor of the machine has been built by inserting inside the tube a Gd alloy. The hot and cold spots have been obtained by using hot and cold air.

The diameter of the machine was equal to 40cm and axial length to 60 cm. The four poles were generated by suitable electromagnets able to generate a field equal to 1T. The following numerical tests were done:

-the calculation of the flux distribution at stand still;

-the calculation of torque at stand still;

-the calculation of the field distribution in rotating condition;

-the achievable speed;

The torque at stand still was experimentally tested

Fig. 7 shows the flux distribution and magnetic field density at stand still for a temperature difference equal to 90 °C. At this temperature difference a torque equal to 1.3 N*m was calculated.

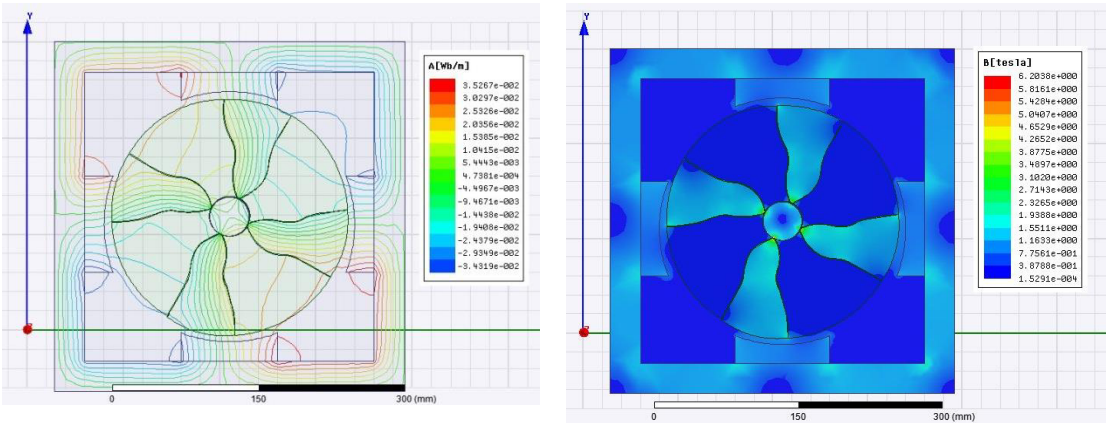

Figure.7 Flux distribution and magnetic field density of the machine

The torque at stand still was experimental tested and the value was equal to 0.9 N*m. This value is 20% lower than the calculated one. This was probably caused by the fact that the 90 °C temperature was not achieved (the temperature difference was in the range of 75 °C).

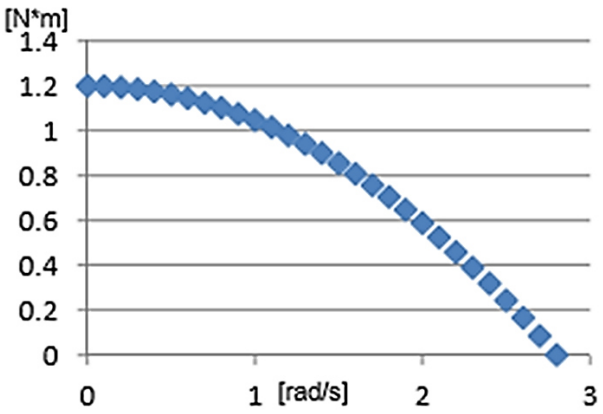

Figure. 8 Mechanical characteristic of the thermomagnetic motor.

The achieved speed at no load condition was equal to 0.09 rad per sec. This speed was in the range of the theoretically calculated speed.

Conclusion

In this study a design and the optimization of a Curie motor has been presented. The mathematical model used to design the motor has been presented and the dq theory of the Curie motor has been explained . It is shown, how the

temperature difference plays a fundamental role for torque generation and that the temperature difference is governed by both thermal conduction as well as advection in the rotor. The use of the mathematical model developed has allowed to optimize and build a continuously rotating thermomagnetic motor.

References

[1] M. Trapanese, A. Viola, e V. Franzitta, «Design and Experimental Test of a Thermomagnetic Motor», *AASRI Procedia*, vol. 2, pagg. 199–204, 2012.

[2] Tesla N., «US Patent number 396121, (1889).» 1889.

[3] K. Murakami e M. Nemoto, «Some experiments and considerations on the behavior of thermomagnetic motors», *IEEE Trans. Magn.*, vol. 8, n. 3, pagg. 387–389, set. 1972.

[4] M. Trapanese, «A dq axis theory of the magnetic, thermal, and mechanical properties of Curie motor», *J. Appl. Phys.*, vol. 109, n. 7, pag. 07E706, 2011.

[5] C. Palmy, «A thermo-magnetic wheel», *Europhys. News*, vol. 38, n. 3, pagg. 32–34, mag. 2007.

[6] L. D. R. Ferreira, C. V. X. Bessa, I. da Silva, e S. Gama, «A heat transfer study aiming optimization of magnetic heat exchangers of thermomagnetic motors», *Int. J. Refrig.*, vol. 37, pagg. 209–214, gen. 2014.

[7] A. Kitanovski, J. Tušek, U. Tomc, U. Plaznik, M. Ožbolt, e A. Poredoš, «Design Issues and Future Perspectives for Magnetocaloric Energy Conversion», in *Magnetocaloric Energy Conversion*, Cham: Springer International Publishing, 2015, pagg. 331–366.

[8] M. S. Choi, S. Um, e Y.-D. Chun, «Electrothermal effects of advanced electromagnetic materials on electrical loss and thermal characteristics of synchronous rotational machines», *J. Mech. Sci. Technol.*, vol. 28, n. 8, pagg. 3335–3343, ago. 2014.

Annex II

Design and Experimental Verification of a Magnetostrictive Electric Power Generator Embedded in Floor Tiles.

Introduction

Recently magnetostrictive technology has been proposed to be used in several energy harvesting devices [1], [2].In magnetostrictive materials, the application of external mechanical stress induces a change in the level of magnetization and therefore an electromotive force (emf) is generated. This emf can be collected in order to produce electrical energy. This effect has been theoretically and experimentally confirmed in metglas [3] Terfenol D [4], [5] FeGa and several other alloys.

Most of these studies are focused on power generation from mechanical vibrations of a single frequency. Unfortunately, the pure sinusoidal mechanical vibration is highly ideal and different from real cases. Some authors[1-2] have examined the possibility to build a power generator by using Terfenol D and have given an expression of the Magnetization in terms of Stoner-Wohlfarth model.

Most papers on this field have adopted static models to describe the principle of operation of magnetostriction based devices. In this paper, on the contrary, we examine the possibility to build a device based on the use of Terfenol D able to convert the energy contained in mechanical vibration generated on a floor by walking persons and we present a mathematical model based on Preisach theory able to predict the variation of the magnetization vs time and therefore the induced emf.

In this paper, in order to give a dynamic mathematical model of the device, we use Dynamic Preisach hysteresis Model (DPM) for magnetostrictive materials operating in hysteretic and time varying nonlinear regimes. This model allow us to design and simulate a magnetostrictive electrical power generator. DPM is a development of classical Preisach Model which is able to include dynamical features in the mathematical model of hysteresis. The magnetostrictive material considered for the power generator is Terfenol-D.

The generator is supposed to be made of several square shaped floor tiles installed on intensively used floor. The tiles are designed to be mechanically loaded by ordinary walking persons and the pressure of each step generates a mechanical stress on the terfenol which is converted in a magnetic field variation

that can be collected in order to produce an electromotive force (emf). The mathematical model used is able to simulate the time variation of the pressure, of the magnetization, of the magnetic field variation and the emf produced in each tile. The tiles, and therefore the generator, is activated from a large number of walking persons (ca. 1000). The gait used to simulate each person is varied according to a normal distribution of the size of the walking population.

The model used is able to reconstruct both the magnetization relation and the Field-strain relation for each tile in the presence of the walking persons. and an electrical model of the connections of the tiles to the conversion system is able to simulate the electrical output parameters of the generator. Finally, it is shown that the power density of such a generator installed in a appropriately chosen area can be comparable to the power density of other harvesting energy technology.

The intellectual path followed in this paper to design a power generator is the following: preliminarly the characteristics of the primary source of energy (gait) is presented (section II), the characteristic of the energy source imposes the mathematical model to be used in the design of the power generator and the model is briefly exposed in section III. The use of the model allows to a design the machine, that is presented also in section III. In section IV preliminarily the mathematical model used is checked against some experimental results and in a second run of experiments the technical features of the built tile are investigated. Finally in section V the conclusions are drawn.

I Cumulative gait: the energy source for a vibrating floor

As already said the converter below presented exploits as source of energy the vibrations induced on a floor by walking people. Therefore it becomes necessary to have a reliable mathematical model of the mechanical stress that a walking person transmits to floor.

Figure 1 is a typical example of the pressure exerted on a surface by a walking and running person. In fig.1on the left it is shown the load impressed during a race, and on the right during a walk. During a race one can see that the force is

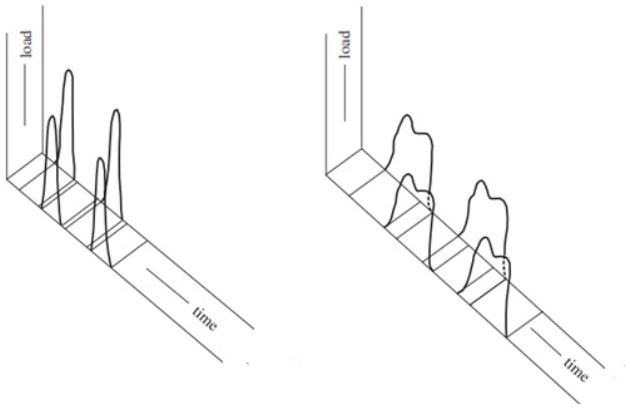

Figureure.1 Typical gaits

discharged to the ground much more quickly and this results in greater stress discharged to the ground, also the feet never touch the ground simultaneously. One cannot say the same when a person walks because the force in this case is discharged to the ground more gently and one can observe a double peak, the time taken to perform the step is greater and the feet for a short period are both on the ground. In Fig.2 it is reported in detail the individual stress due to the contact between the foot and the platform in different modes of walking. On the left, the graphs show the variation of the force / static weight , in function of time. The peak is approximately 0.125 s , then the force is around static weight and again has a peak

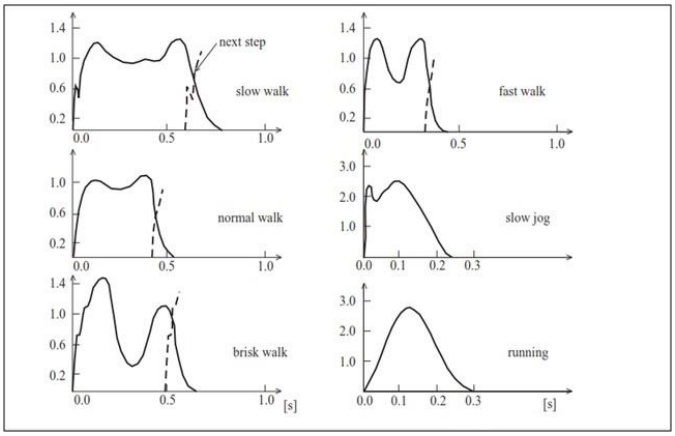

Figure.2 Pressure waveform for several gaits.

The top graph on the right represents a brisk walk, the maximum value of the force due to the stress increases with respect to the previous case, but decreases the time of application.

The second figure on the right ,represents the slow jog , we note that the time of application of the force decreases and the force applied to the surface exceeds twice the static weight , the phenomenon becomes even more evident in the figure in the lower right that represents a race . In this case the applied force reaches almost three times the static weight in a very short time of application , the time required to reach the peak force is approximated in less than 0.15 s , while the time necessary to reset the force is little more than 0.15 s.

These characteristics load vs time have been used as the mathematical model for the vibrations on the floor. These vibrations induce the magnetostriction effect on the floor tiles and cause the emf generation.

II Design of the Floor tile

In order to design a power generator based on the use of magnetostictive materials for energy application, a Preisach like approach has been used. The mathematical details of the model and its identification are reported in [6], [7]. The model is able to describe the magnetization waveform that Terfenol D generates under an external applied pressure waveform. This mathematical model has been validated experimentally (see section 4).

By using the above said model one can compute the output voltage Vout according to the following expression (which is essentially an application of Faraday's law):

$$V_{out} = N \cdot \pi \frac{d^2}{4} \cdot \frac{\Delta M}{t} \qquad (1)$$

Where N is the number of coils, d is the diameter of the coil, ΔM the magnetization variation and t the time needed to walk one step (that was in the order of 1 sec in the case of a walking regime and 0.5s in the case of a run regime). The Magnetization variation was computed (as already said) by using the mathematical model reported in [7]. Eq.1 is the fundamental equation to be used to design a magnetostrictive generator and the critical point is to be able to evaluate accurately the magnetization variation.The dimensions of the coil coincide with those of the Terfenol -d that for the case under consideration are 20 mm high and 8 mm in diameter. As with regard to the number of turns 4 samples were prepared containing respectively 100, 300, 600 and 1000 turns . The ceramic tile that covers the generator has the dimensions of 10cm x 10cm .

In Figure 3 and 4, one can see various parts of the generator.

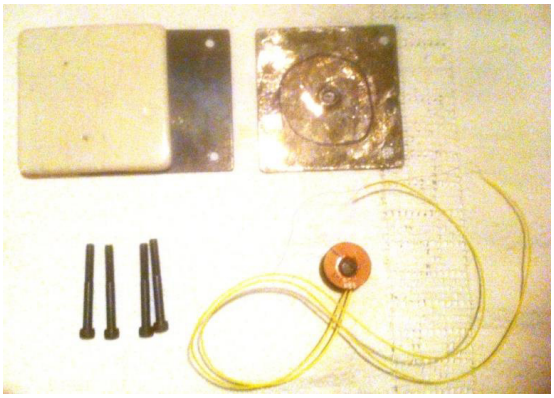

Figure.3 The generator. From upper left corner: the ceramic tile, the lower upper plate, the lower plate, the mechanical joints, the winding with the Terfenol rod in the centre.

The generator consisted of two plates, one winding, one Terfenol rod, four iron mechanical joints, and one ceramic tile.

The plates were made of iron and had dimensions of 10cm x 10cm. The winding were 20 mm high and can have various number of turns. The mechanical joints were 30 mm high. The ceramic tile was square shaped with a side of 10 cm. The plates and the mechanical joints assured the mechanical resistance of the device and provided a closed path for the magnetic flux lines. The tile had a total height equal to 30mm.

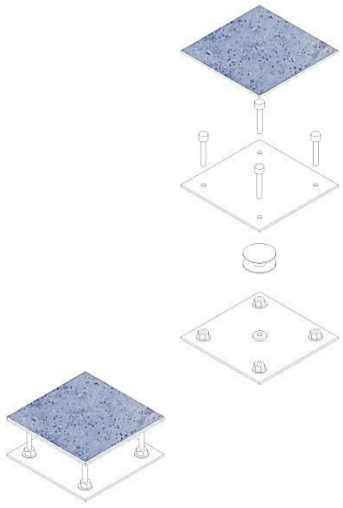

Figure.4 Schematic drawing of the floor tile

The generator is located within a platform. Each tile can contain from one to n generators. The mechanical vibration modifies the shape of the rod and therefore induce a magnetization variation which causes an emf that is collected through the coils. As a result, the waveform of the emf is strictly linked to the magnetization waveform caused by the gait of the walking persons.

III Experimental Methods and Results

A Experimental set up

The principle of operation of the experimental test was that a controlled mechanical load was applied on the terfenol sample inducing a mechanical deformation and therefore, thanks to the magnetostriction effect, a variation of the magnetization of the sample which induced an emf in the winding

The load pressure was applied with a servo-hydraulic machine testing systems (MTS) (Fig. 4). Two teflon guides were locked in place on the two faces of the specimen to guarantee the correct alignment of the punches, and to prevent any movement during the application of the compressive load. The machine was driven by a software that allowed to impose a pre set load waveform. An acquisition systems collected several quantities. The measured quantities were

the displacement, the induced emf, the current and the applied mechanical load.

The experimental test bench is illustrated in fig. 5. The tests were performed on 4 different windings which respectively consisted of 100, 300, 600 and 1000 turns of copper wire. Each winding was wound around a Terfenol D sample 20mm high and with a diameter of 8mm.

Figure.4 The Universal testing Machine

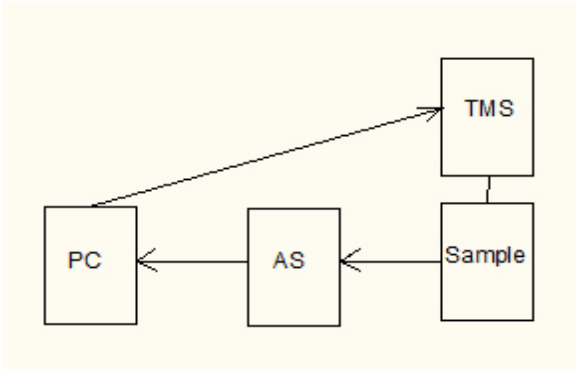

Figure.5 Experimental test bench: PC is the Personal Computer, TMS is the test mechanical system and AS is the acquisition system

B Experimental result

The experimental tests were performed with a twofold objective: on one side the reliability of the adopted mathematical model was tested and on the other side the technical performances of the generator was investigated.

The tests were performed by applying to the sample several types of load.

1)Sinusoidal load;

2)Impulsive load

3)Prolonged sinusoidal load.

The sinusoidal tests were performed at various frequencies (0.1, 1, 2, 5 10 and 20 Hz) for a fixed maximum load ($5*10^3$ kg), the impulsive load tests were performed at various loads (from $1*10^2$ kg, up to $2*10^4$kg), the prolonged sinusoidal tests were performed at 1Hz for a $1*10^3$ kg fixed load.

The sinusoidal tests were done to validate the mathematical model adopted to design the generator. Fig 6 and Fig. 7 show how the mathematical model adopted was able to describe the behavior of the material at low frequency but was not fully adapt to describe the wave form for frequency higher than 5 Hz, where quite a steep shape was detected in some area of the waveform. However, because this steep behavior appears in the loading part of the waveform, we believe it is caused by some imperfections in the mechanical assembling that generates an extra pressure.

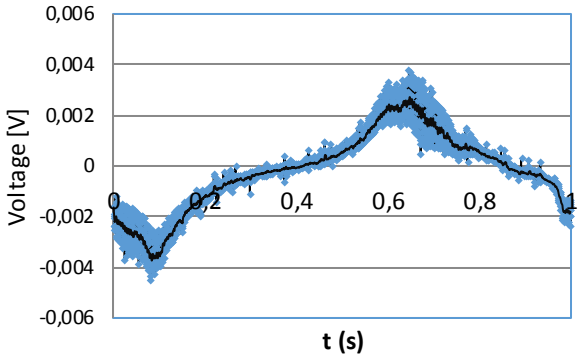

Figure.6 Output voltage at 1Hz. Black line is the line obtained by using the mathematical model and gray line is the experimental line.

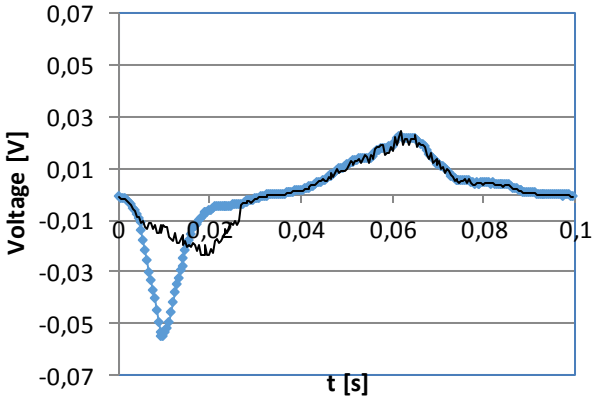

Figure.7 Output voltage waveform at 10Hz. Black line is the line obtained by using the mathematical model and gray line is the experimental line.

The impulsive load tests were done to measure the generation capability of the tiles. The tests were done at open circuit and with a 1Ω resistance with a duration of the impulse equal to 0.1 s and a load equal to $1*10^2$kg. Several windings were tested and results are shown in tab.1.

N of turns	*No load Voltage*	*Output voltage (1 resistance)*
100	10mV	1mV
300	26mV	3mV
600	55 mV	6 mV
1000	96 mV	11mV

Table I. Output voltage under impulsive load

Prolonged sinusoidal load tests were done on each winding that had been built. It consisted on the application of a sinusoidal load of a maximum value equal to 1*103 kg at a frequency of 1Hz. No sample was able to sustain more than 150 cycles . However, the cracks that were caused did not completely destroyed the samples and the generator was able to works continuously for the total time of the test (1 hour) with a degradation of the output voltage lower than 5 %.

IV. DISCUSSION AND CONCLUSIONS

The sinusoidal tests showed that the Preisach like approach used to design the generator is able to describe the voltage generated by our system in a dynamic situation and therefore can be adopted to design magnetostrictive generator.

The impulsive load tests show how at open circuit the system was able to generate a voltage in the order of magnitude of 0.1 V. This value could have been increased by an order of magnitude simply increasing the number of turns (and the designed tile had enough space to allow to accept windings with 30000 turns).

The power generated by our tile was in the order of 1*10-4W under a load of 1*102kg with a time scale in the order of 0.2s. This value means that the power density generation capability of our system for the load above used is in the order of 0.01 W per square meter. This number can appear quite low but it can be greatly enhanced. As matter of fact, in our system a large part of the mechanical load is concentrated not on the Terfenol but on the mechanical joints. In an optimized design most of the load should be applied on the Terfenol and this could be achieved by simply increasing the number of Terfenol rods insterted in the tile. Our tile have enough space for 20 Terfenol converting units. This improvement leads to a power density in the order of 2W per square meter that is a power that can be useful for several applications.

The prolonged sinusoidal load test showed on one side the fragility of the material but on the other side the robustness of the generator that was able to work with a low reduction of the performances even in the presence of broken Terfenol rods. However an improvement on the mechanical assembling of the tile can enhance the durability of the rod .

In conclusion, in this paper we proposed an approach and a mathematical model for the design of a magnetostrictive power generator able to convert mechanical vibrations into electrical energy. The equation used to design the generator was based on Dynamic Preisach hysteresis Model (DPM) for

magnetostrictive materials. We showed that this generator has the potentiality to produce around 2 W per square meter in a densely walked area.

References

[1] H. Zhang, «Power generation transducer from magnetostrictive materials», *Appl. Phys. Lett.*, vol. 98, n. 23, pag. 232505, 2011.

[2] C.Natale, C.Visone, e F. Velardi, «Identification and compensation of Preisach hysteresis models for magnetostrictive actuators», *Physica B*, vol. 306, pagg. 161–165, 2001.

[3] V. R. Challa, M. G. Prasad, e F. T. Fisher, «Towards an autonomous self-tuning vibration energy harvesting device for wireless sensor network applications», *Smart Mater. Struct.*, vol. 20, n. 2, pag. 025004, feb. 2011.

[4] J. Yang, Y. Wen, P. Li, X. Dai, e M. Li, «A New Vibration Energy Harvester Using Magnetoelectric Transducer», *J. Magn.*, vol. 16, n. 2, pagg. 150–156, giu. 2011.

[5] A. Bayrashev, W. P. Robbins, e B. Ziaie, «Low frequency wireless powering of microsystems using piezoelectric–magnetostrictive laminate composites», *Sens. Actuators Phys.*, vol. 114, n. 2–3, pagg. 244–249, set. 2004.

[6] M. Trapanese, V. Franzitta, e A. Viola, «A dynamic model for hysteresis in magnetostrictive devices», *J. Appl. Phys.*, vol. 115, n. 17, pag. 17D141, mag. 2014.

[7] M. Cirrincione, R. Miceli, G. R. Galluzzo, e M. Trapanese, «A Novel Neural Approach to the Determination of the Distribution Function in Magnetic Preisach Systems», *IEEE Trans. Magn.*, vol. 40, n. 4, pagg. 2131–2133, lug. 2004.